Mechanisms of Fatigue Fracture for Nickel Free Titanium Alloys in Biomedical Applications

Submitted By

Muhammad Amjad

Registration No: 05-FET/PHDME/S14

Supervisor: Dr. Saeed Badshah

Co-supervisor: Dr Muhammad Adil Khattak

MECHANICAL ENGINEERING DEPARTMENT

FACULTY OF ENGINEERING AND TECHNOLOGY

INTERNATIONAL ISLAMIC UNIVERSITY, ISLAMABAD

2021

Mechanisms of Fatigue Fracture for Nickel Free Titanium Alloys in Biomedical Applications

Muhammad Amjad

05-FET/PHDME/S14

Submitted in partial fulfillment of the requirements for the PhD degree in Mechanical Engineering at the Department of Mechanical Engineering

Faculty of Engineering and Technology

International Islamic University,

Islamabad

Supervisor

Dr. Saeed Badshah

Co-supervisor:

Dr. Muhammad Adil Khattak

March, 2021

DECLARATION

I **Muhammad Amjad,** Registration No: **05-FET/PHDME/S14** student of PhD Mechanical Engineering in session 2014-2021 certify that research work titled "**MECHANISMS OF FATIGUE FRACTURE FOR NICKEL FREE TITANIUM ALLOYS IN BIOMEDICAL APPLICATIONS**" is my own work. The work has not been presented elsewhere for assessment. Where material has been used from other sources has been properly acknowledged.

Signature of student:.....

Dated:.....

DEDICATED TO

My Family

Certificate of approval

This is to certify that the work contained in this thesis entitled, **"Mechanism of fatigue fracture for nickel free titanium alloys in biomedical application"** was carried out by **Muhammad Amjad** Registration No. **05-FET/PHDME/S14**, and is fully adequate in scope and quality, for the degree of Doctor of Philosophy (Mechanical Engineering).

Viva voce committee:

Dr. Saeed Badshah (Supervisor)
Associate Professor
Department of Mechanical Engineering (FET)
International Islamic University, Islamabad

Dr. Muhammad Adil Khattak (Co-Supervisor)
Materials Engineer
HRL Technology Group, Unit 2, 33-37 Rosedale Street
Coopers Plains QLD 4108 – Australia

Dr. Misbah Ullah (External Examiner-I)
Professor, UET Peshawar

Dr. Manzoor Ahmad (External Examiner-II)
Principal Engineer
PAEC Islmabad Pakistan

Dr. Rafiullah Khan (Internal Examiner)
Assistant Professor
Department of Mechanical Engineering
International Islamic University, Islamabad

Dr. Syed Athar Masood (Chairman)
Associate Professor
Department of Mechanical Engineering (FET)
International Islamic University, Islamabad

Abstract

Biomaterials are synthetic materials, which are implanted to substitute living tissue for a satisfying normal functionalities of the body and can enhance the quality and longevity. Nickel-free titanium alloys are toxic free biomaterials quickly replacing the traditionally used materials. The purpose of this study is investigating the fatigue fracture behavior mechanism of nickel-free titanium alloys in simulated body fluids, and to solve the reliability problems of nickel free titanium alloy implants. In implants crack-like defects are likely to cause fatigue cracks, which is not conducive to the effective performance and design life of the implant. For this purpose, the mechanics and mechanisms of fatigue fracture and cracking of implant materials has been quantified. Influencing factors such as the corrosive environment caused by human body fluid and body weight for different activities have been considered and analyzed. The material mechanics and metallurgical research results of nickel-free titanium alloys under service load will lay the foundation for understanding the fatigue fracture failure of implants.

The study has been structured in experimental and finite simulation sections. The experimental part includes to determine the mechanical properties and study the microstructure of untreated alloys specimen and simulated body fluid (SBF) treated specimen. The mechanical properties include the yield strength, ultimate strength and Young's modulus of elasticity. The fatigue tests include the S-N curve, fracture toughness and fatigue crack growth carried out for both the treated and untreated specimen of implant material. The fractographic analysis of fractured surfaces during tensile test and fatigue crack growth are carried out using Scanning Electron Microscope to quantify the effect of simulated body fluid on fractured surface.

The Finite element part of thesis illustrates the stress state and deformation of implant under actual loading during routine daily activities for different body weights. The loading cycles for different activities and body weights have been selected from previous published research, served as input to the model implant in the FE environment. Total time and step size of simulations are based on 20 years of design life of implant. The material properties like tensile strength, yield strength, Young's modulus and S-N data determined through experiments have been given to FE model for both untreated and SBF treated. The FE simulation results for the daily activity predicts the life of implant for each activity and the determined factor of safety through Gerber formulation which accounts for the mean stress effect during loading. The simulation has been carried out for different body weight for the same daily routine activities and the effect on life of implant has been established.

The fatigue crack growth tests were performed to quantify the effect of simulated body fluid on crack propagation. It has been observed that the treated samples significantly affect the crack propagation. The S-N data has been established for both the SBF treated and untreated samples. The results shows the negligible effect of simulated body fluid on S-N curve due to formation of oxide layer on the defect free surface that act as shielding from corrosion and established a mechanistic model to predict the finite life. It has also been concluded from the experimental results of fatigue crack growth tests that in the presence of crack (defect or scratches) on specimen, simulated body fluid adversely effects the life of materials.

The FE results observed that the implant for the current mechanical properties and activity loading is safe and the factor of safeties are higher. However, the weight of the body influences the factor of safeties and damage of implant and plays a vital role during the implant design and service life. It has been observed that increase of 25 Kg weight from 75 Kg the maximum reduction

in FOS is 48 % for the standup activity, whereas due to SBF treatment the reduction in FOS is 2.0% in standup activity in twenty years.

List of Publications

1. Amjad, M., Badshah, S., Rafique, A. F., Adil Khattak, M., Khan, R. U., & Abdullah Harasani, W. I. (2020). Mechanism of Fatigue Crack Growth in Biomedical Alloy Ti-27Nb. Materials, 13(10), 2299.
2. Amjad, M., Rafai, A., Badshah, S., Khan, R. U., & Ahmad, S. (2018). Finite element analysis of the real life loadings on the ti-27nb hip bone implant. JOURNAL OF ENGINEERING AND APPLIED SCIENCES, 37(2), 15-20.
3. Amjad, M., Badshah, S., Khattak, M. A., Khan, R. U., & Mujahid, M. (2017). Characterization of Nickle Free Titanium Alloy TI-27Nb for Biomedical Applications. Journal of Engineering and Applied Sciences (JEAS), 36(2).
4. Alam, K., Iqbal, M., Umer, J., Amjad, M., & Al-Ghaithi, A. (2020). Experimental study on biological damage in bone in vibrational drilling. Bio-Medical Materials and Engineering, (Preprint), 1-9.
5. Khan, R., ur Rahman, W., Ullah, M., Afaq, K., Amjad, M., & Jan, S. (2016). Age Effect on The Mechanical Properties of Hip Joint Bone: An Experimental Investigation. Journal of Engineering and Applied Sciences, 35(1), 37-44.
6. Khan, R., Jan, S., Amjad, M., Badshah, S., & Ahmad, S. (2017). Crack Closure and Fibre Bridging Contribution in the Stressratio Effect on Delamination Growth Under Fatigue. Journal of Engineering and Applied Sciences, 36(1), 107-114.

ACKNOWLEDGEMENT

First and foremost, praises and thanks to the ALLAH سُبْحَانَهُ وَتَعَالَىٰ, the Almighty, for His showers of blessings throughout my research work to complete the research successfully.

I would like to extend my deepest gratitude to my supervisor Dr. Saeed Badshah for his dedicated support and guidance. He continuously provided encouragement and was always willing and enthusiastic to assist in any way he could throughout the research project. I am also grateful to my Co. Supervisor Dr. Muhammad Adil Khattak from University Technology Malaysia for providing me the opportunity to visit and perform experimental work at UTM under his kind guidance.

I am thankful to Dr.Nazeer Anjum at University of Engineering & Technology Taxila, Dr Yasir at National Textile University Faisalabad and Advance Electronics Lab International Islamic University Islamabad for providing me the experimental facility.

I gratefully acknowledge the assistance of all my colleagues and friends, Dr. Rafi Ullah, Engr. Sajjad Ahmad and Engr. Sakhi Jan Khalil and specially Dr. Mujahid Badshah without their constructive criticism, invaluable contribution and insightful suggestions this would have not been possible.

I am extremely grateful to my parents for their love, prayers and caring through my life. Finally, I am very much thankful to my wife and children for their love, understanding, prayers and continuing support to complete this research work successfully.

Finally, my thanks go to all the people who have supported me directly or indirectly to complete the research work.

Muhammad Amjad

Table of Contents

List of Figures

List Of Tables

1 Introduction

From the last few decades, there has been promising increase of materials applications in biomedical areas and now the field of biomaterials has led to multi-million-dollar business. However, the term "biomaterials" may have encountered different elucidations both in materials science and clinical medicine. Biomaterial is defined as a synthetic material, which is implanted to substitute living tissue for a satisfying normal functionalities of the body and can enhance the quality and longevity [1]. However, the aspect of implant biological bio compatibility and mechanical bio compatibility to the human body are the most importance factors. Implants materials fracture due to fatigue loading, corrosion, wear and toxic effect in a human body that dangers the life of aged patient and may need a revision surgery which leads to economic over burden. Managing implant material corrosion, wear and failure of in-service implants are one of the major technical and economic challenges facing today's engineers and orthopedic surgeon. The in-service life of the implants is strongly exaggerated by the human body environment-fatigue loading, including corrosion and wear. Therefore, for the overall material's load resistance, corrosion resistance and abrasion resistance in the human environment, a comprehensive understanding of the material properties is the basic consideration for the development of the entire biomaterial implant business.

1.1 Background and Rationale

Biomedical Engineering (BME) is the application of design concepts and engineering principles to medical field. Biomedical engineering works as a link between the engineering and medical by combining the design and problem solving techniques of engineering and medical to handle the health care problems [2]. Much of the work in biomedical engineering

consists of research and development, spanning a broad array of subfields as illustrated in Figure 1-1 [2].

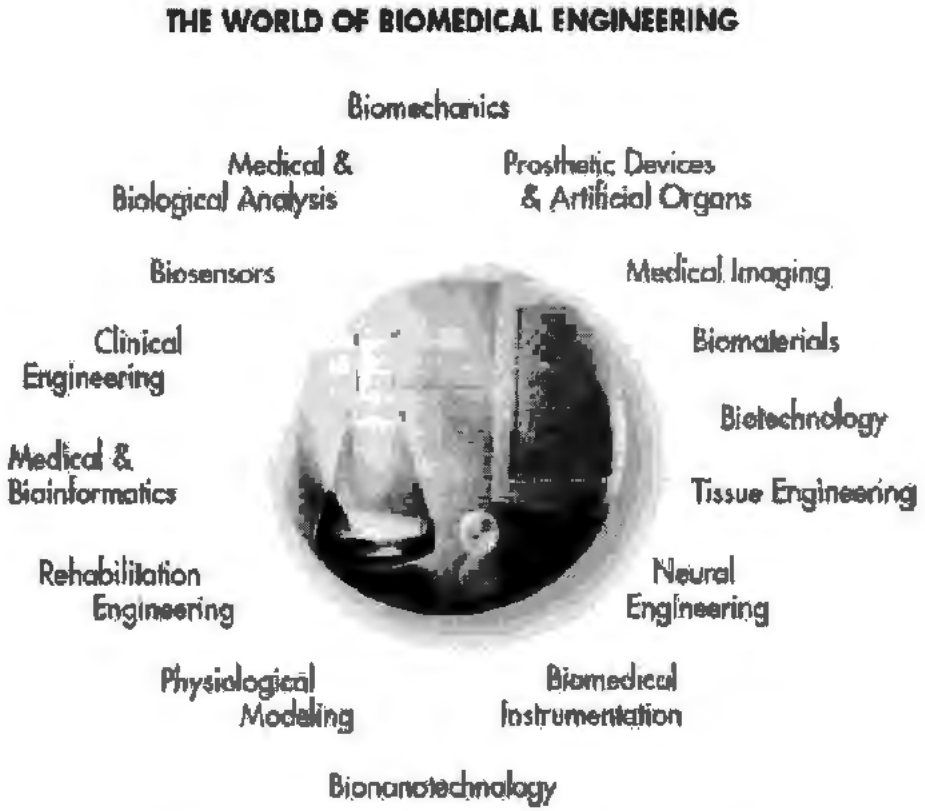

Figure 1-1: The World of Biomedical engineering [2]

The field of biomaterials exists from the era of Egyptian and romans for 4000 years back in the form of Gold and iron for dental implants however the stainless steel, nylon, titanium etc. put in to use after the world war II. After the first conference on biomaterials held at Clemson University in South Carolina in 1969, the field received the recognition it deserves and has received considerable consideration since then. Biomaterials are used in the different parts of the human body as artificial valves in the heart, stents in blood vessels, replacement implants in shoulders, knees, hips, elbows, ears and dental structures [3-5] .With the increase in the population ratio of aged people, arthritis is amongst the main diseases commonly effect

the elders, and sometimes even young ones. It damages the lives of the affected people, causing inconvenience and high pain. The other big reasons for the replacement of failed tissue are the road accidents, fracture due to sports and the global terrorism. So, the demand for the replacement of failed hard tissue due to the causes mentioned is increasing day by day. Amongst all implants, there is an increasing demand for the replacement of knee and hip implants because of the increasing ratio of aged people.

For implants, high level of reliability and integrity is desired due to the potential threats in the human body environment and combined with the life risk of the patient involved. In the human body all the implants have to sustain in the aggressive environment and loadings due to different activities like, sitting, standing, walking, stairs up and down jogging etc. Such conditions lead to environmental fatigue interactions of the implant material. The life of the implant is a key factor to ensure the feasibility of implementing the life extension program of the implant.

Conventional metallic bio materials used as an implant are stainless steel, Co-Cr based alloys, pure titanium and Ti alloys [6]. In the human body the implants operate in a very corrosive environment where body fluids are chlorinated salt water, with a pH in the range of 7.4 to acid, and also contain some other organic acids and ingredients [7]. To meet the demand of longer service life of implant , the artificial materials implants used should avoid the short-term refusal and infection and provide long term biological and mechanical biocompatibility i.e. its high resistance to corrosion in the human body environment, high-wear resistance, long lifetime, high strength, no toxicity to human body etc [6, 8]. Titanium base alloys are widely used as a bio materials implant because of its excellent biocompatibility, low density long in-service life to different fatigue loadings and excellent corrosion resistance [6]. so far, commercially pure (CP) Ti and Ti-6Al-4v are frequently used biomaterial for implants but they can exhibit problems during biomedical applications. The alloys which contains Aluminum,

Vanadium and Nickle having a toxic on the respiratory, circulatory central nervous systems, the digestive organs, kidneys, allergic and immunologic effect, renal Effect and carcinogenesis [9-10]. Newly developed titanium alloys, Ti-25Ta and Ti-27 Nb are without Al, V and Ni due to the health concerns .Ti-25Ta and Ti-27Nb are the low modulus β type titanium alloys with an elastic modulus of 64 and 86 GPa and they have to operate in the corrosive environment at a constant body temperature of 37°C (97.8 °F) The implants material properties and the surgical procedures are the key factors for the success or failure of the implant.

1.2 Research Objective

In this research the mechanism of fatigue fracture in nickel-free titanium alloys and the way in which this mechanism will be influenced by simulated body fluid SBF will be investigated. These investigations would aid to resolve the reliability problems commonly associated with nickel-free titanium alloy implants under cyclic loads during prolong use. In the non-conducive human body fluid environment, the crack like defects would generally result in fatigue cracks to limit the fatigue life of implants. Therefore, investigating the mechanics and mechanisms of fatigue fracture and cracking of implant materials is essential. The former involves the internal deformation and stress state of the implant, while the latter determines the main failure modes associated with material. Influencing factors such as the corrosive environment caused by human body fluid during the synergistic failure process will be quantitatively analyzed. The metallurgical research results of nickel-free titanium alloy and material mechanics under in-service cyclic loads will be utilized to understand the fatigue fracture failure of implants. The relationship between corrosion crack-like defects and nickel-free Ti based alloy implant strength (residual and fatigue) will be identified. The static and fatigue response of nickel-free Ti alloy implants under in services cyclic loads (obtained from experimental studies) would be qualitatively and quantitatively analyzed. The influence of

simulated human body fluid on the service life of nickel-free Ti alloy implants would be established.

1.3 Significance of Research

This research will produce several sets of fatigue data based on S-N and fatigue crack growth rate (FCGR) experiments of the selected material and its corresponding life cycle. The data will be used for screening process for proper selection of biomaterial and its service life in normal and in crack like defects. The orthopedic field of medical industry will directly benefit from this research and will be able for the proper selection of biomaterial and its service life in normal and in crack like defects

1.4 Research Methodology

The methodology for this research will be experimental and analytical having the following steps mentioned below.

1. Procurement of material
2. Preparation of specimen: The dog bone and compact tension test specimen for tensile, fatigue, fracture toughness and fatigue crack growth will be prepared from the sheet of titanium alloy as per ASTM standards.
3. Tensile and fatigue Testing: Untreated and simulated body fluid treated dog bone specimen will be tested on universal testing machine for the stress strain and stress vs number of cycle(S-N) measurement.
4. Fracture and fatigue crack growth testing: Untreated and simulated body fluid treated C.T specimen will be tested for fracture and fatigue crack growth. These tests will be carried out on set of triplet samples in laboratory environment. All the readings will be recorded by using high quality camera.

5. Micro mechanism examination: After fatigue and fracture testing of specimen with and without SBF treatment will be examined for the fracture mechanism due to the fatigue and changes in the microstructure.
6. Finite element Analysis: FEA study of the implant for the fatigue life and damage assessment in daily routine activities of different body loads will be carried out using fatigue data of untreated and SBF treated samples.

1.5 Organization of Thesis

Chapter 2 is about the literature review of the relevant works of different researcher in the field related to the objective of the thesis i.e the effect of human body environment on microstructure, fatigue, fracture corrosion, mechanical properties and finite element analysis studies implants.

Chapter 3 describe the experimental testing of the Ti-27Nb and Ti-25Ta. Chapter include chemical composition, microstructural study, simulated body fluid preparation and procedure for treatment of samples, samples preparation and testing procedure for tensile, fatigue, hardness, fracture, fatigue crack growth and Scanning Electron Microscopy.

Chapter 4 describe the major results attained from the different testing of Ti-27Nb and Ti-25Ta as mentioned in chapter number 3. The results of tensile, fatigue and hardness test on treated and untreated samples are compared to study the effect of human body environment. Spectroscopic Ellipsometry test are carried out to look for the presence of oxide layer formation on the surface of samples. Mathematical relation for the finite life and mechanism of fatigue crack growth has been developed for untreated and SBF treated samples.

Chapter 5 describe the finite element analysis of hip implant of Ti-27Nb. Static and fatigue analysis for different routine activities with different body weights are carried out using the properties of untreated and SBF treated alloys. The results summarize the effect of all the

mentioned condition on the factor of safety, life, von mises stresses and to relate the damage increase against increase in alternating stress due to weight in mathematical form for all activities.

2 Literature Review

2.1 Introduction

This chapter is the review of key literature related to the present research work. This chapter will explain structure of bone, bone diseases, total hip arthroplasty, hip implant replacement methods, feasible materials for hip implant and their properties for biomedical purpose. Figure 2-1shows the structure of literature review in the schematic form.

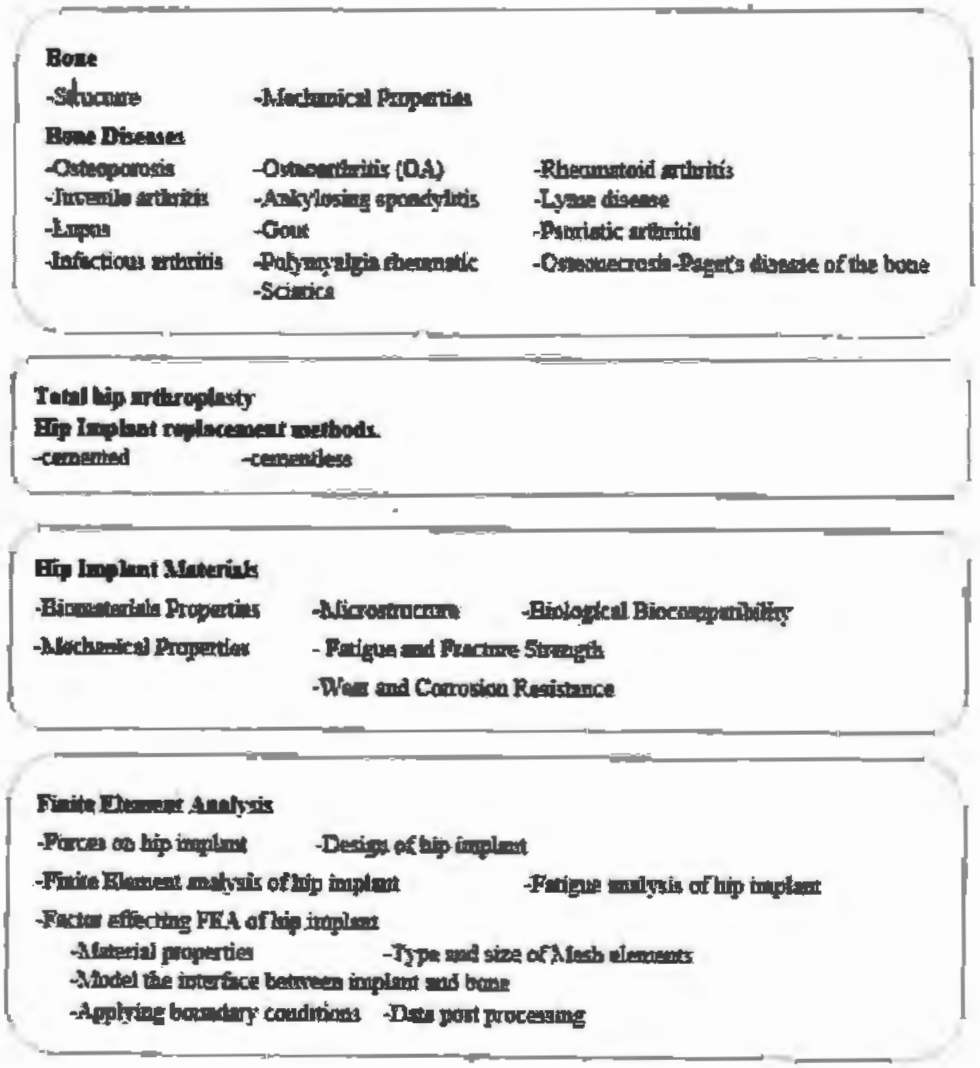

Figure 2-1:Structure of literature review in schematic

In the last part of this chapter, review will be carried out about the computer modeling simulation i.e. Finite Element Analyses (FEA) of hip implant.

Bones are studied in terms of morphology, structure mechanical properties and diseases. In total hip arthroplasty and replacement methods, cemented and cementless methods are reviewed. In the next section review of biomedical alloy materials, microstructure, biological compatibility, mechanical properties, fatigue and fracture strength, wear and corrosion resistance is carried. FEA analysis are summarized in the end of this chapter for the hip prosthesis.

Since 1960, research work on biomaterials for organ replacement and implantation has extended greatly. Organ transplantation, surgical reconstruction and use of artificial organs in case of lost or failure has gained visible development during the last decade. Implants implanted in the human body should meet the standards of high porosity, osteo-conductivity, biocompatibility and biomechanical similarity [11].

2.2 Bone

Bone is a dense thick solid tissue in the human body which provides the structural support to the body beside the guard for the internal organs. For bones lot of information and data is available in literature on skeletal procedures, microscopic structures, mechanical properties and failures of bones. However, a brief introduction to the structural components of bones and its properties are included here to give some taste of understanding of femur structure of bone.

Human bones have different sizes and shapes according to their functions. Some of them are: long bones, such as femurs or tibias, which have the function of resisting flexion and strengthening and are called cortical bones; the second are short bones, such as vertebrae or femoral heads, like spongy materials, also called trabeculae. Or cancellous bone; the third category is the flat bones of the skull and irregularly shaped bones that do not belong to any

category.

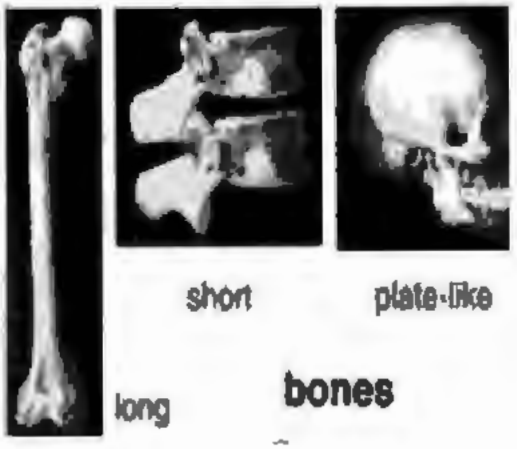

Figure 2-2:Bone shape: long bones-femur, short bones-vertebrae , lamellar bones-skull [12].

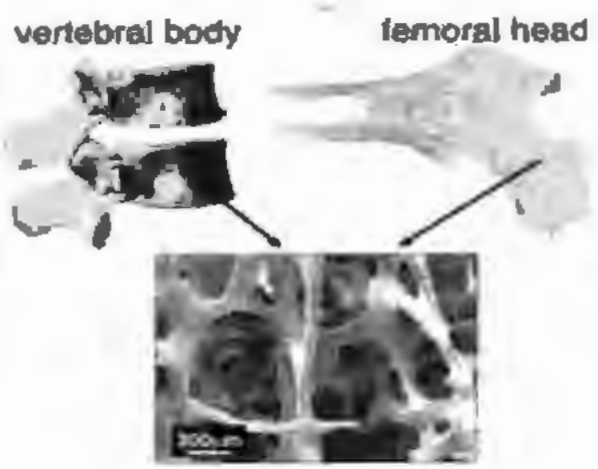

Figure 2-3:The trabecular bone spongy structure found in the vertebrae or femur

Even with different bone shapes, the bone morphology at the tissue and cell level is relatively reliable as shown in Figure 2-2 & Figure 2-3. The thickness of the pillars (or trabeculae) is about a few hundred micrometers. Figure 2-4 shows the structural parts/assemblies of long bones. The end of the long bone is the dry end area. These dry phy end regions are hinged with other bones. The central area of the long bones is called the diaphysis, which surrounds the medullary cavity like a hollow cylinder [13]. Bones are stiff by nature for the prevention from bending and buckling. The bones are also very hard, even if the load exceeds the normal range, they will not break catastrophically [14].

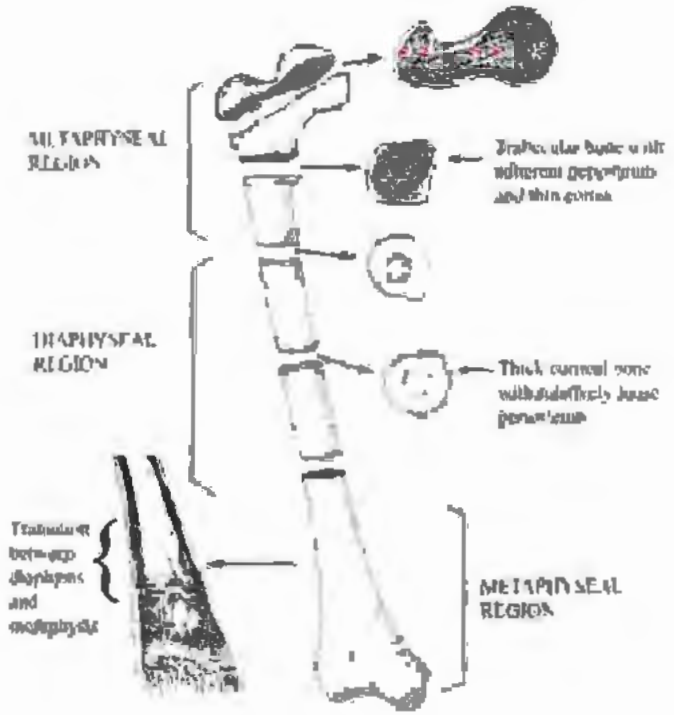

Figure 2-4: Bone structure schematic[13]

Figure 2-5 shows typical values of toughness and stiffness. Proteins (collagen in the case of bone and dentin) are hard but not very stiff. On the other hand, minerals are stiff but not very hard.

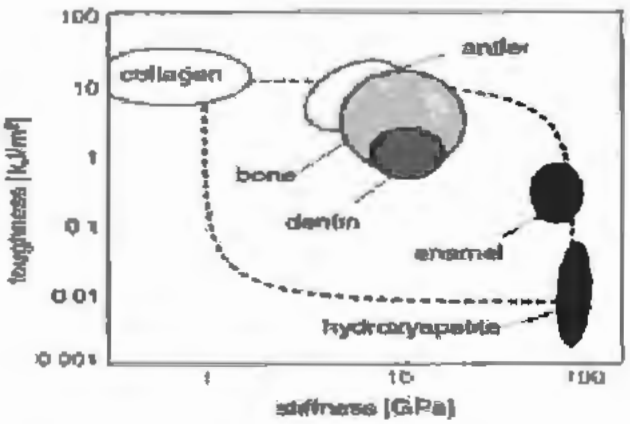

Figure 2-5:Toughness vs stiffness for tissues mineralized with hydroxyapatite [14].

It is obvious from Figure 2-5 that dentin and bone combine the excellent properties of both. The dashed line shown represents the key case of linear and inverse rules of mixing stiffness and toughness.

It is important to mention that trabeculae adjust its orientation in the direction of the applied forces [15]. Individual bones in the body have different distribution of cancellous and cortical bone and 80% of the bone mass in adult human bones is cortical bone [16].

2.2.1 Mechanical properties of bone

Like all structural materials, bones also have a basic stress-strain relationship. Since bone is a vital organ, its nature will change with gender, age, type, location, direction of applied load and test conditions (whether it is dry or wet). The quality and elastic modulus of the cortex and the cancellous part vary. Due to the spongy structure, the strength of cancellous bone is much lower than that of cortical bone [17].

The graph in Figure 2-6 compares the final stress of cortical bone and cancellous bone. The spongy structure, that is, the combination of the cancellous part and the hard element, the cortex, makes the bone a heterogeneous and anisotropic material, which means its characteristics will change in different directions [18].

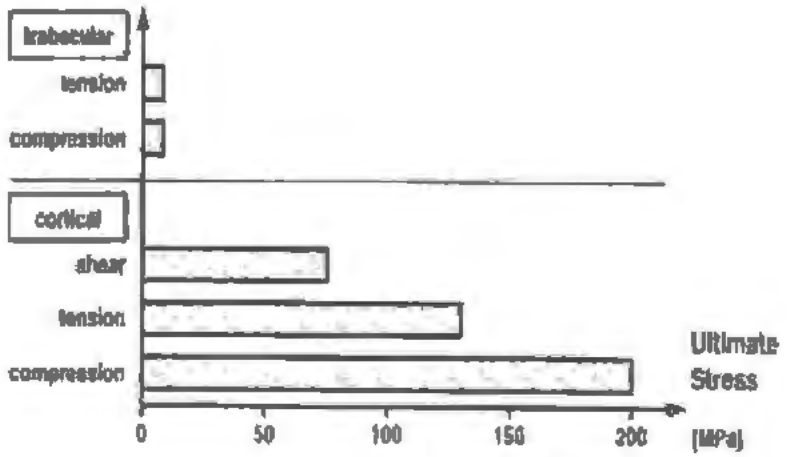

Figure 2-6: Comparison of ultimate stress b/w critical and cancellous bone [18]

In earlier studies different types of conventual mechanical testing techniques for example three point bending , uniaxial tensile and compressive testing were applied for finding out the bone properties, whereas in recent times ultrasound, Magnetic Resonance Imaging(MRI), Computerized Tomography(CT), nano-indentation etc. techniques are used for characterization of bone.

2.3 Bone Diseases

Bone diseases effect both genders. Due to the aging effect and natural deficiencies such as lacking of Vitamin D or C, hormonal imbalances and cell abnormalities the bone loose strength and density naturally. This results in the weaker bones, inflammation in joints, and pain. Around 1.5 million people throughout the world suffer from the bone diseases every year. Some phenomena of diseases in bone and hip are described below.

The osteoporosis is the loss in the mass of bone causing the risk of fracture. Osteoporosis effect the quality of bone and it is also called degenerative disease [19]. Osteoarthritis is the most common disease in the hip joint, its chronic condition is described by the breakdown of the cartilage that provides coushins to the ends of long bones where they meet to form the joint with another part of the body. Osteoarthritis causing the bones to wear out causing pain, stiffness, bone outgrowth called spurs and loss of movement. Pain caused by osteoarthritis phenomena is felt in the groin area. Figure 2-7 showing the femoral head and the spurs generated due to the osteoarthritis in the hip joint [20].

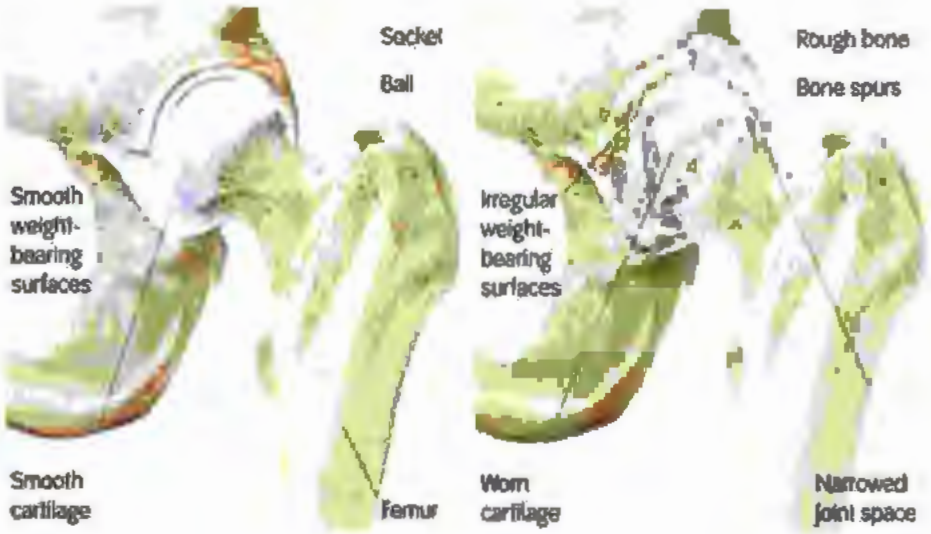

Figure 2-7:Osteoarthritis [20]

In human body immune system protect the body from different type of infections. When immune system mistakenly attack tissues causing rheumatoid arthritis leading to the inflammation in the joints, damage parts of the body, swelling and physical disabilities [21]. Figure 2-8 showing healthy and effected hip joint arthritis.

Figure 2-8: Rheumatoid arthritis [22]

Juvenile arthritis is the term used to portray joint pain when it starts before the age of 16. Juvenile arthritis have several other forms affecting children's. Symptoms include pain in hip joint and swelling [23] as shown in the Figure 2-9.

Figure 2-9: Juvenile arthritis

Ankylosing spondylitis is a rare type of arthritis that mainly affects the spine, causing inflammation and stiffness in the spine. It can also affect the neck part and the hip joint [24]. Lyme disease is a type of infection causing skin rash, fever, flu and joint swelling(arthritis) [25]. Lyme infection can also affect hip joint. Lupus is autoimmune disease in which human body generates antibodies. These antibodies attack the healthy tissues of the body and damage it. Lupus causing inflammation of joints including hip joint as well as heart and respiratory system [26]. Gout is a form of arthritis caused by the excessiveness of uric acid in the body. Gout mainly occur in the foot joints and knees. Gout less commonly cause hip pain [27]. Psoriatic arthritis is the combination of joint pain with skin disease. The skin disease usually occurs before the arthritis and sometime develops after the joint disease [28].

Infectious arthritis is caused by bacteria resulting the infection within the joint. It's usually effects the large joints of the body such as hip and knee joints [29].

Polymyalgia rheumatic is an inflammatory disorder causing muscular pain, symptoms like flu and stiffness. Neck, shoulder, upper arms, thighs and hips are mainly affected by polymyalgia rheumatic [30]. Osteonecrosis also termed as aseptic necrosis or avascular necrosis, happens when blood supply is reduced or stopped to a region of bone and it die and eventually fracture. Osteonecrosis mainly effect the hip joint [31]. Paget's is a chronic disease where unnecessary collapse and development of bone makes the bone weak large and deformed [32]. Sciatica is the inflammation of the sciatic nerve, the largest nerve in the human body. The most common causes of sciatica include nerves being compressed by a herniated disc, or rupture of one of the structures on the vertebral cushion in the spine. Sciatica may be severe pain or burning radiating from the hip [33].

2.4 Total Hip Arthroplasty

As the proportion of the elderly population increases, bone diseases, especially arthritis, are one of the main diseases commonly faced by the elderly. Even young one are sometime suffered from arthritis and damage lives of effected ones, resulting in inability to move and high levels of suffering. The other major reasons for the replacement of failed hard tissue are the road accidents, fracture due to sports and the global terrorism. The demand for the replacement of failed hard tissue due to the causes mentioned is increasing day by day. Amongst all implants, there is an increasing demand for the replacement of knee and hip implants because of the increasing ratio of aged people worldwide and the most exposed part of the body during accident. The implant used in knee and hip joint is shown in Figure 2-10 [34] and Figure 2-11 [35]. According to data collected from total joint replacement surgery, it is predicted that by the 2030, the total number of hip implant procedure will increase by 174% (572,000surgical procedures) and total knee replacement surgery is expected to increase by 673% from the existing rate (3.48 million surgical procedures) [36] .

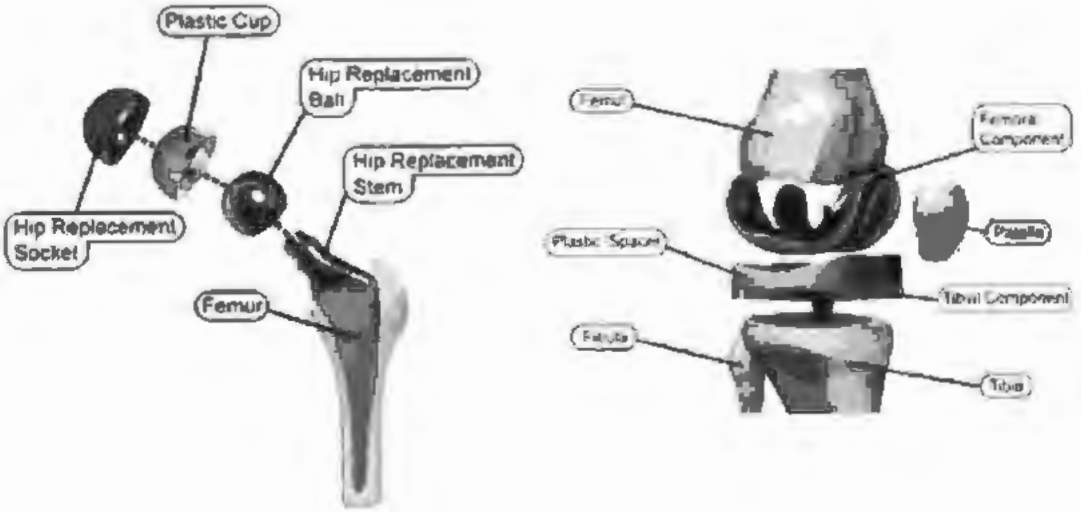

Figure 2-10:Total hip and knee Implant Replacement [34]

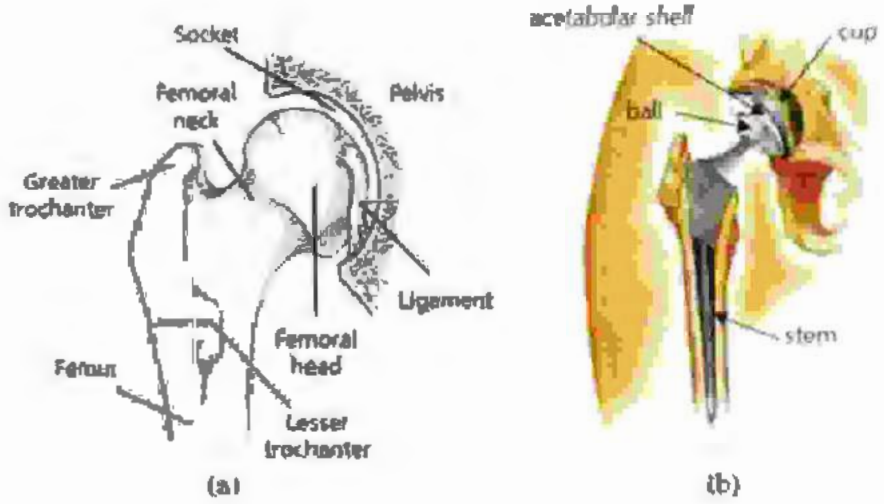

Figure 2-11:Structure of (a) femoral bone (b) Hip implant [35]

Total Hip Arthroplasty or Total Hip Replacement (THR) is the surgical procedure to replace the damaged hip with the artificial one to relieve hip pain caused by hip disease. In hip problems the worn cartilage no longer serves as cushion and expose bone which cause roughness of bones. The ball wear out in the socket when the leg is moved causing pain and stiffness. The effected leg may weaken or shorten, and limp may develop. Total hip

replacement provide smooth working surfaces. The most important purpose of the THR is to release pain improve movability of patient and make the hip more reliable and stable [37].

The entire hip implant has three major parts: stem, ball and cup. The stem part fits in the femur whereas the ball substitutes the sphere-shaped head of femur and the cup, substitutes the damaged hip socket as shown in Figure 2-10. These parts are made up of metal, plastic, alloys or ceramic.

In hip implants the femoral stem, the part attached to the ball is usually made of titanium, cobalt/chromium-based alloys, stainless steel or a titanium and cobalt mix metal [38]. The femoral stems have in different design and shapes. Some stems having porous design for bone ingrowth. The bio materials used for stem part should be bio compatible and possess the same mechanical properties like bone for the replacement [39-42]. But market available stem materials do not have the exactly same properties as bone. Metals for example Co-Cr-Mo, steel, Ti-6Al-4V and have enough fracture toughness and strength, but having high stiffness, that's leads to the stress shielding.

Acetabular component (socket) is the semi cup shaped piece represents socket. This cup shaped piece is fit into human body resurfaced socket. This piece is typically made of polymer but is rarely made of ceramic or a combination of plastic and metal. Polymers like polyethylene and polymethylmethacrylate have sufficient fracture toughness, low stiffness but low in strength.

Femoral head (ball) directly fits into the new, plastic lined Socket (Acetabular cup) and is attached to the femoral stem. There are many designs, shapes and sizes of femoral heads. These are usually made of ceramic. Ceramics are very hard materials such as alumina and hydroxyapatite, having good compression but have low fracture resistance.

2.5 Hip Implant Replacement Methods

There ae two methods of hip replacement i.e. cemented and cementless. Cemented total hip arthroplasty involves filling the side of the bone with cement to fix it. It is the faster method of rehabilitation. Due to the variable fatigue loading this can cause cracks (fatigue fracture) in cement and with the passage of time cause loosening of stem and become unstable.

Cemented hip implant is more stable and reliable for the aged patients (over the age of 60years) who have less activities, resulting less stresses on the cement [43]. Callaghan, et al. [44] reported 90 % success of cemented hip implant for the patient of 25-year age. Out of 62 of hip procedures 14 revision surgeries were carried out, of which 03 cases were performed due to laxity caused by infection, and the remaining 3 cases were performed due to aseptic laxity. Willert, et al. [45] worked out a micro movement at the bone cement interface for a range of cement thicknesses.

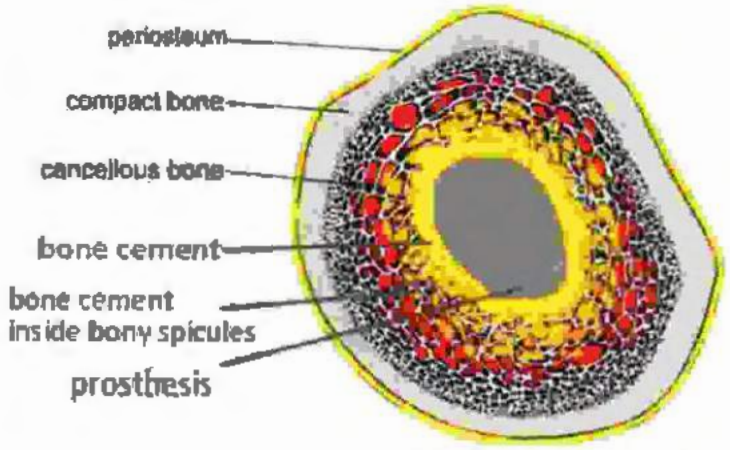

Figure 2-12: showing the bone structure and cemented area [46]

According to analysis, cement thickness affects the stress level and microscopic movement. The increase in cement thickness leads to an increase in proximal shear stress and an increase in microscopic motion at the interface. High slip leads to the production of cemented debris, that cause osteolysis.

The small cement debris which are separated due to the loosening and wear around the stem portion are absorbed in cells surrounding the joint resulting inflammation with pain. As the bone weaken the implant become unstable [47].

In cementless method no cement is used, and the implant is directly attached with the bone. In such implant there are pores for the ingrowth of bones. The stem part in the implant is more stiffer then the bone and takes major portion of the body weight load due to which the bone is not properly loaded and its natural phenomena when the bone is not loaded then with the passage of time the bone become weaker and is more bare to the fracture. this phenomena is called stress shielding [46] .

Cementless implant fixation procedure has extensively investigated to evade the loosening issues [48]. Different porous materials are used for coating or texturing of cementless implant to allow bone ingrowth. Healing time of cementless implants is around 2 to 4 months which is more than cemented implants because for stability cementless implants depend growth of new bone. In cementless implants the gap with bone should be less then 2mm for the ingrowth bones therefore, close contact between the implant stem and bone is crucial. Weak bonding between the stem and bone will result into the loosening. Many surgeons are currently using cementless hip implants for elderly and young patients, it is still recommended that young people (under 50) undergo cementless THR surgery with good bone quality and can ensure bone ingrowth of patients. The fit of the implant is very important for cementless implants. Fretting often causes malfunctions. Engh and Bobyn conducted a study of 307 cases of cementless THR after two years of surgery and 89 cases of cementless THR after five years [49]. The conclusion is that the tight fit of the femoral isthmus is very important for superior bone fixation. Observing that a good tight fit can reduce pain, they also proposed that if the stem is filled with medullary canals, the prognosis will be beneficial to bone growth. They report that stems with smaller diameters have almost no stress shielding in 88% of cases, and

stems with larger diameters cause more bone loss through stress shielding [49-50]. Hip implant needs lifelong, stable and pain free fixation to be used clinically. Cemented fixation of implants has provided less satisfactory results in active and younger patients [51-52] and it involves some chronic problems, such as the release of toxic monomers and heat necrosis [53-54]. Cementless hip prostheses are a better choice for osseointegration in the porous bone body that is tightly integrated between the diaphysis and bone, which is important for stability, survival, and resistance to osteolysis [55-57].

2.6 Hip implants Materials

The term "biomaterials" may have encountered different interpretations both in materials science and clinical medicine. Biomaterials field exists from Egyptian and romans era about 4000 years back in the form of Gold and iron for dental implants, however the stainless-steel nylon, titanium etc. put in to use after the world war II [1]. After the first conference on biomaterials held at Clemson University in South Carolina in 1969, the field of biomaterials received the recognition it deserves and has been receiving extensive attention ever since. Biomaterials are man-made or natural materials used to make structures or implants to replace lost or diseased biological structures to restore shape and function. Therefore, biological materials help to improve the quality of human life and longevity. The field of biomaterials has shown rapid growth to meet the needs of an aging population. Biomaterials are used in different parts of the human body, such as replacement implants in ears, elbows, shoulders, knees, hips, tooth structures, heart artificial valves and stents in blood vessels [3-5]. It is also used as a heart simulator and urinary tract reconstruction. Among all these, the number of implants used for hip ,spine and knee replacement is very large. Human joints suffer from degenerative diseases, such as arthritis, which cause pain or loss of function. Due to excessive load or lack of normal biological self-repair processes, degenerative diseases cause the mechanical properties of bones to decline. It is estimated that 90% of the population over the age of 40 suffer from such

degenerative diseases, and the elderly population has increased sharply in the past few years, and it is estimated that it will increase by 7 times.

In order to enhance the stability and durability of the implant, many materials are used and are in use. However, all materials used for hip implants should have biocompatibility, corrosion resistance, non-degradable, non-toxic, low wear, and have the highest manufacturing standards and quality control at a reasonable cost.

Hip Implants can be assessed according to the type of materials used. Research has been conducted on hard bearing surfaces with different combinations for total joint replacement. The clinical report of wear shows that the wear rate of metal on plastic, ceramic on plastic, metal on metal, ceramic on metal and ceramic on ceramic has the highest and lowest wear rate [58]. However, conventional metallic biomaterials such as stainless steel, Co–Cr based alloys, pure Ti, and Ti alloys have been widely used in the medical field for many years [6]. The issue related to these materials is its failure after long-term use due to many reasons, such as low corrosion and wear resistance, high modulus and lack of biocompatibility with the bone. So, the success of an implant requires the formation and maintenance of a functional interface between the physical environment and the implant [59].

Titanium is used extensively in human body like surgical instruments, attachment wire, dental implants, pacemakers, heart valves, intramedullary rods, bone plates, artificial joint prostheses and wheelchairs In the human body the implants operate in a very corrosive environment where body fluids are chlorinated salt water, with a pH in the range of 7.4 to acid, and also contain some other organic acids and ingredients to which titanium is totally immune [60]. Titanium is one of the major materials used in different industries. This element was originally discovered by Gregor in England in 1790, although it wasn't recognized well until Klaproth named it the first son Titans in the mythical earth in 1795. The atomic number of

titanium is 22 with atomic weight of 47.9. As a transition element in period 4 group IV of periodic table, titanium has an incompletely filled D shell in the electronic structure [61].

The titanium alloys are superior then its counterparts due to their good combination of mechanical properties to include excellent specific strength (σ/ρ), stiffness, fatigue resistance, low density, high corrosion resistance, good erosion resistance in the aggressive environments and excellent bio compatibility [62]. Among these properties, control of the elastic modulus has been extensively investigated because of the fact of higher elastic modulus of implant resulting in the stress shielding [63]. Stress shielding is caused by the difference of elastic modulus of implant and bones because of the distribution of inhomogeneous stresses which results in the implant loosening and refracture of bone. Therefore, metallic biomaterials with a similar modulus to that of bone i. e low modulus metallic biomaterials are required. Advancement in the material sciences made it possible to get the toxic free titanium alloys with the desired properties near to bone and to avoid hazardous effects in human body [34].

Some of the biomaterials made from titanium alloys reported recently are Ti–Mo–Al system alloys, Ti–Mo–Ge system, Ti–Mo–Ga system, Ti–Mo–Nb–Si system, Ti–Mo–Zr–Fe system, Ti–Sn–Nb–Ta system, Ti–Mo–Zr–Sn system Ti–Fe–Ta system, Ti–Nb–Ta–Zr system, Ti–Nb–Sn system, Ti–Nb–Zr system ,Ti–Nb–Hf system , Ti–Ta–Zr system , Ti-Nb system , Ti–Ta system ,Ti–Mo system ,Ti–Zr system[64-71] . Most of these alloys contain considerable amounts of Mo Sn, Ta , Zr and Nb.

2.6.1 Biomaterials Properties

Material properties and the process used to obtain the required properties during the manufacturing of the metal part are essential to ensure that the implant in use has the required performance.

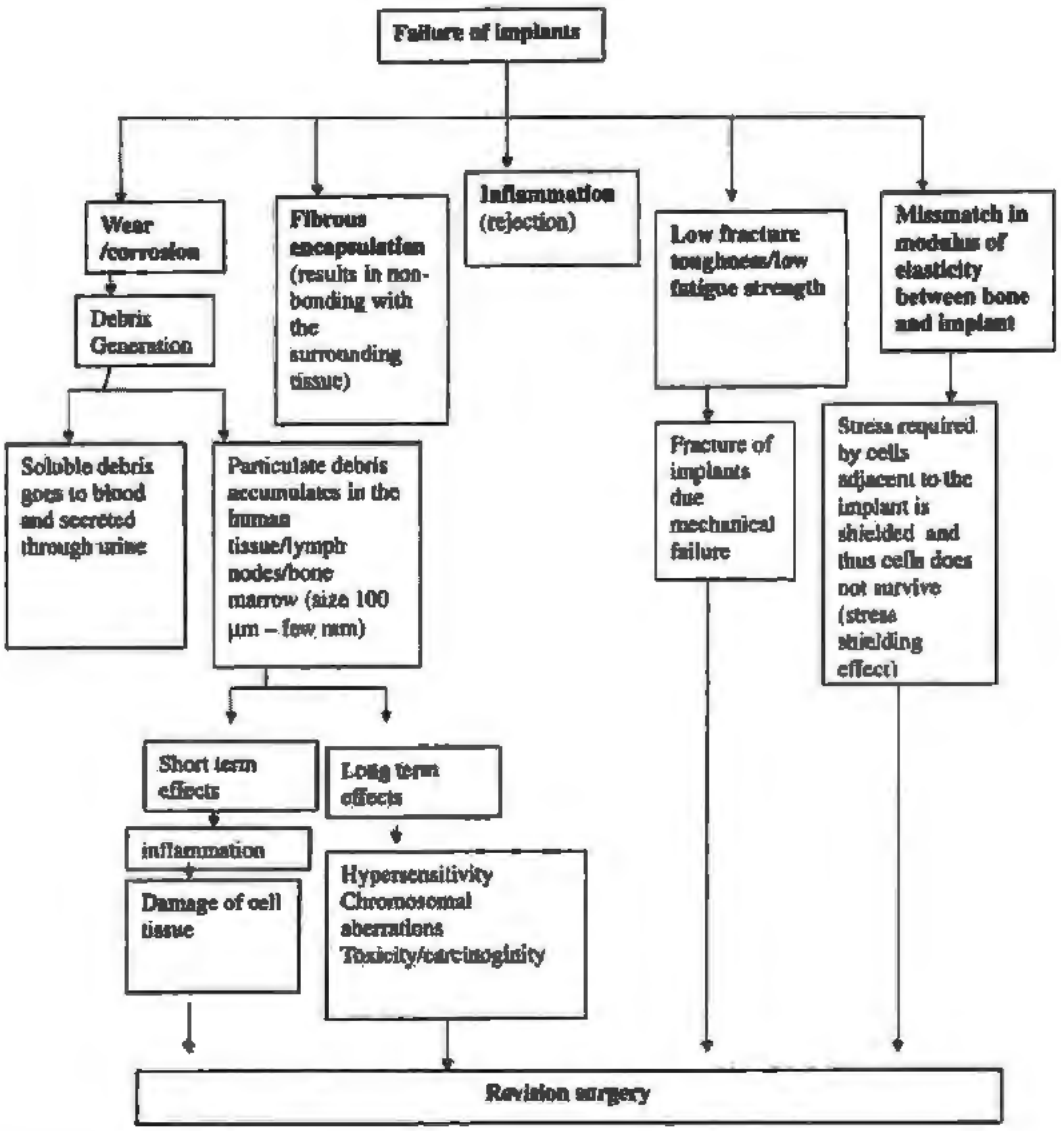

Figure 2-13 Various causes for failure of implants that leads to revision surgery [34].

Although mechanical failure is unacceptable for most engineered structures, this is especially true for surgical implants, as this type of surgery can cause patient pain and in some cases death (such as heart valve components Fracture) or require complex and life-threatening revision surgery [72]. The various reasons for revision surgery are shown in Figure 2-13 [34]. The most important properties are crystalline structure (BCC, FCC, HCP), biological biocompatibility, Mechanical biocompatibility i.e. hardness, tensile strength, reduced elastic

modulus, enhanced corrosion resistance, less wear and the fatigue strength (Material response to repeated cyclic loading or strain). The material fatigue strength is the determination of the prolonged life success of implant response to the cyclic loading [7, 73-76]. Ti alloys have good combination of all these properties like excellent stiffness, biocompatibility, corrosion resistance, low density, less wear and high fatigue strength that make it superior than other metallic biomaterials.

2.6.2 Microstructure

Titanium is a polymorphic metal as it has more than one type of crystal structure [1] . Ti is grouped into three groups i.e. Alpha (α), Alpha-Beta (α+β) and Beta (β) alloys [7, 62, 77, 78]. Some of the common elements used as a α, α+β and β stabilizers are FE, Mn, Al, Mo, V, Cr, H, O, Nb, Ni, N, Sn, Ta, C, Zr. Stabilizer like AL, Mo, V, Fe, Cr, Ni has some toxic effects, whereas the desired properties can be achieved by the stabilizer like Ta, Nb Zr etc. The α-stabilizers can increase the β-transus temperature, and the β-stabilizers can lower the temperature. Neutral elements have less effect on β-transus temperature. On other hand, β-stabilizers are classified into β-isomorphous and β-eutectoid elements. β-isomorphous increase the stability of β phase in all composition of the alloys, while the β-eutectoid cause eutectoid transformations of β phase, as shown in Figure: 2-14 [79].

The α-alloys are formed by single solid solution of α-phase. Temperature properties of α-alloys are high, but due to their intrinsic properties they don't permit microstructural modifications for the improvement of their properties by heat treatment [78]. α-alloys has the higher elastic modulus in comparison with the rest of two because of the crystal structure of α phase, which is the main component phase of α-type Ti alloys, is hexagonal closed packed. The β-phase improves the strength and workability of the alloys and the modulus of elasticity is lower than that of α and α+β alloys, with a body centered cubic crystal structure [62, 63]. The α+β alloys contain 4 to 16% of β-stabilizers. The most regularly used alloy in this category is

Ti-6Al-4V. Near-β alloys (also called metastable β-alloys), contain small amount of α-stabilizers and 10 to 15% of β-stabilizers [78]. These alloys can be optimized for high strength and toughness, upto the strength above 1400 MPa.

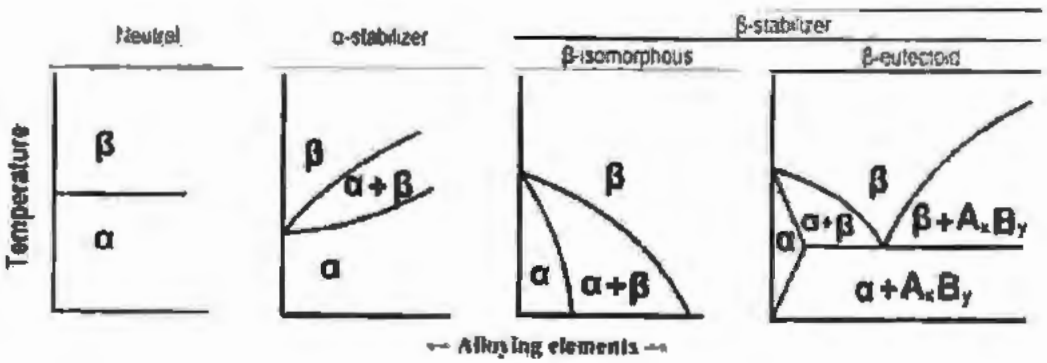

Figure: 2-14 Illustration of influence of alloying elements on the α and β fields [79].

Young's modulus of α and β-structure are about 100–120 GPa and 60–80 GPa respectively. . However, the β structure exhibits low strength. The strength along with ductility of the β phase can be increased by alloying or having the fine microstructures, Although the coarse structure is more resistant to fatigue crack growth and creep, the equiaxed microstructure usually has higher fatigue strength and ductility, and is an ideal choice for superplastic deformation, while the lamellar structure has higher fracture toughness, and it exhibits excellent resistance to fatigue crack growth and creep. The bimodal microstructure combines the advantages of equiaxed structures and lamellar structure to achieve a well-balanced characteristic curve [80].

2.6.3 Biological Biocompatibility

The implant biocompatibility is distinct by its metal sensitivity, toxicity and carcinogenicity from metal ions that have been released in the body. Biological biocompatibility need to be calculated to reduce implants failure and risk to patient's life. Metal ions released into human body due to abrasion and corrosion of the implant materials. This release of ions causes many pathophysiological effects [81]. For this reason, the effects of

alloys, metals and elements have been remained the field of interest for researchers. One of the major issues related with implants in human body is corrosion. Due to corrosion metal ions are released into body tissues and fluid that weakens the implant and cause harm to the body. Corrosion arises in two ways. One is physical erosion of implant by wearing as in case of artificial joints and the second cause by electrochemical corrosion.

A small number of elements like Fe, Mn, Mg, Zn are essential within a human body for normal biological functions. toxic reactions may be caused by excessive amounts of these elements. These implants release metals ions that may leads to mutations, local inflammation and sometime cancer as well. Table 2-1:Metal tolerance in human body towards different metal elements in implants [72].

Table 2-1:Metal tolerance in human body [1].

Metal	Normal Amount	Comments
Fe	4-5g in whole body	Element of red blood cells. One of the least toxic trace elements
Co	Related to B_{12} amount	Element of vitamin B_{12} No biological function of free Co. May pure Co is toxic to bone tissue. Co-Cr alloys are not toxic. High dose may be carcinogenic.
Cr	2.8 µl/ 100g in blood	Toxic and affecting cell viability and diminishing DNA synthesis. Hexavalent Cr is carcinogenic.
Mn	12-20 mg in whole body	Essential elements in cells. One of the least toxic trace elements.
Mo	1-3 ppm in liver	Necessary to certain enzymes to function, toxic in high dose. Also, possible interfere with metabolism of Cu and P.
Ni	5 mg/L in blood	Essential element for limited biological activities. High dose is toxic and may be carcinogenic.
Ag	No lined in the body	No inert in the body. Strong inhibitory and bactericidal effects.
Ti	0.8 mg/day	No normal function, but not carcinogenic.
Al	0.12 mg/day	Having adverse effects. Causing deficiencies in bone calcification and neutral disorder
V	0.002 mg/day	Toxic

The cytotoxicity of typical surgical implant alloys and pure metals indicates that vanadium is classified as a sterile abscess (toxic) group and aluminum is classified as a capsule (soar tissue) group. Nickel is also known as a sensitizing and carcinogenic element, and shows one of the highest sensitivity in metal allergen tests [82, 83]. The alloys which contains aluminum, vanadium and nickel having a toxic on the respiratory, circulatory, central nervous systems, the digestive organs, kidneys, allergic and immunologic effect, renal effect and carcinogenesis[9, 10]. Majority of implants available in the market and also shown in Table 2-2 contain; vanadium, aluminum and nickel. Therefore, the researcher worked hard for the

development of Al, V and Ni free β titanium alloys such Ti-29Nb-13Ta-.6Zr(TNTZ), Ti-1Mo-6Zr-2Fe, Ti-35Nb-5Ta-7Zr(TNTZ), Ti25Ta and Ti-29Nb .

2.6.4 Mechanical Properties

The human bones are subjected to different types of forces in different directions. These loads may be due to external forces, forces applied by muscle, weight of body and by the gravity. The loads are acting on body in multi directions causing forces may different from five types: , torsion, shear, tension, compression or curvature [84]. The Bio implant material replaced for bone failure is expected to fulfill all the criteria for the subjected loadings in the bones. The biomaterials should have sufficient tensile and compressive strength and modulus equal or near to that of bone. The measured values of the compressive strength and tensile strength of bones are quite different in different cases. Different bones in the human body need to withstand different forces, so the strength between different bones is very different. In addition, age is an important factor, and strength usually decreases with age. The tensile strength reported in longitudinal direction is 60-70 (MPa) and in transverse direction is ~ 50(MPa) and for compressive strength of 70-280 (MPa) in longitudinal direction and ~50 (MPa) in transverse direction [85]. Human bones elastic modulus having the variation from 4 to 30 GPa depending on direction of measurement and types of the bones [64, 75]. Current implant materials are required to be having modulus of elasticity near to bone otherwise in case of higher stiffness than bone resulting in bone resorption around the implant and thus leads to the implant loosening causing the death of bone and is known as "stress shielding effect"[6]. The tensile strength of the biomaterial shown in Table 2-2 is in accordance/ higher than the tensile strength of the bone whereas the young's modulus of the biomaterials is on the higher side. The tensile strength of titanium alloys usually varies from 240 MPa to 1400 MPa with young modulus of 103 GPa for pure titanium, and for the commonly used Ti-6Al-4V, its value varies between 900 and 1200 MPa and young's modulus of about 110 GPa [79]. The Young's

modulus change with β_phase stability. The least stable single β_phase alloys show minimum values in Young's modulus in the β_type alloys [86].

Table 2-2: Mechanical Properties of Titanium Alloys for biomedical applications [76, 87-94]

Alloy	Type of Alloy	Yield Strength σ_y	Tensile strength (UTS) (MPa)	Yield Strength σ_y	Elongation (%)	Modulus (GPa)	RA(%)
1. Pure Ti grade 1	α	170	240	170	24	102.7	30
2. Pure Ti grade 2	α	275	345	275	20	102.7	30
3. Pure Ti grade 3	α	380	450	380	18	103.4	30
4. Pure Ti grade 4	α	485	550	485	15	104.1	25
5. Ti-6Al-4v ELI (mill Annealed)	α+β	795-875	860-965	795-875	10-15	101-110	25-47
6. Ti-6Al-4v annealed	α+β	825-869	895-930	825-869	6-10	110-114	20-25
7. Ti-6Al-7Nb	α+β	880-950	900-1050	880-950	8.1-15	114	25-45
8. Ti-5Al-2.5Fe	α+β	895	1020	895	15	112	35
9. Ti-5Al-1.5B	α+β	820-930	925-1080	820-930	15-17	110	36-45
10. Ti-15Sn-4Nb-2Ta-0.2Pd (Annealed)		790	860	790	21	89	64
(Aged)		1020	1109	1020	10	103	39
11. Ti-15Zr-4Nb-4Ta-0.2Pd (Annealed)	α+β	693	715	693	28	94	67
(Aged)		806	919	806	18	99	72
12. Ti-13Nb-13Zr (Aged)	β	836-908	973-1037	836-908	10-16	79-84	27-53
13. Ti-12Mo-6Zr-2Fe) (Annealed)	β	100-1060	1060-1100	100-1060	18-22	74-85	64-73
14. Ti-15Mo (Annealed)	β	544	874	544	21	78	82
15. Tiadyne 1610 (Aged)	β	736	851	736	10	81	
16. Ti-15Mo-5Zr-3Al9 (ST)		838	852	838	25		48
(Aged)	β	1000-1060	1060-1100	1000-1060	18-22	80	64-73
17. 21RX (annealed) (Ti-15Mo-2.8Nb-0.2Si)	β	945-987	979-999	945-987	16-18	83	60
18. Ti-35.3Nb-5.1Ta-7.1Zr	β	547.1	596.7	547.1	19	55	68

19. Ti-2Nb-13Ta-4.6Zr (Aged)	β	864	911	864	13.2	80
20. Ti-25Ta	β	480	595	480	20	64
21. Ti-27Nb	β		740			60

Some representative low modulus titanium alloys used in biomedical are Ti–40Ta, Ti–50Ta Ti–Mo–Sn, Ti–25Ta, Ti–29Nb–13Ta–4.6Zr (TNTZ), Ti–35Nb–7Zr–5Ta (TNZT), Ti–15Mo–2.8Nb–0.2Si–0.26O, Ti–16Nb–10Hf, Ti–15Mo (ASTM F2066), Ti–12Mo–6Zr–2Fe (ASTM F1813-97), Ti–13Nb–13Zr (ASTM F1713-96), and Ti-27Nb with tensile strength of 600 MPa to 1100 MPa and modulus of elasticity 55-85 GPa. Some authors believe that the use of appropriate heat treatment and the addition of biocompatible alloying elements (such as Ta,Zr and Nb) to titanium are the basis for gaining titanium alloys with best suitable mechanical properties (ie, low elastic modulus) [74, 95] . Figure 2-15 also lists some titanium alloys for biomedical applications.

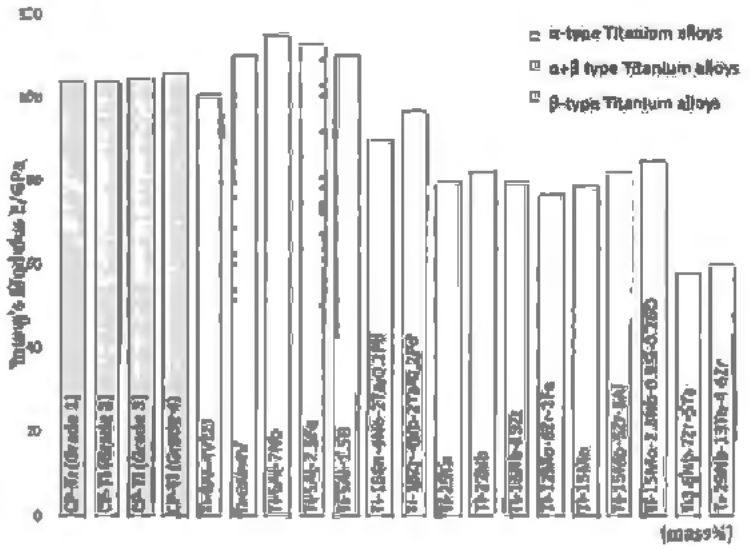

Figure 2-15: Young's moduli of representative α-type, (α + β)-type and β-type titanium alloys [96].

2.6.5 Fatigue and Fracture strength

In addition to obtaining sufficiently high yield strength to prevent unacceptable shape changes during functional loading, the implant must also be prevented from complete facture. During human movement, cyclical loads are applied to the orthopedic implants, resulting in

alternating plastic deformation of small microscopic areas where the stress is concentrated due to notches or uneven microstructures. Therefore, the fatigue resistance is a critical property for the longevity of implants in service [72]. This may happen with relatively low number of cycles (≤104 cycles) (high repeated strains lead to low cycle fatigue) or millions of cycles (low cyclic strain leads to high cycle fatigue). The fatigue strength and yield strength of materials are dependent on the microstructure control, composition of alloy and previous history of material thermo-mechanical processing. Although increase in yield strength and decrease in ductility due to strain hardening leads to the initiation of fatigue crack [97]. Fatigue strength is greatly affected by surface treatment, finishing and processing. Therefore, alloy displays series of significant mechanical properties, which is controlled by appropriate heat treatment and processing. The careful selection of material processing procedures is the important parameter for the achievement of optimal static and dynamic (fatigue) properties of metallic implants. Fatigue strength of biomedical titanium alloy at 107 cycles are shown in Figure 2-16 showing the fatigue strength of different biomaterial titanium alloys at 10^7 cycles and other used metallic biomedical materials alloys such as Co type alloys; Co–Ni–Cr–Mo and Co–Cr–Mo stainless steels; SUS 316L and AISI 316 LVM. Figure 2-17 showing the fracture toughness of titanium biomaterials alloys. Some of the β type titanium alloys listed in Figure 2-17 has almost same fracture toughness that of α and α+β alloys but they don't contain toxic or hazardous elements like Al, V and Ni.

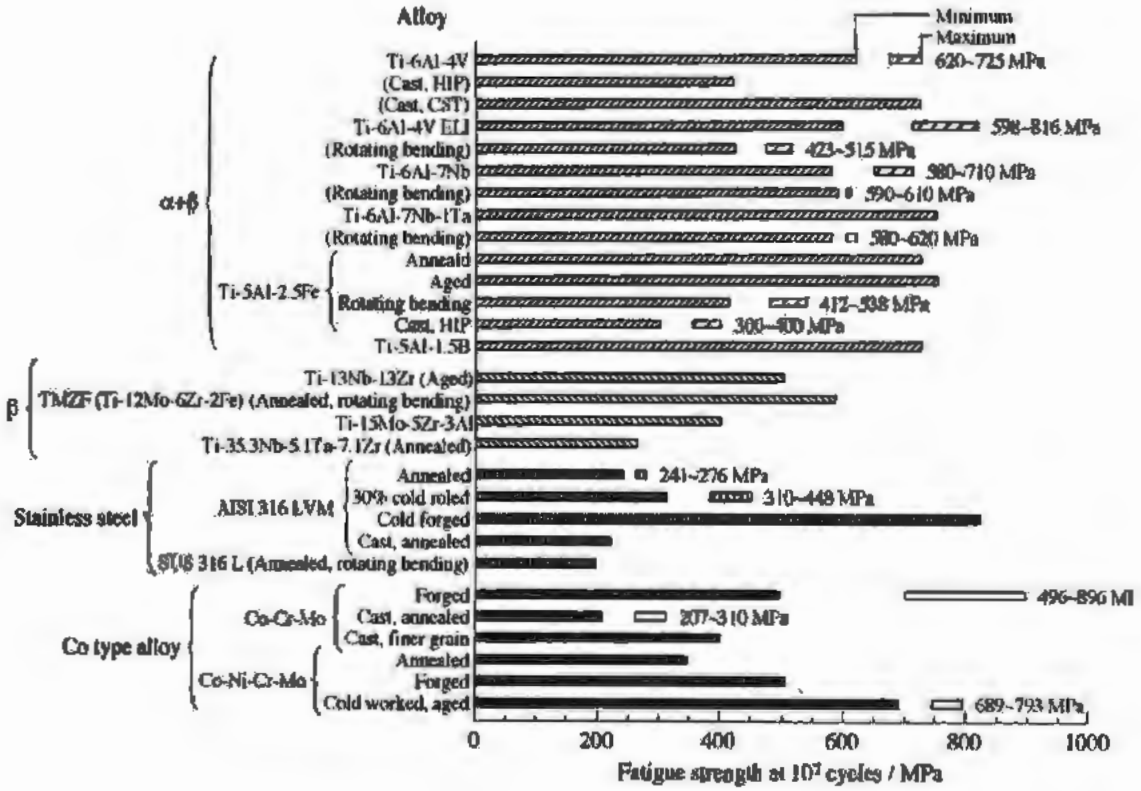

Figure 2-16: fatigue strength at 10^7 cycles of biomedical titanium alloy. Data without designation of rotating bending are those obtained from uniaxial fatigue tests [98].

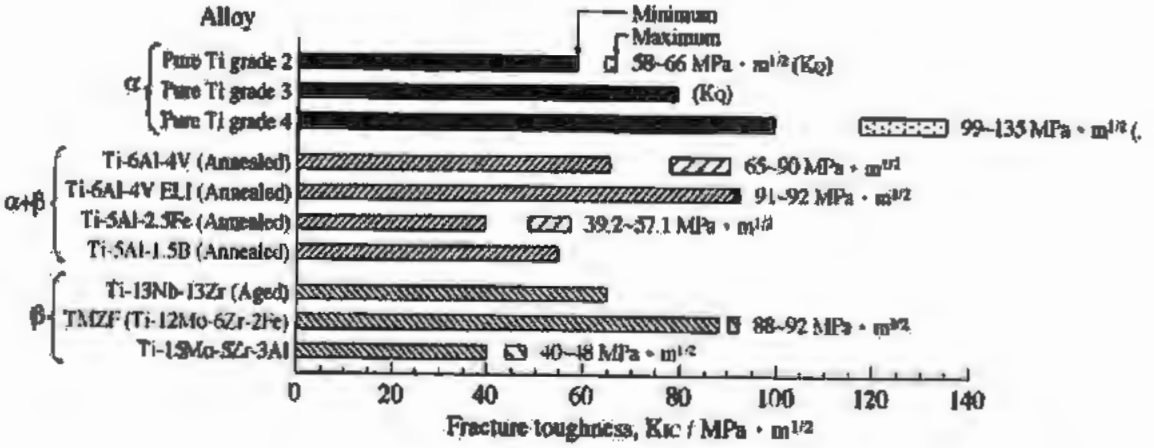

Figure 2-17: Fracture toughness of biomedical titanium alloy. KQ means invalid fracture toughness [98].

2.6.6 Wear and Corrosion Resistance

Corrosion of bio implants is the gradual degradation of materials by electrochemical attack in the electrolytic environment of the human body. A bio implant should have very high corrosion and wear resistance in highly corrosive body environment (blood and other constituents of the body fluid [99]. The corrosion in the implants that occur are uniform, galvanic, pitting, stress corrosion cracking, intergranular corrosion and fretting (rupture of protective oxide layer) and fatigue corrosion [100]. After the fixation the implant success depends on the interaction of living tissues and implant materials. Surface oxide layers (coating) protect most of the materials from the environmental effect. These oxide films protect the material from corrosion and help in tissue compatibility [101]. The effect of the environment on the surface oxide layer is highly reliant on the composition of base material. The titanium alloys implants damaged mainly due to fatigue [102]. The reason for this is the synergistic effect i.e. the formation of surface corrosion pits caused by dissolution of Ti^{2+} ions in human body [103, 104]. The concern for titanium and titanium alloys are due to the known toxicity linked with alloying elements and the known morbidity of particles emitted because of the decomposition of the oxide layer linked with the degradation of metal implants. For example, the case of the commonly used bio-implant material Ti-6Al-4V alloy, the vanadium oxide in the passivation film dissolve and causes the generation and diffusion of openings in the oxide layer [105]. However, the addition of Nb as an alloying elements will enhance the passivation effect by forming Nb-rich pentoxide dioxide, which is extremely stable in the human body environment, results high resistance to the corrosion [106]. Ti-Ta alloys also revealed that the release of metal particles from the surface oxide layer can be decreased by the addition of Ta. This phenomenon occur because of the formation Ta_2O_5 oxides layer which are highly stable [107]. In low modulus titanium alloys the alloying elements are usually Ta and

Nb. Therefore, the corrosion resistance of the passivation film is dependent on the layer thickness formed and the properties of alloying elements in titanium and its alloys.

2.7 Finite Element Analysis

Effect of hip implant loading i.e. gait forces and body loading are under consideration from long time. For this purpose, a research method i.e. Finite Element Analysis (FEA) is in use for the calculation of these loading effects. Mechanical testing is expensive in comparison with the FEA . Alternately, FEA is faster and can provide contour plots of stresses in the whole structure. Finite Element Analysis is particularly advantageous in the preclinical analysis of implants and other biomechanical structures. Due to the high level of subject variability, ethical constraints and cost, the scope of mechanical testing in vivo or in vitro is limited. Through finite element analysis, the comparative performance of different prosthesis materials and designs can be studied, and the full effect of surgery and post-operative patient variability considering different variables e.g weight and daily routine activities effect can be predicted. Extensive research has so far been conducted in the quest to achieve a more perfect and accurate hip implant designs and materials.

Finite Element Analysis is also used to find out wear, contact analysis and fatigue life evaluation of implants by using different engineering software like, ANSYS, ADINA and ABAQUS, etc.

One of the most critical steps in the FE analysis is the accurate application of forces on the implant. Several experimental studies have reported their force measurements that can be utilized in the FE analysis. In one such study,Bergmann et.al measured the forces on an instrumented hip implant for different daily activities [108-113] . Reports of the results shows that the stresses applied on the bone and implants were influenced by direction and magnitude of forces as well as by the weight of the patient and the type of activity. The study also reported force increase of about 870% of body weight for some activities. In another similar study,

Stansfield and Nicol [114]. In this research the forces on hip joints were calculated by using three-dimensional leg model in different modes of walking i.e. slow walking, normal and fast speed walking (0.97 to 2.01 m/s). In addition to these experimental works several models have also been proposed to estimates forces on the implants. Hurwitz, et al. [115]. This model was used for the measurement of forces variation in muscles and their net effect on the hip forces. Similarly, MavČiČ, et al. [116] The model has also the capability to analyze the biomechanical and radiographic parameters of an adult hip joint in a one-legged standing posture. Early failures of the contemporary hip implants is not rare. An investigation on the failure of cemented hip implant showed a higher failure rate within two years of surgical procedure [117]. The FE analysis can be an extremely useful tool for the design development and improvement of contemporary hip implants. Huiskes and Res find out the relationship between bone desorption and stress shielding around hip stem by using finite element model [118]. This relationship shows important fluctuations in bone morphology. This research recognized that the use of flexible stem can reduce stress shielding while it can enhance proximal interface stresses, that's leads to increase rate of loosening because of the interface micro motion and debonding. Turner, et al. developed 3D nonlinear finite element model in ABAQUS to study the dislocation or loosening of cemented hip implant [119] A convex curved shape acetabular lip was designed to decrease the tendency for dislocation. This new design increases the resistance torque during dislocation by 28% [120]. Gross and Abel performed the finite element analysis of hollow stem hip implant for the reduction of stress shielding in the femur [121]. A 2D finite element model was developed, consisting of plastic layer, graft, cement and bone using plain strain elements. The graft layer was taken as an elasto-plastic material while the plastic bone and cement are taken as linear elastic materials [122]. As a part of the design innovation efforts a robust total hip implant was designed under the effect of ecological variables viz., cancellous bone elastic modulus, joint force angle and implant bone interface

friction [123, 124]. Finite element analysis was carried out by Senapati and Pal on the 3-dimensional (Axi-symmetric) model and concluded that more flexible stem cause more proximal load transfer [125].

Several researchers used composites materials for the implant design to get the required properties. They developed numerical optimization technique for the designing of fiber reinforced composite implant. The two design objectives i.e. stress shielding based and failure based were used to design carbon fiber reinforced composite implant for lowering the stress shielding and potential for bone remodeling [126-129]. A new design of hip implant was proposed by Shirandami and Esat made of Composite material i.e polyethylene-hydroxapatite for good bone compatibility and stiffness [130]. Weisse, et al. optimized the proof tests procedure for hip joint ball heads to eliminate defective samples in the manufacturing process prior to implantation in to the human body [131].

Finite element modeling was reviewed in the areas of analysis and design of orthopedic devices, analysis of skeleton and analysis of tissue growth by Prendergast [132]. A prototype of femoral prosthesis was designed and fabricated from controlled stiffness composites having a core made up of cobalt-core surrounded by layers of flexible composites. The purpose of this new design was to compare the performance of multi modulus prosthesis with that of prosthesis made up of single modulus material [133-134].

For maximization of fatigue life of the cemented hip implant, a method was developed by Hedia, et al. to optimize the shape of cemented hip implant [135]. For anatomic custom design implants a new methodology for its design and manufacturing was developed.

Testing method for hip implant was developed by Tanner, et al. [136]. The implant is placed in the proximal part of the femur and force is applied through the greater trochanter through the acetabulum. A study on the mechanism and appearance of 172 retrieved femoral

stem was carried out.. In this study 74 out of 172 were found stable in vivo. After examining the rest of pieces at nano, macro and micro level it was concluded that 93% of the stem wear was due to micro motion in the stem portion because of stem design [137]. Scannell and Prendergast [138] did the FEA study on the changes in the bones around the hip implant and proposed a technique for the implants to be pre-clinical tested by computational methods. Li, et al. and Zhou, et al. established a femur model utilizing different models of material degradation and failure criteria to study numerically the femoral components failure by using FEM [139-141]. In another study a hip implant having hallow stem was analyzed by using FEM. The hollow stem was used to reduce the stress shielding effect in the femur while keeping the required low level of stress in the cement [121]. Peters, et al. studied the relation between different hip implant design and its corresponding strains in the cement by using FEM analysis and concluded that maximum stresses in the cemented prosthesis occur on the distal ends [142].

Comparative study of finite element analysis was carried out for the debonding of stem cement interface and damage accumulation in the cement mantle concluding that the debonding process is different for each stem depending on the design of the stem [143] . Joshi, et al. in their analytical study on existing femoral prosthesis design concluded that through the new design reduction in stress shielding can be reduced [144]. Comparative study for proper stress distribution in different stem design was carried out through FEM analysis for finding the fluctuation area for the evaluation of fixation. From the study it is concluded that there is variation in the area or place of stress distribution in different designs [145]. Thermo mechanical finite element analysis model was developed for the simulation of wear test to estimate transient contact stresses and for the prediction of temperature increase due to friction in the implant components. The analysis helped in understanding the behavior of acetabular cup material and the temperature influence on wear forces and interfaces [146]. Baleani, et al. predicted maximum stresses reported in the hip implant stem by the ISO experimental test

setup [147]. These stresses were calculated using finite element analysis and beam element theory. For the assessments of the accuracy of theoretical calculations, strain measurements were utilized. Fatigue tests were also carried out for the evaluation and prediction of stem performance. For minimizing the stress concentration in the cement layer around the metal stem of hip prosthesis the finite element analysis and gradient projection method were used for optimization of stem shape [148].

Four designs of cemented hip prosthesis were selected for FEA investigation of cancellous bone stresses for the determination either they can be used for the prediction of migration of different version of prosthesis [149]. Research is done on the CT scan images attained after surgery for the development of finite element model of human femur. The results revealed that the CT scan images provide accurate information and the effect anticraft are almost zero at 2mm distance from the hip implant [150]. Prendergast and Taylor used FEA to identify that due to the stress shielding i.e stress induced bone loss in the femur is the main cause of loosening in the hip implant [151]. McNamara, et al. also inspected the bonding between prosthesis and bone on proximal load transfer using FEA on femur [152]. Prendergast, et al. investigated the effect of young's modulus of cement layer and stem material on the stresses in the prosthesis and proposed the criteria for the selection of material on the fatigue strength [153].

For fatigue analysis, femoral components are investigated in combination of computational and experimental methods for finding out the fatigue crack propagation from stem -cement interface using torsional loading model [154]. Fatigue damage phenomena in bone -cement bonding subjected to shear stress is determined [155]. By applying von-Mises stress train theory a general damage model was established to find out creep fatigue response for the bone-cement bonding under different types of loading. Qausi 3-dimensional finite element model for the damage evaluation, fatigue analysis and sensitivity analysis of total hip

implant showed moderate sensitivity to the stem young modulus and significantly sensitive to young's modulus of cement and friction coefficient of stem cement [156, 157]. Raimondi and Pietrabissa in their study on in-vivo hip implant stem for investigation of fatigue recommends the use of standard testing specification of ISO 7206 for getting more accurate result as compared to that of existing typical fatigue test on hip implant stem [158]. Cemented hip prothesis was also studied by Hung, et al. by using finite element analysis methods for the investigation of fatigue behavior [159]. Ortega, et al. carried out the failure analysis of a fractured hip implant stem [160]. From fractography and numerical results its concluded that failure was due to the weakening of bone due to stress shielding and design parameters of implant, causing stress concentration in the localized area.

Material properties are one of the most important considered for FE simulation. The approximation of actual physics is quite complicated due to the assignment of material properties to natural tissues and bones. Similarly, the process become more complicated by considering the conditions at interface between the implant and bone. Accordingly researchers have proposed several simplifications to the model material properties [123].

For model meshing, there are no predetermined standards for selecting the appropriate element size and type and the user can define their own appropriate size and type of mesh in the finite element method. Therefore, compared with a finer mesh, the use of a coarser mesh can reduce the running time of the simulation and the accuracy of the results. Tetrahedral element types are usually used for high-quality meshes due to their specific shapes. This is also a simple and straightforward way to automatically generate them in FEA software.

Stolk, et al. evaluated the mesh density effect on THR model. They compare the bonded and non contact/debonded implants. Through comparative studies, they showed that de-bonded implants are more sensitive to the density of mesh as compared to the bonded. They also found that there may be uncertainty and inaccuracy in the result due to sudden changes in the mesh

size [161]. Ramos and Simoes studied common element types in femoral geometry and compared their results. Convergence tests were carried out using hexahedron (bricks with 8 nodes and 20 nodes) and tetrahedron (tetrahedron with 4 nodes and 10 nodes), and the von-Mises stress and principal strain at specified points of the femur were compared [162]. Comparison of von-Mises stress distribution with the theoretical one reveals that results obtained from tetrahedral element used for femur model meshing is closer to the theoretical value. However, it is found that the hexahedral element is relatively more stable and is less affected by the refined mesh size.

The sides of the bone and implant interface are not always connected to each other. Because, in order to transfer the load across two interfaces, another type of element is needed. Therefore, the use of cementless implants is very important, because the key issue is the development of fibrous interface between implant and bone. The loosening of implant may not only be caused by the wear particles in the osteolytic bone, but also may be caused by the formation of fibrous tissue. Aspenberg and Herbertsson proposed that the formation of fibrous tissue is the key issue [163]. As for modelling of interfacing between bone & implant different approaches are being used. Several researchers have used specific material properties and a chain of bone graft contact pair parameters. Some researchers worked on the implant integrity by applying loads, while others try to formulate rules to simulate the dynamic behavior of the tissue surrounding the implant. The finite element software provides various parameters to define the nonlinear behavior of the contact surface between two objects, which depends on the material of the part and another parameter, such as the type of contact element. Where contact elements can either be surface-to-surface, node-to-node and node-to-surface. For large interfaces in hip replacements (such as bone implant interfaces), the surface-to-surface or node-to-surface accuracy is higher. Bernakiewicz and Viceconti studied sensitivity of results retrieved from finite element for various parameters like convergence tolerance and contact

stiffness and concluded that in accuracy of results, subject parameters play an important role [164].

For the simulation of hip replacement, the load is applied to the center of the femoral head. Different scenarios are being taken into consideration while applying load on implant. Such as fast walking, normal walking , stairs up , stair down, sit down, stand up etc . Bergmann et al. in 2001 measured the parameters for boundary conditions of aforementioned different cases. Duda, et al. studied the behavior of thigh muscle strength, body weight, and hip and knee contact force in finite element analysis. Compared with the case where muscle action is not considered, their internal load is reduced by 50% under most possible load conditions [165]. Cristofolini, et al. verified similar results.. He experimented with a custom nylon band clamp on the surface of the femur to simulate muscle strength and hip contact [166]. Stolk, et al. pointed out that the abductors have the greatest impact on all muscles in the femur. The constrained rigid body motion is very important and has a direct impact on the results of any finite element analysis. The common standard is to limit at least 6 degrees of freedom (DOF) at the middle backbone node or to limit the node at the distal con [167].

In the post-processing performance indicators, one of the key parameters is stress distribution and strain. Compared with non-biological materials, the modeling of biological materials such as bones is much more complicated. Because it adapts to external conditions and shows uniform strain under load [119].

3 Materials and Methods

3.1 Introduction:

In this chapter, the research framework is described and presented. The experiments performed to fulfill the scope of the research are identified. Metallurgical studies chemical analysis, simulated body fluid preparation and mechanical tests are adequately elaborated in this chapter. The following section discuss research framework.

Figure 3-1 showing the schematic for research framework for Ti-27Nb and Ti-25Ta as received samples for normal and simulated body treated material for 504 hrs and 816 hrs. This research includes the three major portions i.e. 1) Experimental, 2) Analytical and 3) finite element simulation. The first part includes the Tensile testing, fractur toughness, fatigue crack growth, hardness, microstructure evaluation and fractography on the simulated body treated samples and untreated samples. The mechanical testing is carried out using Instron machine. The fatigue crack growth propagation test is carried out at 4 Hz and at R=0.1 in high cycle fatigue region to study the effect of simulated body fluid on the fatigue crack growth propagation. The fractography of tensile and crack propagated samples are carried out for any transition or change in microstructure of the treated samples. X-diffraction tests and spectroscopic ellipsometry of the treated and untreated sample are carried out to study any corrosion effect on treated samples. The fatigue and tensile properties for treated and untreated material were used for the finite element analysis of hip implant using ANSYS software. Static and dynamic analysis of hip implant were carried out for different daily routine activates incorporating the treated and untreated material properties.

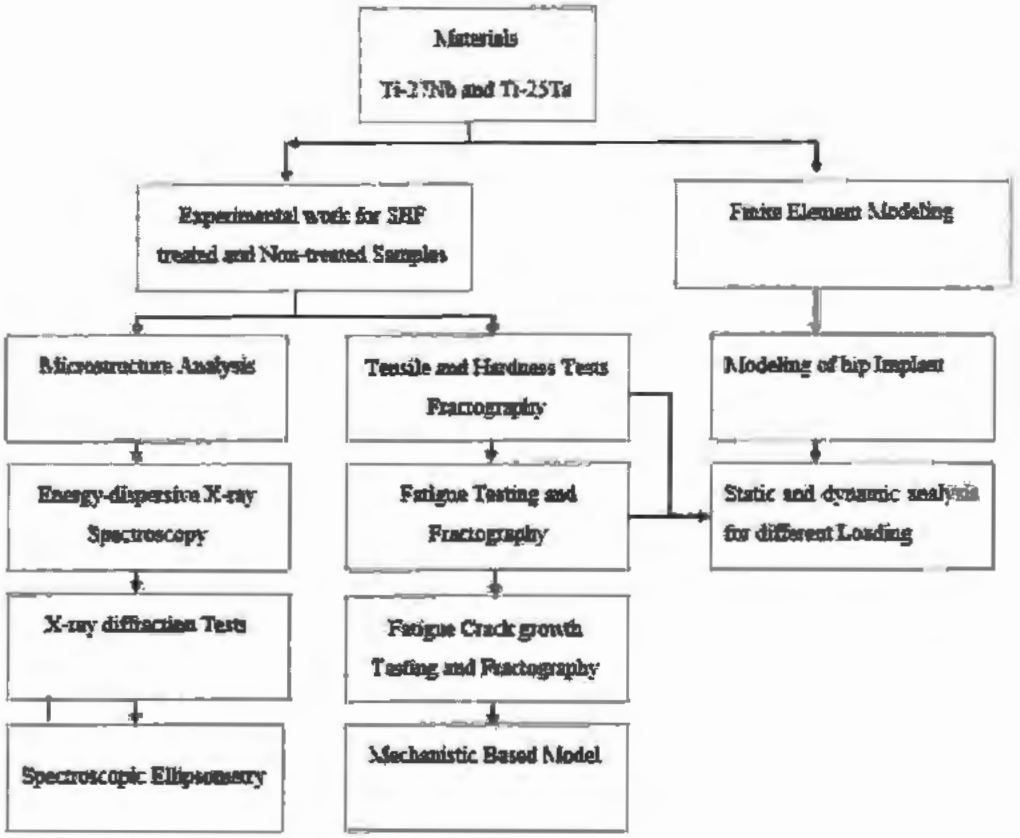

Pigure 3-1: Schematic of research framework

The following subsections sections describe the material, chemical composition, specimen preparation and the test procedures for corresponding tests programs.

3.2 Material

Titanium-27% Niobium (Ti-27Nb) and Titanium-25% tantalum (Ti-25Ta) bio materials are employed in this research study. The selection of these bio materials are on the basis whether the alloys are carcinogenic (cancer causing), genotoxicity (DNA damaging), mutagenic (mutation causing), cytotoxicity (cell destructing/ killing), allergenic and whether it can resist corrosion. Titanium is 3D transition metal, niobium is 4d transition element and tantalum is 5d transition element. As 3D transition metals are approved for implantation in

human body but except titanium all other metal in this group exhibit some degree of negative biological impact. Whereas 4D transition metal are not widely used for implants. the niobium and zirconium of this 4d transition group are extremely biocompatible in vivo having low ionic cytroxicity in vitro, no mutagenicity recorded and having good resistance to the corrosion. Tantalum is 5D transition metal and exhibit excellent corrosion resistance, low cytotoxicity and good osteo compatibility.

Table 3-1: Showing the concern of the titanium niobium and tantalum biological impact [82].

Periodic position	Element	Biocompatible	Cytotoxic	Prone to Corrosion	Mutagenic	Genotoxic	Carcinogenic	Allergic	others
3d	Ti	Yes	Med	No	No	No	No	No	No
4d	Nb	Yes	Low	No	No	No	No	No	No
5d	Ta	Yes	Low	No	No	No	No	No	No

All these parameters for the titanium niobium and tantalum show the good biological impact that's why the titanium-niobium and titanium-tantalum alloys are used for orthopedic implantation.

3.2.1 Chemical Composition

Ti-27Nb and TI-25Ta were purchased from Shaanxi Baoji Pelifly Titanium Industry Co., Ltd china in the form of 300mm x 300mm x 3mm sheet. Ti-27Nb alloy is made up of Titanium (Ti) with 26.01 ± 1.05 wt. % of Niobium (Nb). Minor alloying elements include iron (Fe), oxygen (O), carbon (C), hydrogen (H) and nitrogen (N) as impurities. The relevant amount of constituent alloying elements for base metal are shown in Table 3-2.

Table 3-2: Nominal composition of Ti-27Nb biomaterial (wt.%)

Element	Base Metal (wt. %)
Fe	0.21
C	0.03
N	0.025
H	0.008
O	0.21

Ti-25Ta alloy has also two main constituent elements titanium (Ti) and Tantalum (Ta) 24.8 ± 1.05 wt. %. minor alloying elements include iron (Fe), carbon (C), nitrogen (N), hydrogen (H) and oxygen (O) as impurities. The relevant amount of constituent alloying elements for base metal are shown in Table 3-3

Table 3-3:Nominal composition of Ti-25Ta biomaterial (wt.%)

Element	Base Metal (wt. %)
Fe	0.18
C	0.03
N	0.02
H	0.010
O	0.19

Figure 3-2 also shows the Energy Dispersive Spectroscopy (EDS) analysis pattern of received samples of Ti-27Nb at the fracture surface area, indicating the existence of Ti and Nb in the sample within the required range.

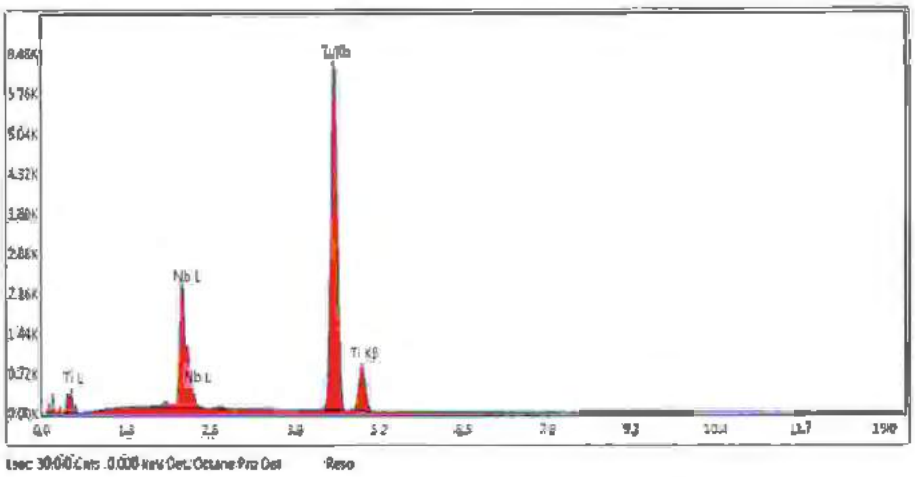

Figure 3-2: EDS results of Ti-27Nb alloy.

3.2.2 Microstructure analysis

For the microstructural evaluation of the material, optical microscope was used at magnification range of 100X-500X. The specimens were prepared using silicon carbide abrasive paper ranging 100-1200 grit size. After grinding the specimen, nylon cloth with addition of diamond paste was used to mirror polish the specimen from 15-1 microns. Finally etching was done using 75cc HNO_3 and 25cc H_2O to study of microstructural properties of the specimen. The specimens were studied using Olympus BX60 optical microscope Figure 3-2, for the resulting microstructure of Ti-27Nb Figure 3-3. Photomicrographs at different positions and magnifications were taken. Detail discussion on microstructure of Ti-27Nb alloy in as-received condition and surfaces of fractured specimen were analyzed with the help of Scanning Electron Microscope (SEM) to observe the morphology of fatigue crack growth surfaces of an ambient and SBF treated specimen. Analysis results are presented in chapter 4.

Figure 3-3:Olympus BX60 optical microscope

3.2.3 Experimental Procedures

As mentioned earlier the material was received in the form of flat plate. First task is the cutting of plate for the sample preparation in the desired dimensions. EDM wire-cut machine is used for the sample preparation to minimize the effect of heat on material during cutting process. Samples for the tensile, fatigue and fatigue crack growth (FCG), and fracture toughness are produced as per required dimensions using EDM wire-cut machine.

3.3 Simulated Body Fluid (SBF)

Simulated body fluid is used for in vitro study as from the literature study it is apparent that apatite layer formed on the biomaterials surface bond to living bone and having the same properties that are produced on the biomaterial surface in the living body i.e. in vivo study. By using this method, the in vivo experiments can be remarkably reduced. Table 3-4 shows the powder regents grade chemical used for the preparation 1000 ml of SBF in the lab by the method of Kokubo and Takadama [168].

Table 3-4: Reagent, amounts in gm, weighing containers, purity and formula weight for preparing 1000 ml SBF [168].

Order	Reagent	Amount	Container	Purity (%)	Formula weight
1	NaCl	8.035 g	Weighing paper	99.5	58.443
2	$NaHCO_3$	0.355 g	Weighing paper	99.5	84.0068
3	KCl	0.225 g	Weighing bottle	99.5	74.5515
4	$K_2HPO_4.3H_2O$	0.231 g	Weighing bottle	99	228.222
5	$MgCl_2.6H_2O$	0.311 g	Weighing bottle	98	203.3034
6	1.0_M-HCl	39 ml	Graduated cylinder	—	—
7	$CaCl_2$	0.292 g	Weighing bottle	95	110.9848
8	Na_2SO_4	0.072 g	Weighing bottle	99	142.0428
9	Tris	6.118 g	Weighing paper	99	121.1356
10	1.0_M-HCl	0–5 ml	Syringe	—	—

For preparation of 1000ml SBF we put 700 ml of ion exchanged and distilled water in 1000 ml plastic jar without any scratches instead of glass containers. Heated the water to 36.5± 1.5°C under stirring.

Different regents ranging from 1st to 8th were dissolved in 700 ml solution ion exchanged and distilled water at a temperature of 36.5 ± 1.5 °C as per the categorization of Table 3-4. The regent given at serial number 9 and 10 are added in the solution in order to get the required pH. special care was taken for maintaining the temperature and pH level under 7.45 as suggested in literature. After the preparation of SBF the chemical analysis was carried out for the confirmation of ion concentration in comparison with blood plasma is described below Table 3-5.

Table 3-5: Nominal ion concentration of human blood plasma vs SBF [168].

Ion	Ion Concentration (mM)	
	SBF	Blood plasma
Cl^-	147.8	103.0
Na^+	142.0	142.0
K^+	5.0	5.0
Ca^{2+}	2.5	2.5
Mg^{2+}	1.5	1.5
HCO^-_3	4.2	27.0
HPO^{2-}_4	1.0	1.0
SO^{2-}_4	0.5	0.5
pH	7.4	7.2-7.4

SBF is a supersaturated solution with respect to apatite, an inappropriate solution preparation method leads to precipitation of apatite in solution. Prepared SBF can be preserved in refrigerator at 5-10 °C and can be used within month after preparation.

For soaking the sample in SBF the volume of SBF was found using the equation 3-1.

$$V_s = \frac{S_a}{10} \qquad (3\text{-}1)$$

V_s= volume of SBF (ml)

S_a= Surface area of Sample (mm^2)

The required volume of SBF was poured in the plastic jar and placed in the bigger jar containing pure water. The temperature of the water was kept at 36.5 °C with the help of heating filament. At 36.5 °C temperature of SBF the test specimen was submerged in the SBF and are caped as shown in the Figure 3-4.

Figure 3-4: Specimens inside Jars containing in SBF with heating filament

During the test hours the SBF pH was checked on regular basis. After soaking at 36.5 °C for a period of 504 hours and 816 hrs the test samples are taken out and gently washed with pure water and then dried in desiccator.

3.4 Tensile and Fatigue Testing

To establish the stress strain diagram of Ti-27Nb and Ti-25Ta the tensile test was carried out for the normal and simulated body fluid treated samples. Test is conducted to obtain properties of material before and after SBF treatment. The tensile test specimens were prepared according to ASTM E8 [169] . The prepared test specimen having rectangular cross section with the enlarged ends for gripping and geometry drawing is shown in Figure 3-5. The mechanical properties noted from diagram are young's modulus, tensile strength, and yield strength. Experiments are performed as per ASTM A370 standards [170].

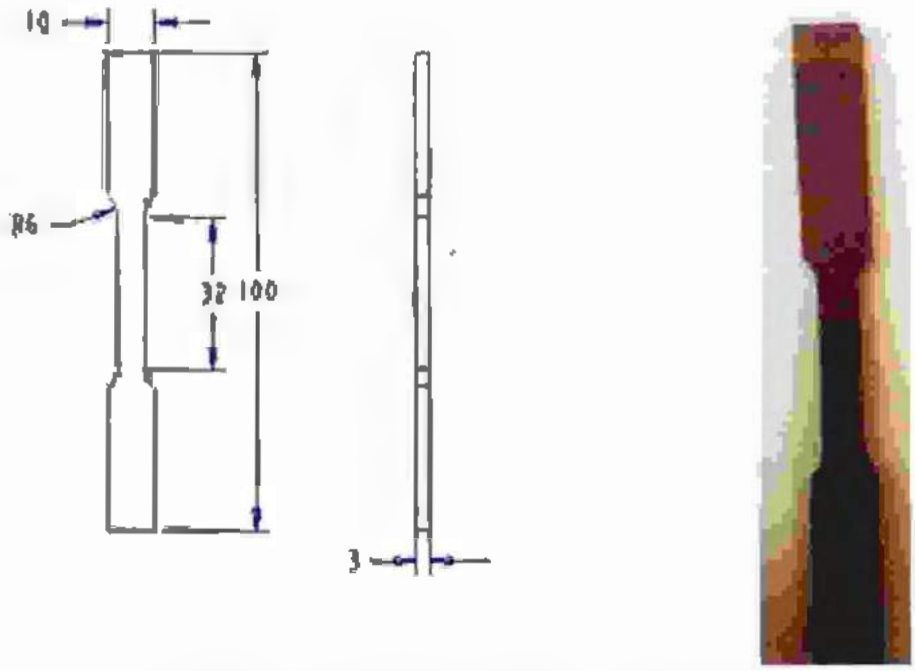

Figure 3-5:Geometry of Specimen and final prepared specimen

Set of triplets of dog bone specimen for Ti-27Nb and Ti-25Ta were tested. Test system INSTRON 600 UTM were used for testing. The specimen was clamped in the jig as shown in the Figure 3-6.

Figure 3-6: Instron 600DX Universal Testing Machine.

The load was applied at the rate of 10 N/minute. During tests, the displacement and load were recorded by the machine computer. The test was stopped when the specimen was finally ruptured.

The stress σ and strain ε was calculated using equation: (3-2) to (3-4) respectively

$$\sigma = \frac{F}{A} \tag{3-2}$$

$$V_s = \frac{S_a}{10} \tag{3-3}$$

$$\varepsilon = \frac{\delta}{l} \tag{3-4}$$

In above equations, A is the area of cross-section, F is the applied load, δ is the specimen's deformation, l is initial length of specimen and ε is the strain. Young modulus 'E', is calculated from stress-strain data, using equation (3-5).

$$E = \frac{\sigma_{max}}{\varepsilon_{max}} \tag{3-5}$$

Where σ_{max} is the maximum stress and ε_{max} is the maximum strain at failure.

For obtaining the total fatigue life, the dog bone specimen at Figure 3-5 was used. The surface of the specimen is mirror polished as per the methodology discussed in the microstructure analysis section for reducing the surface roughness effect. The tests were carried out on Instron 8875. Fatigue testing is carried out using load control method. The stress amplitude ratio was R(σ) = -1. Following parameters were recorded during the fatigue testing: number of cycle N, load P, the maximum/minimum stress σmax/σmin.

$$R = \frac{\sigma_{min}}{\sigma_{max}} \tag{3-6}$$

$$\sigma_{mean} = \frac{\sigma_{max} + \sigma_{min}}{2} \quad (3\text{-}7)$$

$$\sigma_a = \frac{\sigma_{max} - \sigma_{min}}{2} \quad (3\text{-}8)$$

After testing the S-N curves for ambient and 504 hrs treated sample were plotted using stress amplitude vs number of cycles to the failure.

3.5 Hardness Tests

The main purpose of this test is to compare the effect of SBF treated Ti-27Nb and Ti-25Ta with the non treated specimen in term of hardness. The study on the effect of simulated body fluid on material hardness were carried out to the material. In this study the hardness of TI-27Nb non treated specimen is compared with the treated specimen of 504 hrs. and 816 hrs. and same procedure for the Ti-25Ta specimen. The test specimens for hardness tests were manufactured from the same alloy's sheets. The schematic of location for hardness test is shown in Figure 3-7.

Figure 3-7:Schematic of location of Hardness Tests

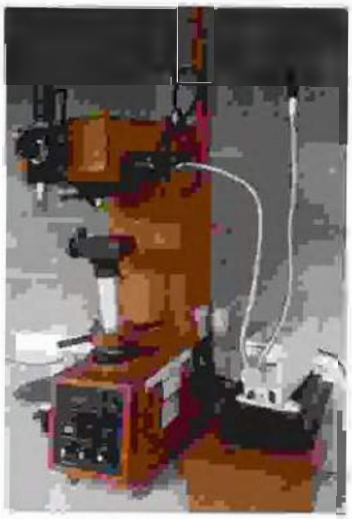

Figure 3-8: Mastuzawa Sciki co Ltd Japan Model DVK-2

In the current research vicker hardness test is carried out on Mastuzawa Sciki Co. Ltd. Japan Model DVK-2 as shown in the Figure 3-8 with the diamond point of pyramid shape. These tests were carried at room temperature and pressure conditions. The vicker hardness tester (Hv) with a load of 1 Kgf was kept for 10-15 seconds.

3.6 Fracture toughness

Compact Tension (CT) specimen are fabricated by the wire cut machine to reduce the effect of local heating. The dimension of the specimen used for fracture toughness in this study is W= 35 mm, a= 14.7mm(notch) and the thickness, B= 3mm. These dimensions are chosen to satisfy the relationship as per ASTM E399[171], Irregularities and surface porosities on the specimen were removed by grinding. The fracture toughness specimens were placed in SBF for 504 and 816 hours as per the test matrix in Table 3-6.

Table 3-6: Test matrix for fractur toughness testing of normal and SBF treated samples.

	Normal	SBF-504 hour	SBF-816 hour
Specimen ID	FT-1	FT-4	FT-7
	FT-2	FT-5	FT-8
	FT-3	FT-6	FT-9

Out of nine specimens of Ti-27Nb and Ti-25Ta, six specimen were placed in the SBF. Specimen ID FT-4 to FT-6 were taken out of SBF after 504 hours of treatment. FT-7 to FT-9 were treated for 816 hours. After taking out the specimen from the SBF are washed with pure water and dried.

Standard fracture toughness tests are carried out as specified in ASTM E-399 on the CT sample. This test is very strict, effective and valid test that must satisfy some criteria regarding the specimen thickness, crack length and crack length to weight ratio. Servo

hydraulic fatigue testing machine (Instron 8875) is used for conducting the fracture toughness tests. The maximum length of stroke for this machine was 300 mm. All the tests were performed at 25 °C which was the ambient temperature of the laboratory. The specimen geometry and in-test specimen are shown in Figure 3-9.

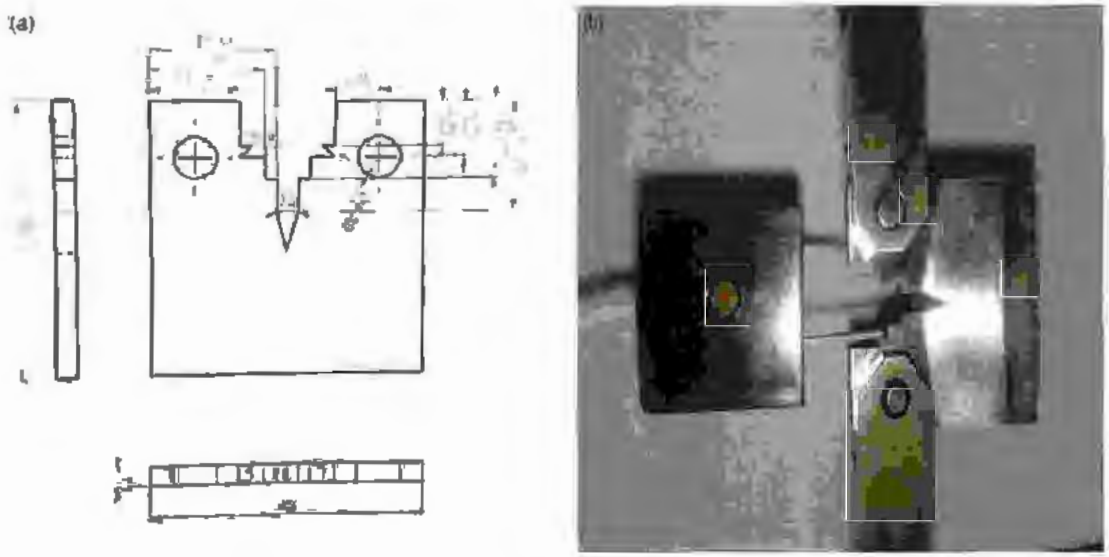

Figure 3-9: CT specimens (a) Geometry (b) Photo of in test specimen

As per ASTM standard, the stress intensity factor during the stages of pre-cracking should not exceed 80% of K_{IC}. Based on the initial calculations the value of Kmax is $25Mpa\sqrt{W}$. 10 Hz frequency (f) and 0.1 load ratio (R) were set on the machine for the generation of pre-cracking. All the parameters like load ratio $-1 \leq R \leq +0.1$ and frequency $f <$ 100Hz were in line with ASTM E399.

Pre crack of desired length i.e. 1.3mm minimum was achieved after 1.5 hour of cyclic loading. Subsequently, the specimen is loaded with monotonic load till the complete failure. Load and displacement of crack mouth are monitored and recorded. Extensometer was used for the measurement of the crack mouth. These recorded data were used for the plotting of force versus displacement curve. As per ASTM 399 three types of curves for load and displacement can be expected as shown in the Figure 3-10.

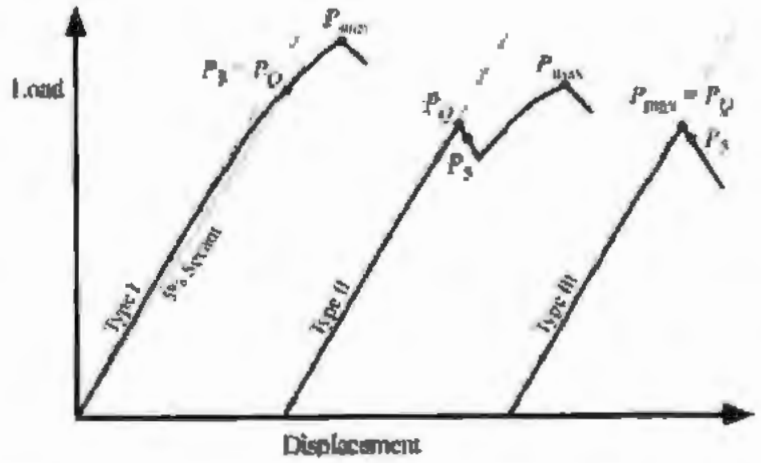

Figure 3-10: Load versus displacement behavior in a K_{Ic} test [171].

The P_Q i.e. critical load can be expressed in different ways for different curves shapes. In the type one curve the line from the origin with 5% secant line should be constructed to determine P_5. The P_Q is then defined as if the force at every point on which precedes P_5 is lower than P_5 is P_Q, if however, there is maximum force preceding P_5 which exceed it, then the P_5 will be the maximum force. The determination of crack length and P_Q are used for provisional fracture toughness K_Q computation.

The K_Q value is calculated using Equations (3-9) and (3-10).

$$K_Q = \frac{P_Q}{\sqrt{BB_N}\sqrt{W}} . f[a/w] \qquad (3\text{-}9)$$

Where $f\left(\frac{a}{w}\right)$ is the dimensionless function and is can be stated as:

$$f\left(\frac{a}{w}\right) = \frac{\left(2+\frac{a}{W}\right)\left[0.866 + 4.64\frac{a}{W} - 13.32\left[\frac{a}{W}\right]^2 + 14.72\left[\frac{a}{W}\right]^3 - 5.6\left[\frac{a}{W}\right]^4\right]}{\left[1-\frac{a}{W}\right]^{3/2}} \qquad (3\text{-}10)$$

The K_Q value calculated from equation 3-9 will be valid K_{IC} results if all the requirements for the validity mentioned in ASTM399 are met i.e

$$0.45 \leq \frac{a}{W} \leq 0.55 \quad (3\text{-}11)$$

$$B, a \geq 2.5\left(\frac{K_Q}{\sigma_{YS}}\right) \quad (3\text{-}12)$$

The 1st requirement of validity is met if the dimension satisfies the equations (3-11) and (3-12) .The 2nd requirement of validity is to make sure that the test conducted is in plain strain condition, as plain strain and plain stress varies based on the thickness of the specimen. Whereas the K_Q value is considered to be valid K_{IC} result, only if:

$$P_{max} \leq 1.10P_Q \quad (3\text{-}13)$$

Then $K_Q = K_{IC}$

The P_{max} is the maximum force the specimen can sustain should be calculated. If P_{max}/P_Q ratio does not exceed 1.1 then K_Q be calculated appropriate to the specimen configuration. If the value exceed 1.10 then the test is no valid K_{IC} , then test method E1820 on elastic -plastic fracture toughness should be adopted.

3.7 Fatigue Crack Growth Testing

Figure 3-11 shows geometry and the final prepared samples for fatigue crack growth measurement test.

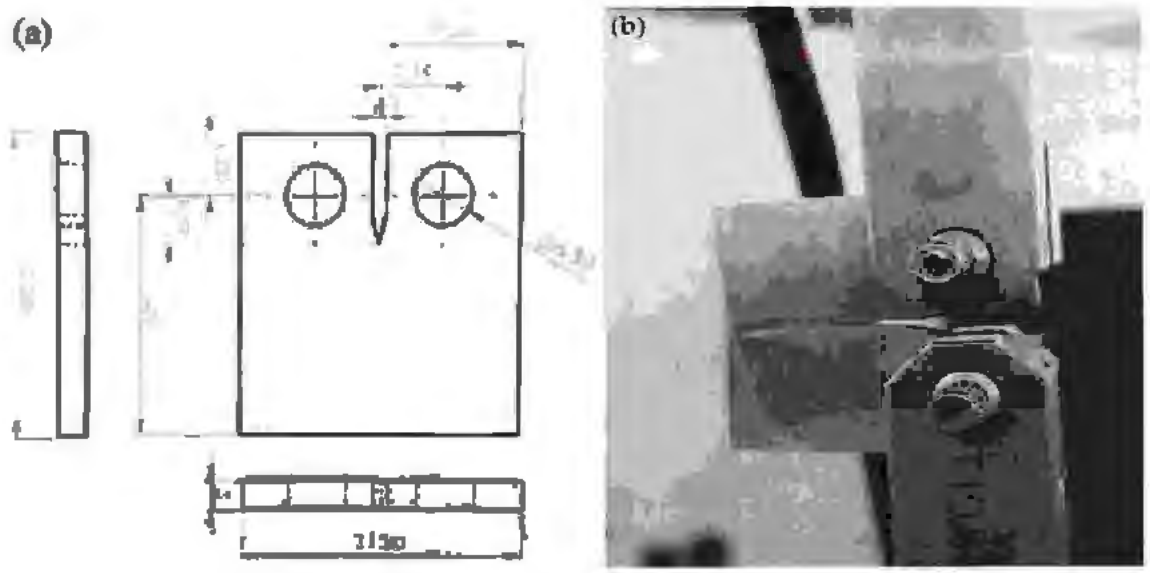

Figure 3-11: (a) Geometry of the CT Specimen for fatigue crack growth test (b) In Test Specimen

Fatigue crack growth experiments are performed on the same Instron 8875 machine used for fracture toughness testing. ASTM E 647 standard is used for fatigue crack growth measurements i.e. *da/dN* as a function of *delta K* [172]. The fixture and specimen used in the test are almost identical to the fracture toughness tests specimen. Tests are carried out in the lab environment at 25^0 C. All the specimen are first pre-cracked by applying cyclic loading up to 1.3mm. During test the crack growth is measured by optical technique using travelling microscope. During this fatigue crack growth test frequency was set to 4 Hz. The load control method is applied to the fatigue test at load ratio of R=0.1. The displacement, force and number of cycles are monitored and recorded during the fatigue tests through software.

3.8 Scanning Electron Microscopy

Samples for fractographic study, were cut from the fractured tensile specimens and the fractured surface of CT specimen. The top corner of the fracture surface was examined in the SEM S-3400 as shown in Figure 3-12. The voltage during SEM examination was 5kV. SEM images of the fracture surface were taken in the range 25X-5000X.

Figure 3-12: Hitachi SEM S-3400

4 Experimental Results

Experimental procedures of tensile, fatigue, fracture toughness, crack growth and SEM are described in the previous chapter. Current chapter presents the results of these tests. The results are presented graphically however for some tests tables are also given as supporting material. The significance of the results are elaborated through discussion.

4.1 Tensile Test Results

The stress-strain diagrams of the Ti-27Nb and Ti-25Ta are shown in Figure 4-1 a-d and Figure 4-2 a-d respectively. The yield strength of the Ti-27Nb is 757 MPa and 733 MPa and the ultimate tensile strength of 862 MPa and 833 MPa for untreated and treated specimen. The material exhibits reasonable amount of plasticity up-to failure. The material is less ductile as compared to its counterpart materials e.g. Ti-6Al-4V, however the strength is approximately 12% less than Ti-6Al-4V. This is beneficial for implant due to its lower dimensional change.

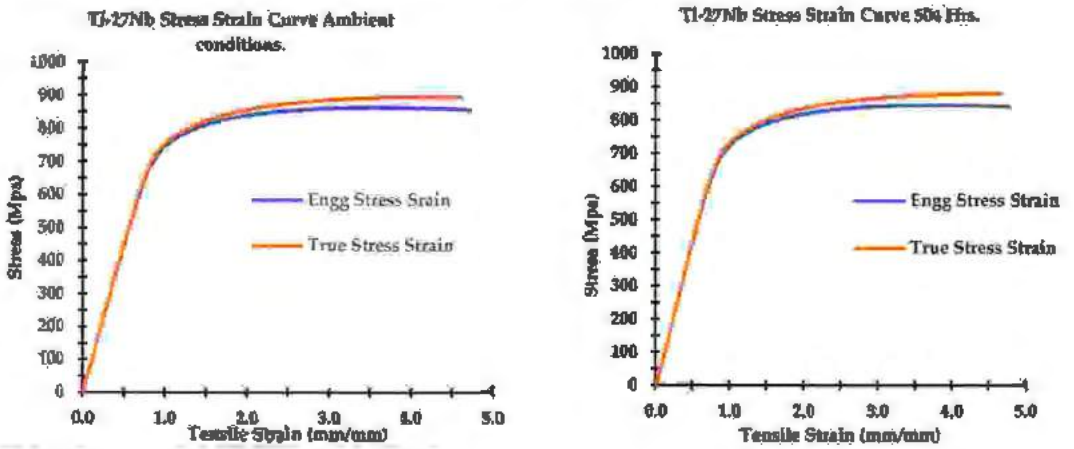

(a) (b)

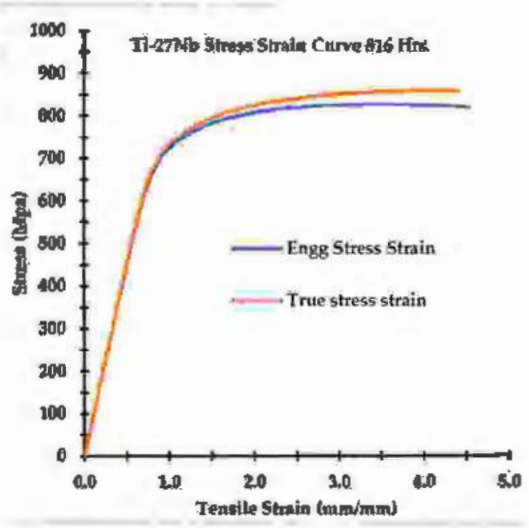

(c)

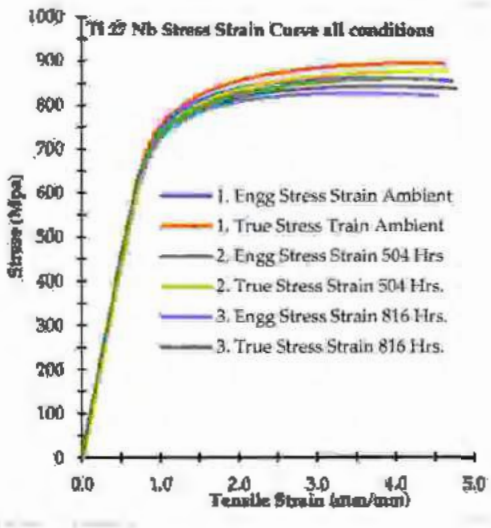

(d)

Figure 4-1: Stress Strain Curve Ti-27Nb (a) Ambient Conditions (b) 504 Hrs (c) 816 Hrs (d) Combined

The true stress is same to engineering stress up-to yield point however its value slightly deviates from the engineering stress after yielding point. The elastic modulus of the material is ~86 GPa. The elasticity is lower than its commonly used bio implant materials e.g. Ti6AL4V (110 GPa). Due to its lower elasticity, the stress shielding will be less in this material.

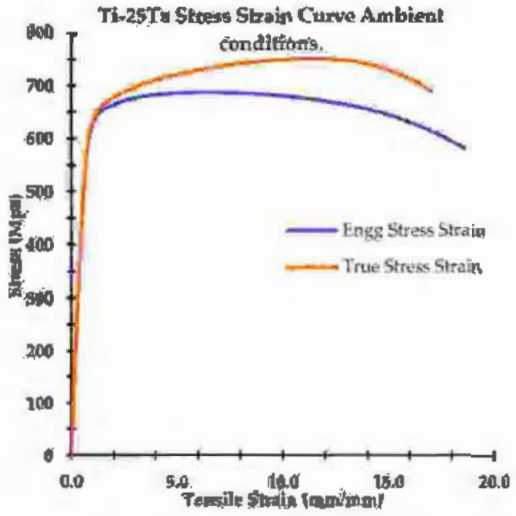

(a)

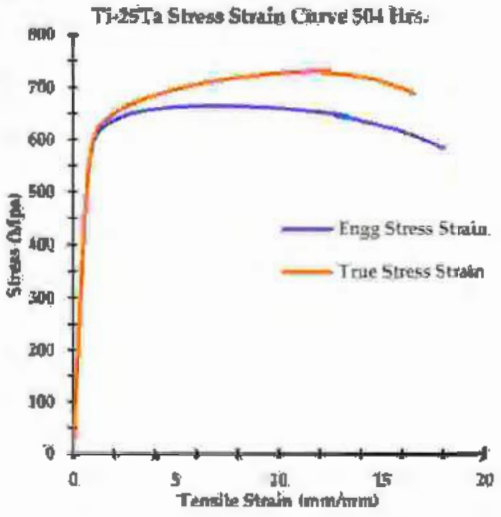

(b)

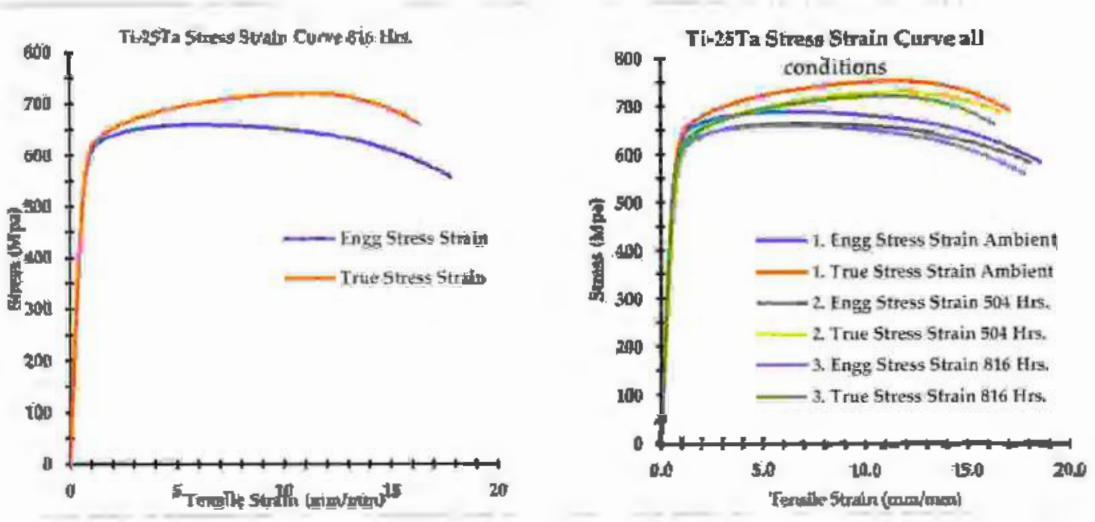

(c) (d)

Figure 4-2: Stress Strain Curve Ti-25Ta (a) Ambient Conditions (b) 504 Hrs (c) 816 Hrs (d) Combined

Theses specimen were tested as per ASTM E8. The results are given in the Table 4-1.

Table 4-1: Tensile Tests Results

S.No	Specimen	Yield strength (Offset 0.2%) (MPa)	Ultimate strength (MPa)	Modulus (Gpa)
1.	Ti-27Nb	757.39	862.15	86.50
2.	Ti27Nb (504 Hrs Treated)	733.21	843.65	85.72
3.	Ti27Nb (816 Hrs Treated)	733.05	842.23	85.7
4.	Ti-25Ta	608.58	688.09	88.15
5.	Ti25Ta (504 Hrs Treated	582.55	664.600	80.60
6.	Ti25Ta (816 Hrs Treated	582.3	664.5	80.6

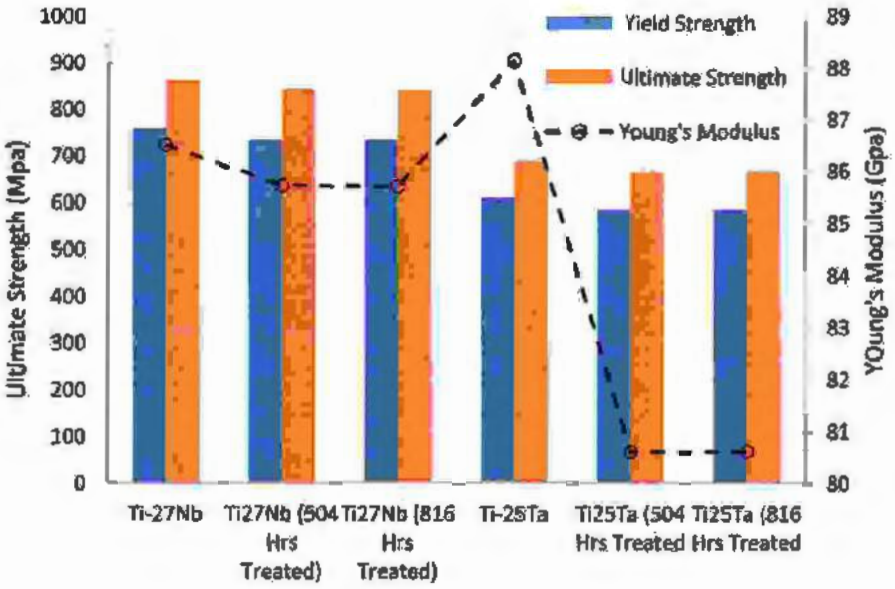

Figure 4-3: Tensile Properties of Ti-27Nb & Ti-25Ta

The results shown in Figure 4-3 reveals that there is a slight variation in the untreated and 504 hrs treated specimen of Ti-27Nb and Ti-25Ta. The percentage difference of variation for yield strength, ultimate strength and modulus is 3.2%, 2.14% and 0.9% respectively for Ti27Nb. Whereas there is almost negligible variation in the test values of 504 and 816 hrs treated Ti-27Nb specimen. Similar behavior is also observed for the Ti-25Ta the average variation recorded for untreated and 504 hrs treated specimen is a 4.18% for yield strength, 3.14% for ultimate strength and 8.5% in modulus. It may be concluded that variation in the above mechanical properties of treated and untreated specimens is negligible for the current test series. The reason for the negligible effect on the above properties may be attributed to formation of a very thin oxide layer on the treated specimen for protection against corrosion. The oxide layer on treated specimen were measured using Spectroscopic Ellipsometry tests. The values of layer thickness are given in Table 4-2, however further tests for example microstructural analysis using SEM and TEM may give in depth view of the effect of SBF treatment on Ti-27Nb and Ti-25Ta.

Table 4-2:Spectroscopic Ellipsometry Results

S.No	Material	Average Thickness(nm)	Error(%)
1.	Ti-27Nb untreated	14.6	2.4
2.	Ti-27Nb(504Hrs Treated)	43.84	1.23
3.	Ti-27Nb(8164Hrs Treated)	61.25	1.05
4.	Ti-25Ta	9.82	2.3
5.	Ti-25Ta(504Hrs Treated)	22.45	1.98
6.	Ti-25Ta(816 Hrs Treated)	33.72	1.52

4.2 Fatigue Life Test:

Fatigue life testing is carried out on untreated and treated samples for finding the fatigue strength upto 10 million fatigue cycles. The observed test data during fatigue tests is tabulated in Table 4-3.

Table 4-3: Fatigue test data

Sample No	No. of Cycles for Untreated sample	No. of Cycles for SBF treated	Alternating Stress (MPa)
1	1	1	860
2	4	3	810
3	27	28	752
4	35	34	752
5	320	380	651
6	1540	1800	559
7	3153	2915	559
8	36259	20590	479
9	25402	22357	479
10	125231	95000	429
11	300035	325000	429
12	380810	360423	429
13	2811240	2583651	350
14	1008005	1256123	350
15	10051120	9861451	343

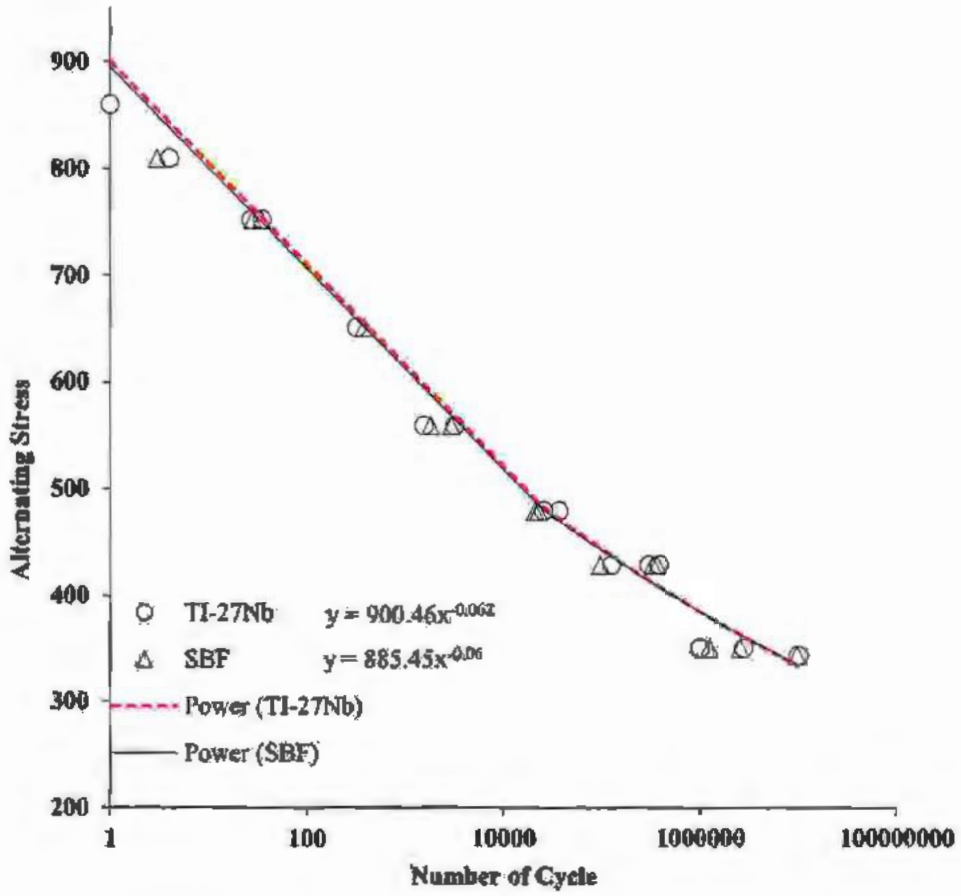

Figure 4-4: S-N Curve for Ti-27Nb (Treated and Untreated samples)

The S-N curve for ambient and 504 hrs SBF treated specimens is plotted in Figure 4-4. The effect of SBF treated and non-treated samples has negligible difference in the total fatigue life of the material. The difference of 1.88% was observed in the fatigue life at alternating stress level of 343 MPa.

A trend line was fitted to the fatigue life test data using power law. The fitted curves is shown in the Figure 4-4. The model for the finite life of untreated specimen is as follows;

$$\sigma_a = 900.46\, N^{-0.062} \tag{4-1}$$

$$log(\sigma_a) = log(900.46N^{-0.062}) \tag{4-2}$$

$$log(\sigma_a) = log(900.46) - 0.062logN \quad (4\text{-}3)$$

$$log(\sigma_a) - log(900.46) = -0.062logN \quad (4\text{-}4)$$

$$log\left(\frac{\sigma_a}{900.46}\right) = -0.062logN \quad (4\text{-}5)$$

$$N = \left(\frac{\sigma_a}{900.46}\right)^{-1/0.062} \quad (4\text{-}6)$$

Where σ_a is the maximum stress, N are the maximum number of cycles before failure of specimen, 900.46 and -0.062 are the curve fitting parameters. This model can predict the life of the TI-27Nb in untreated condition for any stress level.

The model for the finite life of 504 Hrs is as follow

$$\sigma_a = 885.45\ N^{-0.06} \quad (4\text{-}7)$$

$$log(\sigma_a) = log(885.45N^{-0.06}) \quad (4\text{-}8)$$

$$log(\sigma_a) = log(885.45N^{-0.06}) \quad (4\text{-}9)$$

$$log(\sigma_a) = log(885.45) - 0.06logN \quad (4\text{-}10)$$

$$log(\sigma_a) - log(885.45) = -0.06logN \quad (4\text{-}11)$$

$$log\left(\frac{\sigma_a}{885.45}\right) = -0.06logN \quad (4\text{-}12)$$

$$N = \left(\frac{\sigma_a}{885.45}\right)^{-1/0.06} \quad (4\text{-}13)$$

Where σ_a represents the maximum stress, N are the maximum number of cycles before failure of specimen, 885.45 and -0.06 are the curve fitting parameters. This model can predict the life of the TI-27Nb in treated condition for any stress level. The treatment time in simulated body fluid (SBF) is selected as 504 hrs for the current study. The predicted life curve shows a negligible variations for the selected treatment time. The predicted life model of the specimens

is serving as input for the Finite Element Model of implant for the purpose to carry out fatigue analysis of implant for different daily routine activities. The fatigue life will depend upon the maximum stress at local level in the stress field in the implant. The fatigue life can be found out using this model in treated and untreated condition as input at each integration point of material.

4.3 Hardness test results

Hardness test was carried out along the longitudinal and transverse direction. Twenty data points are taken along the longitudinal direction and four data points are taken along the transverse direction as shown in Figure 4-5 for both SBF treated and non-treated specimen of Ti-27Nb and Ti-25Ta.

Figure 4-5: Hardness Test Specimen

Vicker hardness number was calculated by dividing applied force by surface area of pyramidal depression.

$$HV = \frac{2P}{d^2}\sin\frac{\alpha}{2} \qquad (4\text{-}14)$$

Where P is the force in kilograms and d is in millimeter.

After analyzing the data the average come out to be 273 Hv for Ti-27Nb and 231 Hv for Ti-25Ta. Same average values are recorded for untreated and SBF treated samples of Ti27Nb and Ti-25Ta. It is also observed that no significant change in the hardness value was observed along the edges of the samples.

4.4 Fracture Toughness

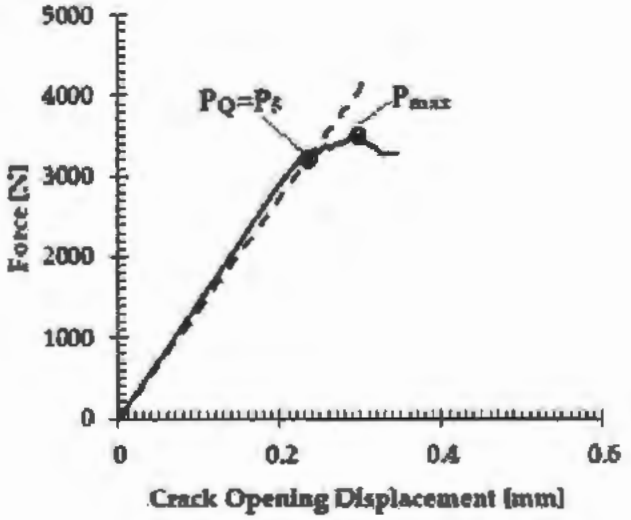

Figure 4-6: Load Vs Crack opening displacement

The K_Q value will be valid if $Pmax \leq 1.10\ P_Q$. Then K_Q will be the fracture toughness (K_{IC}). Figure 4-6 shows the relation between load and corresponding displacement for fracture toughness tests od Ti-27Nb. Same behavior has also been reported for other alloys of Ti. The fracture toughness derived by using equation (3-9) and Figure 4-6 is 50 MPa.√m. This value of fracture toughness is near to another titanium alloy Ti-6Al-4V which has value of 65 MPa.√m [98].

4.5 Behavior of Fatigue Crack Growth

A high-resolution camera of 10 Mega Pixel is used to closely observe the crack length (a) is while the number of load cycles (N) noted from display monitor of machine. Seven-point incremental polynomial technique is used according to ASTM E647 to record the growth rate of fatigue crack. Figure 4-7, Figure 4-9and Figure 4-11 shows the differences in growth rate of fatigue crack vs number of cycle under ambient, specimen treated for 504 and 816 hrs respectively for Ti-27Nb. The experimental results obtained are analyzed using the Paris law which is:

$$\frac{da}{dN} = C(\Delta K)^m \quad (4\text{-}15)$$

Where *da/dN* presents the growth rate of fatigue crack, ΔK represents range of stress intensity factor while coefficient "*C*" represents the line intercept on log-log plot and exponent "*m*" represents the slope. Both "*C*" and "*m*" are constant. The Paris law relation of specimen placed ambient, treated for 504 and 816 hrs are as follows

$$\frac{da}{dN} = 1 \times 10^{-7}(\Delta K)^{2.12} \quad (4\text{-}16)$$

$$\frac{da}{dN} = 1 \times 10^{-5}(\Delta K)^{2.09} \quad (4\text{-}17)$$

$$\frac{da}{dN} = 1 \times 10^{-5}(\Delta K)^{1.92} \quad (4\text{-}18)$$

Figure 4-8, Figure 4-10, Figure 4-12 and Figure 4-13 shows relation between the growth rate of fatigue crack and stress intensity factor ΔK on log-log scale for specimen tested at ambient, treated for 504 and 816 hrs in SBF solution. The experiments have been conducted in the set of triplets. An observance of an error less than 2% for nearly all the experiments reflect low standard deviation. In case of untreated specimen the curve for crack growth is of typical sigmoidal shape (S shape curve). All three regions i.e. threshold, Paris and critical growth regions are clearly visible. As compared to untreated specimen the curve obtained for the SBF treated specimens are almost straight suggesting no threshold growth region. Thus, resistance to crack growth is far superior in case of untreated as compared to treated specimen. Similarly it can be concluded that crack growth in SBF as compared to untreated specimen will take place at even lower SIF values.

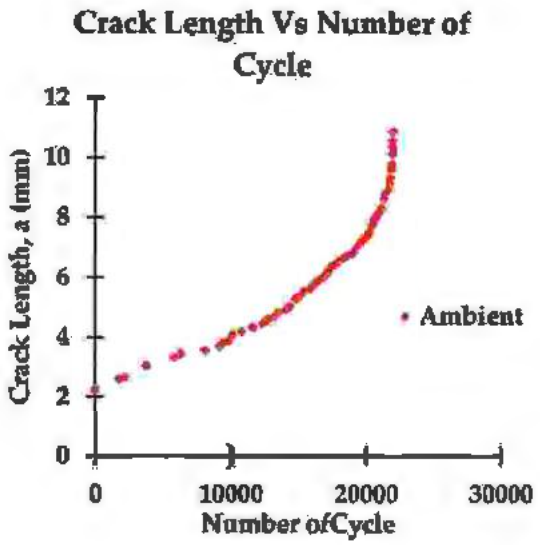

Figure 4-7: Crack length vs Number of Cycle of Ti-27Nb for untreated specimen

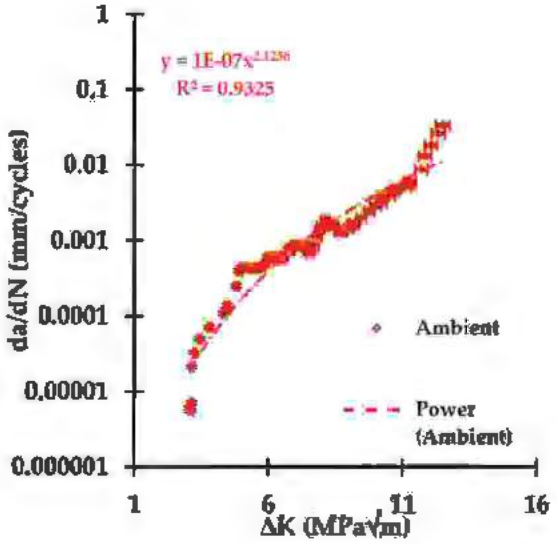

Figure 4-8: da/dN vs ΔK of Ti-27Nb for untreated specimen.

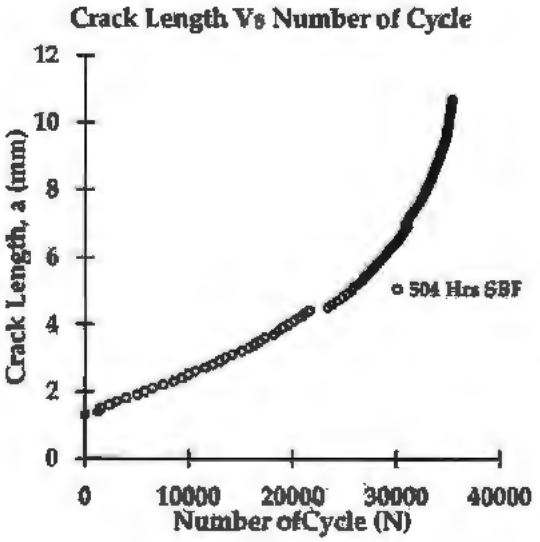

Figure 4-9: Crack length vs Number of Cycle of Ti-27Nb for 504 Hrs SBF treated Specimen

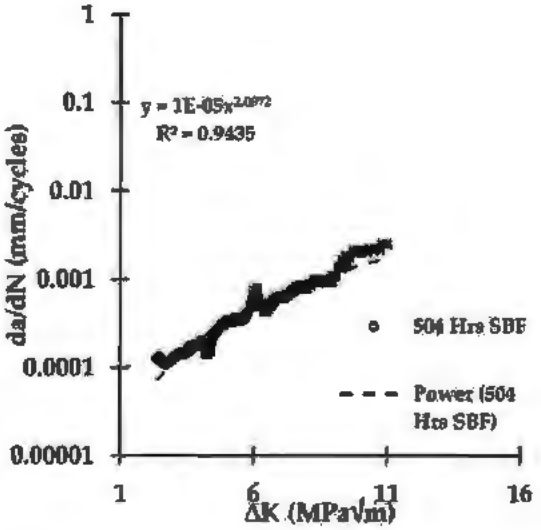

Figure 4-10: da/dN vs ΔK of Ti-27Nb for 504 Hrs SBF treated Specimen.

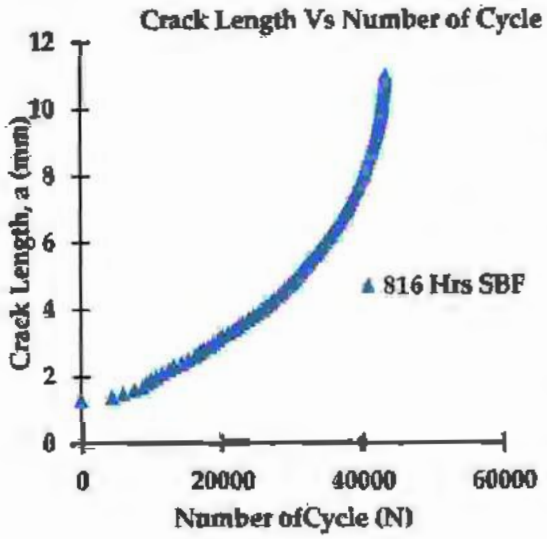

Figure 4-11: Crack length vs Number of Cycle of Ti-27Nb of 816 Hrs SBF treated Specimen

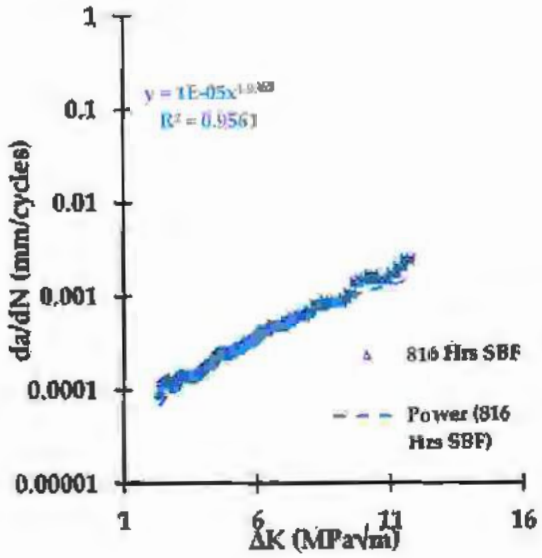

Figure 4-12: da/dN vs ΔK of Ti-27Nb for 816 Hrs SBF treated Specimen

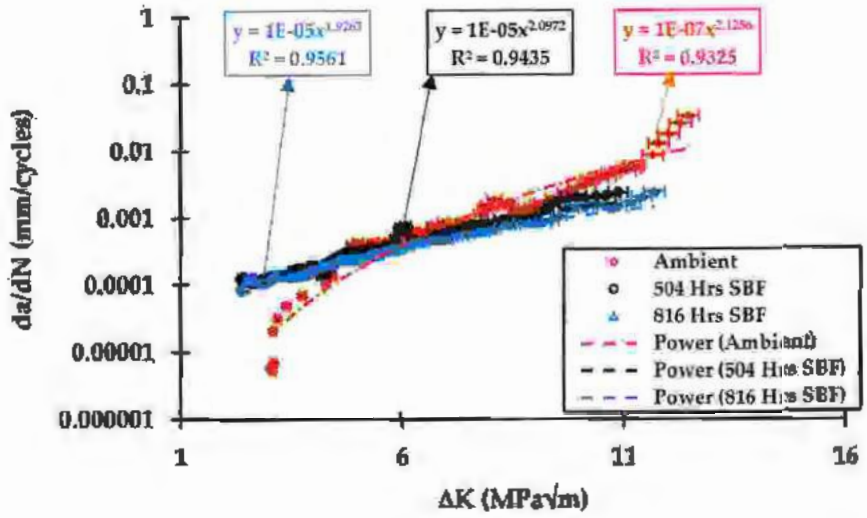

Figure 4-13: da/dN vs ΔK results for untreated, 504 hrs. and 816 hrs. in SBF for Ti-27Nb.

4.6 XRD Results

For finding crystallographic structures and crystal phase composition analysis of the Ti-27Nb and Ti-25Ta specimen were carried out using X-ray diffractometer (D8 Advance BRUKER) using Cu Kα radiation (λ=1.5406 Å) in the diffraction angle (2θ) ranging from 10 to 70°.

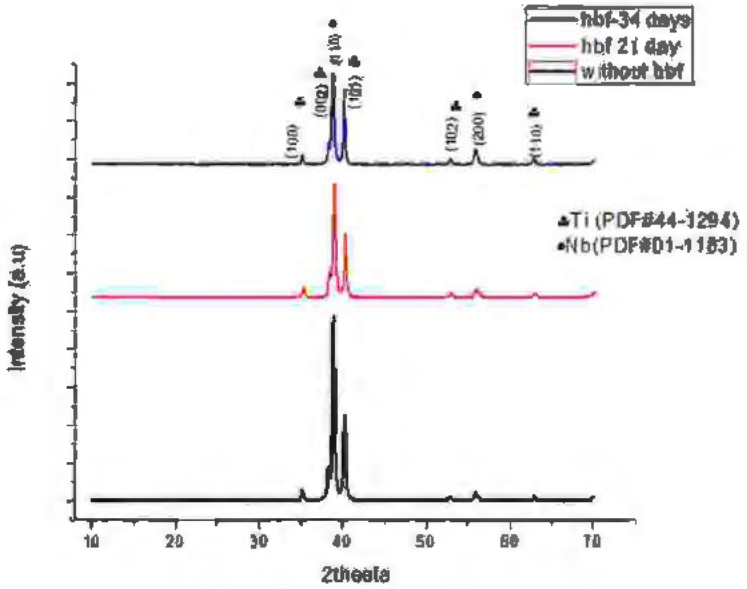

Figure 4-14: XRD pattern of Ti-27Nb

The XRD patterns of Ti-27Nb alloy before and after adding to SBF solution (pH 7.4) for 504 and 816 Hrs are shown in Figure 4-14. As can be seen from Figure 4-14, that Ti27Nb alloy show α phase (hcp structure) β phase (bcc structure) [173]. The diffraction peaks at 2θ values of 35.09, 38.42, 40.17, 53.00, and 62.95° are consistent with the (100), (002), (101), (102), and (110) crystallographic planes of Ti hcp structure (JCPDS NO. 044-1294), while the 38.47 and 55.55° corresponding to the (100), (200) crystallographic planes of Nb bcc structure (JCPDS NO 01-1183). The crystal phases of the Ti-27Nb remains the same before and after adding to SBF solution which is the indication that there is no obvious change in the crystallinity phase is observed and also no peak shift is seen in any of the sample. It means that

there is no change in the composition of structure of the material occur before and after adding to SBF solution in Ti27Nb.

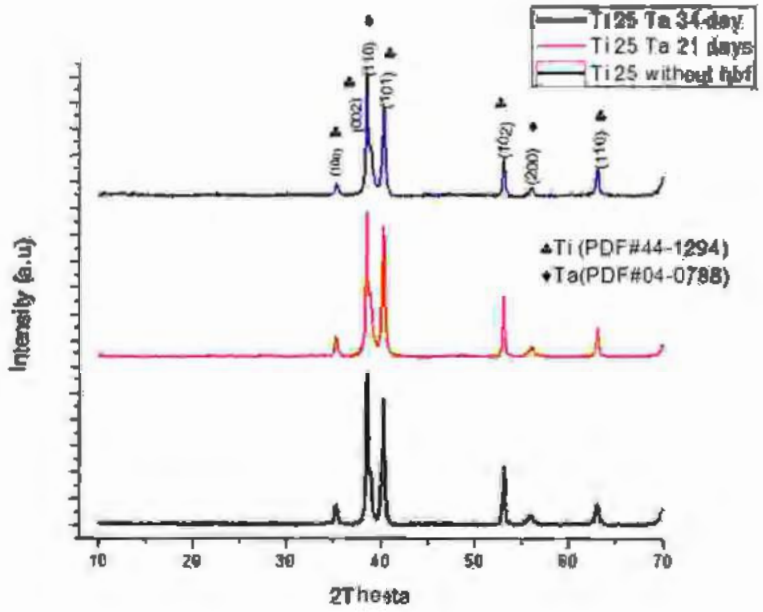

Figure 4-15: XRD Pattern of Ti-25Ta

Figure 4-15, show the XRD patterns of the Ti25Ta alloy before and after adding to SBF solution (pH 7.4) for 21 and 34 days. The XRD diffraction peaks that appeared in spectra can be radially indexed to alpha (α) phase (i.e., hexagonal closed-packed, hcp) for Ti and beta (β) (i.e., body-centered cubic, bcc) phase for Ta with the JCPDS NO. 044-1294 and JCPDS NO. 004-0788 respectively [174, 175]. The α peaks of the Ti25Ta can be labelled as $\acute{\alpha}$, as this is the metastable martensitic non-equilibrium form of the equilibrium stable α phase, with the same crystal structure. The pronounced diffraction peaks were observed at 2θ values of 35.09, 38.42, 40.17, 53.00, and 62.95° corresponding to the (100), (002), (101), (102), and (110) crystallographic planes of Ti, while the 38.47 and 55.55° corresponding to the (100), (200) crystallographic planes of Ta. The solution pH changes from 7.4 to 7.3 after 816 hrs. It is clear from the Figure 4-15 that there is no obvious peak shift occur after treating Ti25Ta in SBF fluids for 504 and 816 hrs that indicate that crystal phases of the Ti-25Ta remains the same,

however the intensity of XRD peaks decreases slightly which may implies the hardening of the sample [176].

4.7 Microstructure Evaluation of Ti-27Nb:

The fracture behavior, fatigue resistance and yield strength of titanium based alloys are mainly affected by the volume fraction of phases and morphology of microstructure. It is observed that the microstructure of the selected material is characterized as bi-modal (i.e. α + β) having Widmanstätten lath structure [177]. Widmanstätten bi-modal microstructure usually shows highest fatigue limit, fatigue crack growth resistance and maximum fracture toughness [178, 179]. Figure 4-16 shows the micrographs of as-cast Ti-27Nb alloys at two different magnification by optical microscope which clearly indicate the near equiaxed grains of alpha and transformed beta (i.e α+β) phase. The dual phase i.e α+β offer a combination of strength, ductility and the advantage in term of fatigue resistance. In such microstructures, the bi-modal (i.e α+β) structure composed of primary near equiaxed shaped alpha-grains (light phase) with a mean size of 9μm and colonies of very disperse lamellar matrix of transformed beta (β) phase (dark portion). The fine acicular shape can be observed in both micrographs like a basket-weave which demonstrate the Widmannstetter structure. The volume fraction of the beta-phase in following Ti-27Nb alloy is 0.61 measured by Fiji-Image j software, which is very large compared to Ti-6Al-4V (i.e. 0.12). This change in volume fraction, morphology and distribution of the two phases is attributed to the addition of Niobium which is strong beta-phase stabilizer.

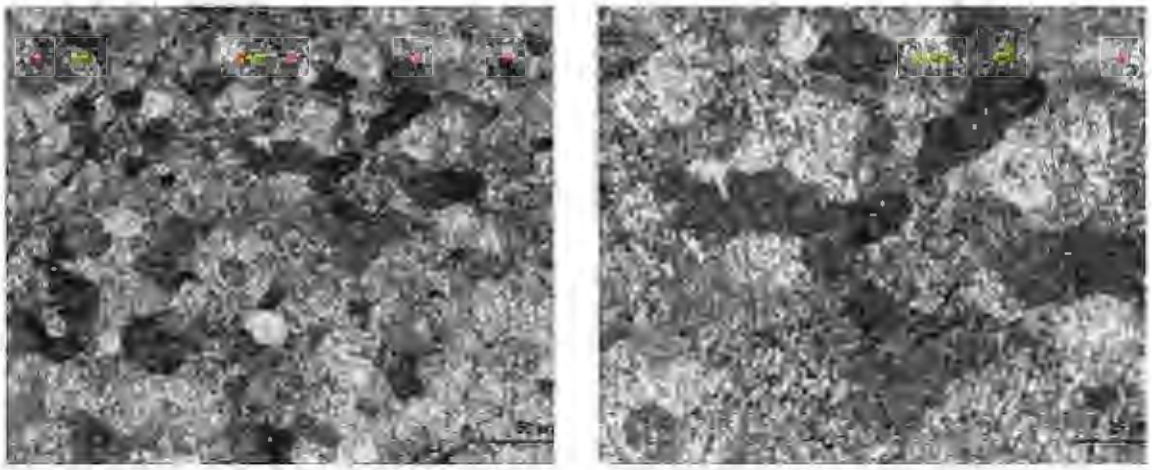

Figure 4-16: Ti-27Nb microstructure in a basket-weave arrangement, where the α phase is the white grains, while the β phase is the dark grains at magnification of 100x and 200x.

4.7.1 Fractography:

The fracture surfaces of tensile tested specimens in Figure 4-17, fatigue crack growth and fracture toughness specimen were examined by Hitachi S-3400N Scanning electron microscope (SEM) at 20 KV for both macroscopic and microscopic study. In Figure 4-18 (a) the macrograph showing a fracture surface of mixed behavior of brittle and ductile phases with no extensive plastic deformation. In central interior portion of the specimen, irregular and fibrous appearance which is indicative of ductile phase while some portion especially near edges of the specimen clearly showing no gross plastic deformation which is indicative of cleavage facet brittle fracture. While on microstructure level, the Figure 4-18 (b) showing dimples characteristics that's indicate a intergranular fracture and faceted textures surface that's indicate the trans granular fracture which is the demonstration of a typical mixed ductile and brittle fracture respectively.

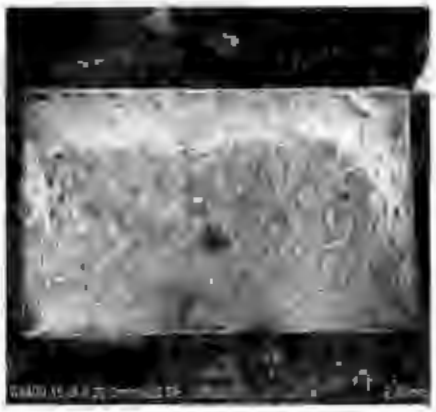

Figure 4-17: Fracture surfaces of tensile tested specimens of Ti-27Nb by using SEM

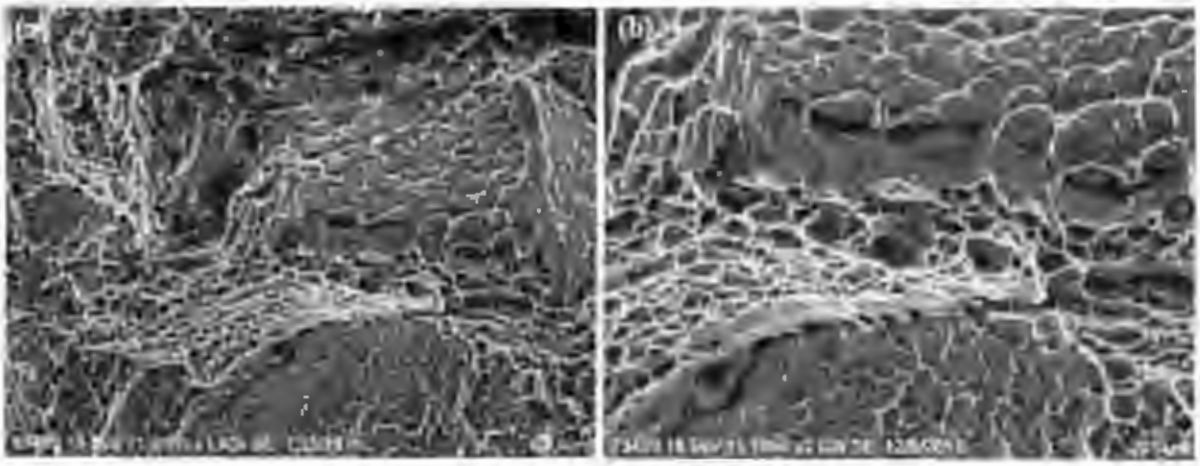

Figure 4-18: Macrograph showing the fractured surface

Figure 4-19 shows the Field emission scanning electron microscopy micrographs of tested untreated specimen fatigue crack characteristics, crack propagation path and microstructure. Figure 4-19a shows the widmanstätten lath structure and Figure 4-19b shows the path of tortuous crack propagation with branch crack. The fracture toughness of the curved crack path is higher than the flat crack path, because it consumes more energy during crack propagation [180].

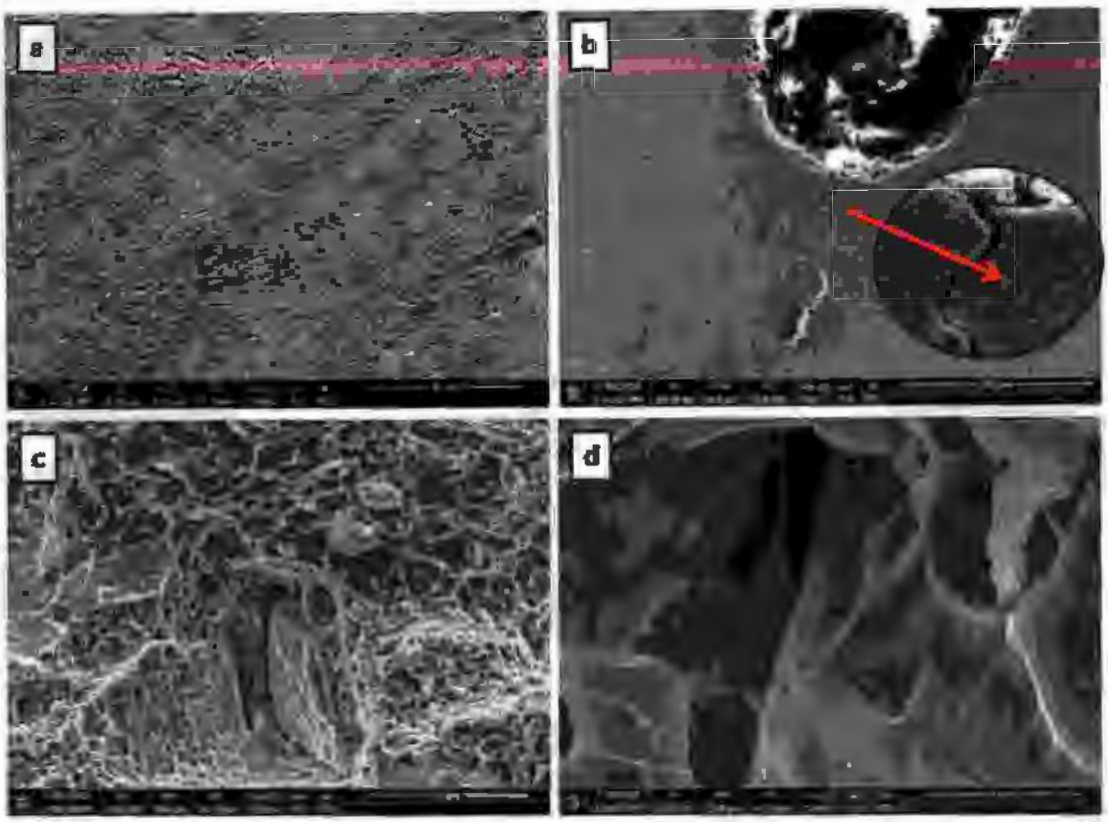

Figure 4-19: Ti-27Nb specimen field emission scanning electron microscopy (FESEM) micrograph under fatigue loading. (a) Widmannstetter lath structure (b) branching and deflection of crack (c-d) fracture surface.

This is usually occurred due to the colonies of lath α and β in the bi-modal microstructure, which act as effective slip barrier to stop the slip transfer to adjacent colonies. The crack changed the direction during propagation while crossing the boundaries of these adjacent colonies, leads to secondary crack creation and crack branching. The stresses redistribution caused by the crack branching reduced the crack growth rate [181]. The crack branching and redirection, consequently, occurred which eventually increased the toughness and resistance of the material to crack propagation. Figure 4-19c shows the fracture surface of the sample which exhibited mixed morphology of trans granular ductile and brittle behaviors in the form of dimples and cleavage facets respectively. In bi-modal microstructure, cleavage facets usually formed at primary α-grains, whose large boundaries comprise weak sites. Striations, which are main feature of fatigue fracture, have also been observed in Figure 4-19d. These striations demonstrating the position of crack tip at the given cyclic load and creating

ridges that is spreading from the initiation site. These ridges are perpendicular to the direction of fatigue crack propagation as clearly shown in micrograph.

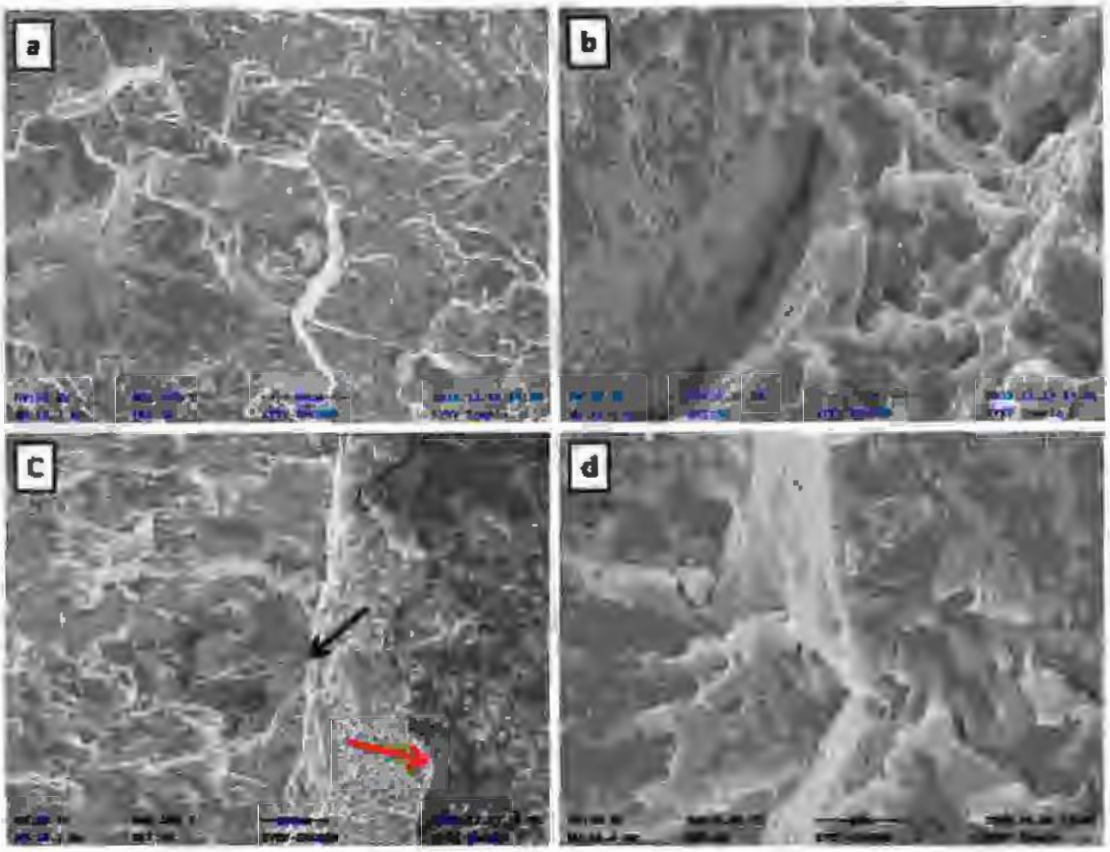

Figure 4-20: Ti-27Nb SEM fracture surface micrograph placed in SBF for (a-b) 504 hrs (c-d) 816 hrs.

Figure 4-20 showing Ti-27Nb specimen fracture surface, placed in the SBF for 504 and 816 hrs. Appearance of fracture surface of the specimen placed in SBF for 504 hrs as in Figure 4-20 a and b shows intergranular and transgranular faceted fracture mode. The intergranular mode is mainly related to brittle failure. In brittle failure, the preferential crack propagation is located at the grain boundary. Change in the fracture mode from transgranular to intergranular fracture leads to reduction in ductility of alloy [182]. This intergranular fracture is attributed to the corrosion fatigue. Corrosion fatigue occurs at the grain boundaries of alloys when in contact with SBF. When titanium alloys are used in different chemical solutions, brittleness has been observed [98, 183, 184]. This results in fast crack growth propagation and relatively straight

profile. Figure 4-20 c and d showing the specimen fracture surface placed in SBF for 816 hrs. The red arrow in Figure 4-20c shows the creation of thick oxide layer due to the oxidation by SBF and the black arrow shows the crack initiation site. The crack surface shows rougher fracture surface and the cleavage which leads the materials to fast crack propagation and brittle failure due to corrosion fatigue. It is known phenomenon that cleavage cracks grow faster than crack which shows striations [185]. By evaluating the fatigue crack growth (da/dN) and fracture surface of the sample, it can be found that the longer the material is placed in the fluid, the faster the fatigue crack growth. This is due to corrosion fatigue caused by the chemical environment of simulated body fluids. In this environment, the longer the sample is immersed in the simulated body fluid, the higher the fatigue crack growth caused by corrosion fatigue, which has also been reported in different studies [98, 180, 181, 184, 186]. Furthermore, no fatigue striations are observed in SBF treated specimen in contrast to untreated specimen which also confirm the fast crack growth propagation behavior in treated specimen.

5 Finite Element Analysis of Hip Implant

This chapter presents the static and fatigue analysis of hip implant made from nickel free titanium alloys through Finite Element Simulations. The static response of implant is characterized by quantifying the equivalent stress and Factor of Safety (FOS) against static loads for various activities. In a similar manner the fatigue character of implant is described through fatigue life, fatigue FOS and damage. The static and fatigue analysis for two nickel free titanium alloys (i) Ti-27Nb (ii) Ti-25Ta is performed as part of this research. While the results of only Ti-27Nb are made part of this discussion, results for Ti-25Ta are provided in Appendix B to avoid repetition. Additionally, the influence of SBF on the fatigue character of implant is also quantified. However, some results were a mere repetition of their counter parts for the untreated implant. Therefore, they are also not made part of the main discussion and are presented in Appendix-A.

5.1 Numerical Method

The hip implant is analyzed in transient structural analysis because the loads on implant in various activities varies with time. The analysis reported in this thesis have been performed in the transient structural analysis system with in the ANSYS Workbench. The governing equation which is the linear general equation of motion solved for these analysis is written in matrix form as follows:

$$[M]\{\ddot{x}\} + [c]\{\dot{x}\} + [k]\{x\} = \{F\} \qquad (5\text{-}1)$$

Where, $[M]$ is the structural mass matrix with $\{\ddot{x}\}$ as the nodal acceleration vector $[C]$ is the structural damping matrix with $\{\dot{x}\}$ as the nodal velocity vector. $[k]$ is the stiffness matrix with $\{x\}$ as the nodal displacement vector and $\{F\}$ is the applied load vector.

In equation (5-1), $[M]\{\ddot{x}\}$ represent the inertial loads, $[c]\{\dot{x}\}$ the damping loads and $[k]\{x\}$ represent the stiffness loads. In transient analysis the complete general form of this equation is solved.

5.2 Geometry and Mesh

Hip implant model is selected from the world renowned synergy product range and its solid model is reconstructed in the Autodesk Inventor as shown in the Figure 5-1.

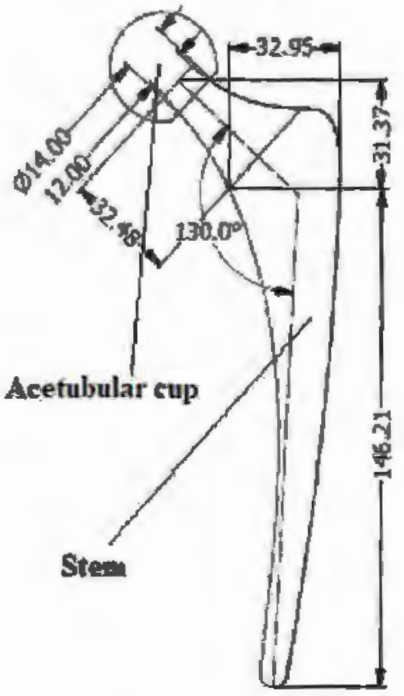

Figure 5-1: Geometric model of the Hip Implant

The hip implant is assigned Ti-27Nb material with mechanical properties already provided in Table 4-1. The solid model is a two-body part consisting of acetabular cup and stem that is transformed into a single multi body part to generate a conformal mesh on the mating surfaces. Selective body meshing technique is used with patch confirming tetrahedral mesh method. The meshing strategy is adopted such that to dedicate most of the elements to the neck area where the maximum stress is expected as already reported in [187, 188]. The mesh generation is started from the neck region followed by the stem and acetabular cup. Four meshes with different grid densities are generated and spatial discretization study is conducted

to establish the spatial accuracy of simulations. **Error! Reference source not found.**Table 5-1 provides the details of all generated grids and Figure 5-2 provides a pictorial representation of the relative grid density in different portion of the hip implant for Mesh 3. This mesh is utilized for all simulations reported in this thesis.

Table 5-1: Detail of meshes utilized mesh sensitivity study

Mesh Description	Mesh Number of elements		
	Acetabular Cup [Nos.]	Stem [Nos.]	Total [Nos.]
Mesh-1	11540	23607	35147
Mesh-2	17325	35448	52773
Mesh-3	17741	76558	94299
Mesh-4	17986	204935	222921

Figure 5-2: Pictorial representation of Mesh 3 utilized for FE analysis

For the selected mesh 3, the neck regions is meshed with a body sizing of 1.33 mm whereas rest of the stem and acetabular cup is meshed with a body sizing of 2 mm. Transient structural analysis is conducted for the mesh sensitivity study with load case representing the walking activity and problem constraints explained in the proceeding section. The equivalent Von Mises stress mathematically represented as:

$$\sigma_e = \left[\frac{(\sigma_1 - \sigma_2)^2 + (\sigma_2 - \sigma_3)^2 + (\sigma_3 - \sigma_1)^2}{2}\right]^{1/2} \qquad (5\text{-}2)$$

Where σ_1, σ_2 and σ_3 are the maximum, middle and minimum principal stresses respectively. The maximum Von Mises stress is selected as the solution variable for the grid independence check because it will be used as the stress component for fatigue analysis. The value of von Mises stress increases with increasing grid density as shown in Figure 5-3.

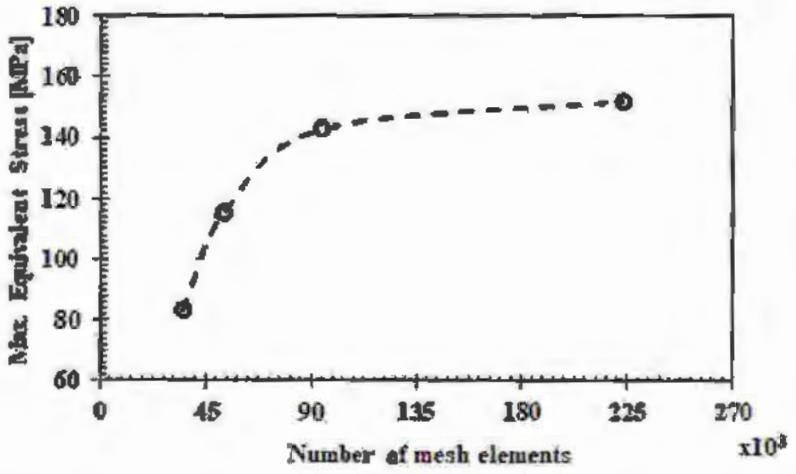

Figure 5-3: Simulated values of Max. von Mises stress with different density grids

This increase is almost linear for the 1st three meshes and becomes monotonic between mesh-3 and Mesh 4. The difference in von Mises stress value between mesh 3 and mesh 4 is only about 6% and therefore it is decided that further increase in the grid density is not required. As this would largely increase the computational time with minimal improvement in the accuracy of simulation results.

5.3 Simulations setup

Time settings for the transient structural analysis is set such that the total simulation time is set up to match the total time of load application for each activity in the experimental measurements of Bergmann, et al. [189]. The total simulation time of each activity is divided into 150 equal steps to determine the time step for the transient analysis. The details of total simulation time and time step for each activity for all simulations is shown in Table 5-2.

Table 5-2: Total time and time step for simulation of different activities.

S.No	Activity	Total Simulation Time [sec]	Simulation Time Step [sec]
1	Walking	1.123	0.007
2	Stance	9.103	0.060
3	StandUP	3.195	0.021
4	SitDown	3.628	0.024
5	StairUp	1.505	0.010
6	StairsDown	1.489	0.010
7	KneeBend	5.439	0.036
8	Jogging	0.737	0.005
9	Cycling	1.449	0.010

The hip implant is assigned a fixed boundary condition on the faces highlighted in purple as shown in Figure 5-4. This boundary condition would constrain all degrees of freedom on the highlighted surface of implant. This boundary condition type has been selected as this closely resembles the actual way in which the hip is implanted in human body. The co-ordinate system

Figure 5-4: Support condition for Hip implant

for the hip implant in FEA is constructed such that to match the co-ordinate system used for the experimental data. This enabled to directly apply the loads from the excel sheets of experimental data without any manipulation. Loads are applied at the center of the mating surface of the acetabular cup and implant which is the origin of the coordinate system utilized for the FE model. Loads for the Finite Element Analysis (FEA) of hip implant are utilized from the experimental measurements of Bergmann, et al. for the two body weights of 75 kg and 100 kg [189]. These loads are graphically reproduced in Figure 5-5 (75 Kg body weight) and from Figure 5-6 (100 Kg body weight) for different activities.

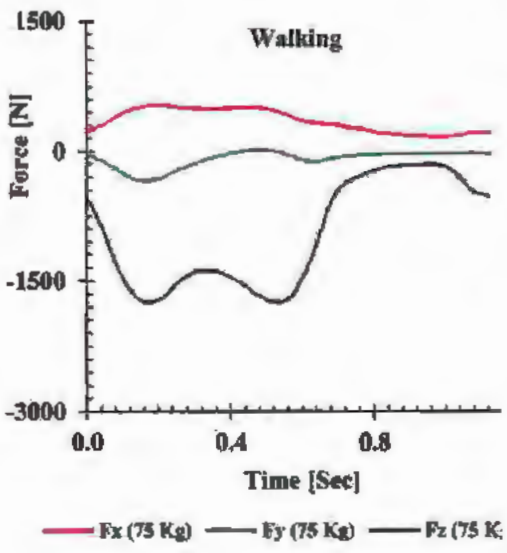

(a) walking

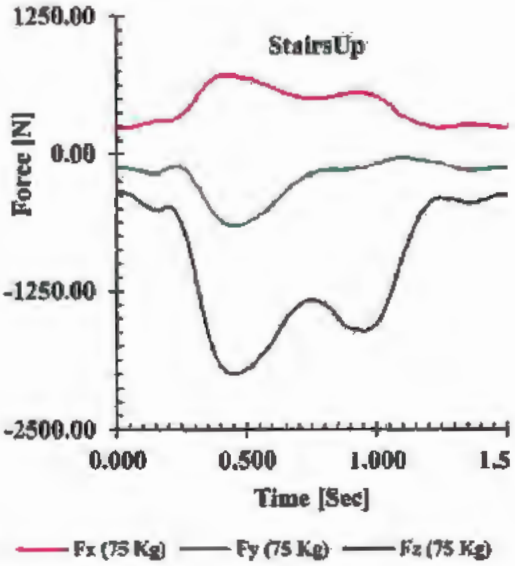

(b) Stair up

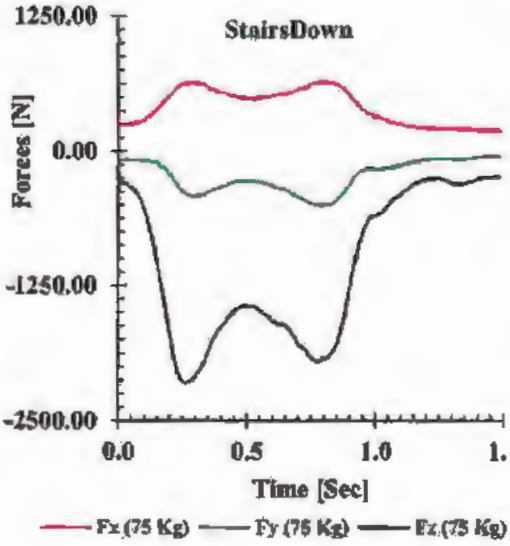

(c) Stair down

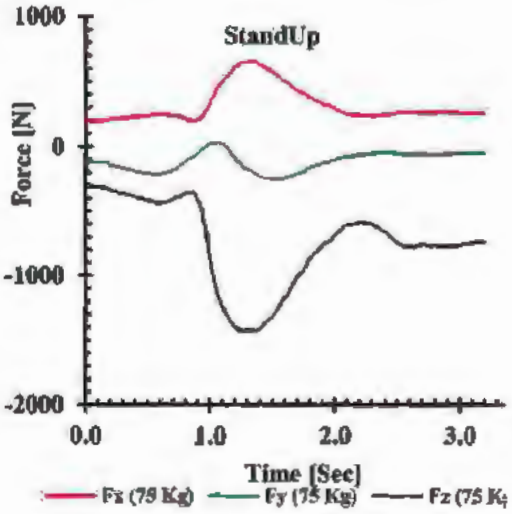

(d) Stand up

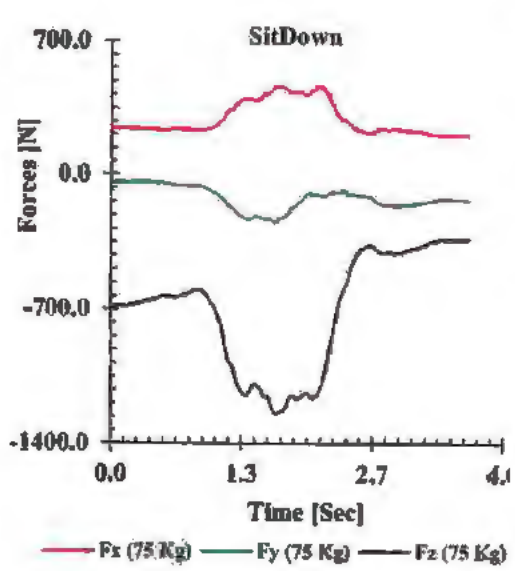

(e) Sit down

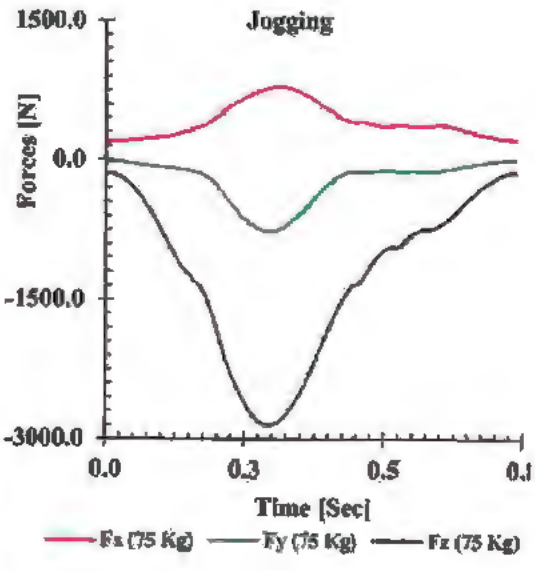

(f) Jogging

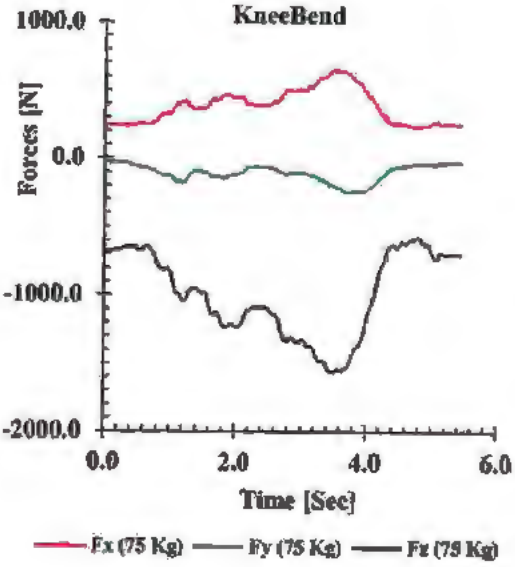

(g) Knee Bend

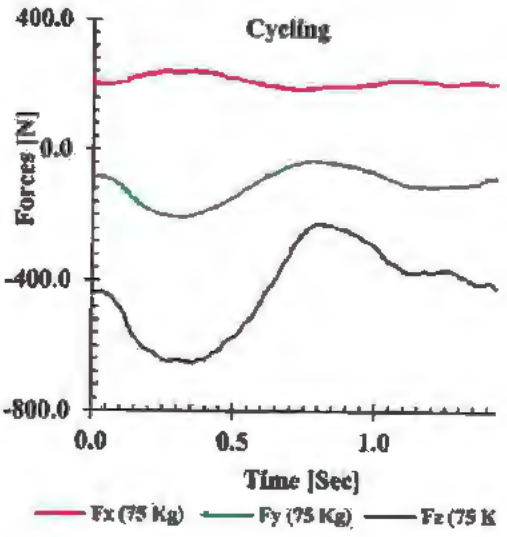

(h) Cycling

Figure 5-5: Measured Forces for 75 kg

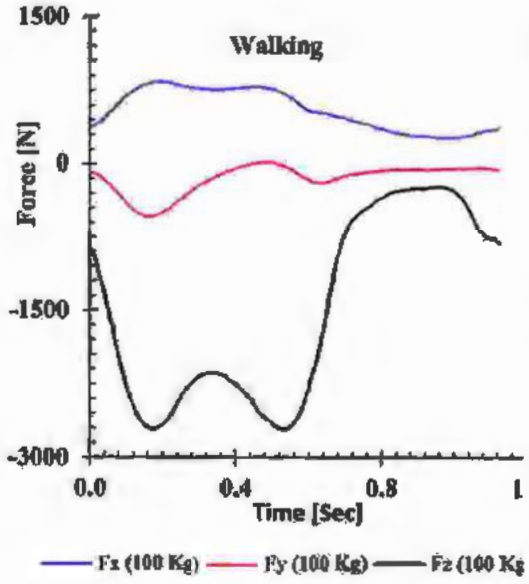

(a) Walking

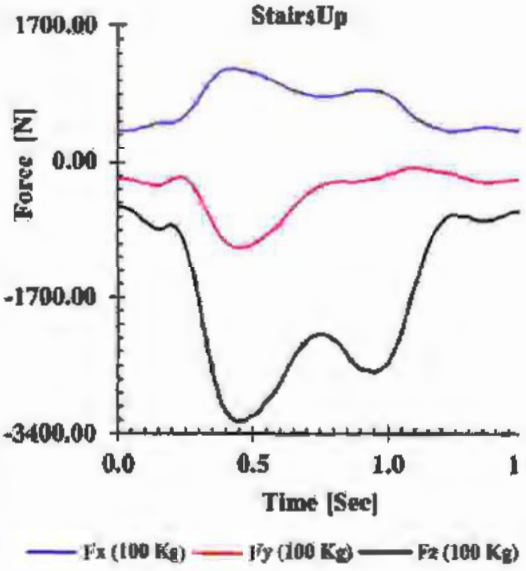

(b) Stairs up

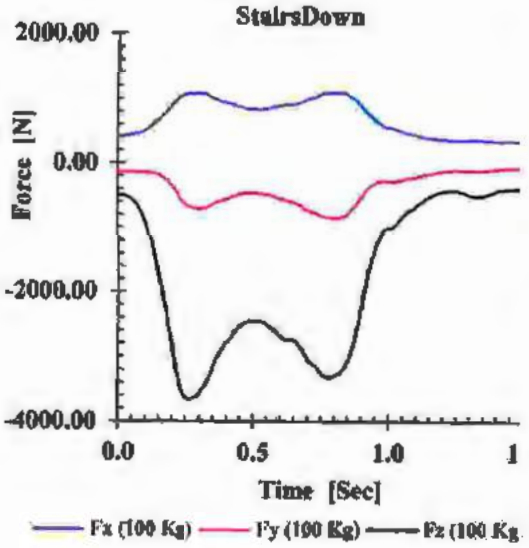

(c) Stairs down

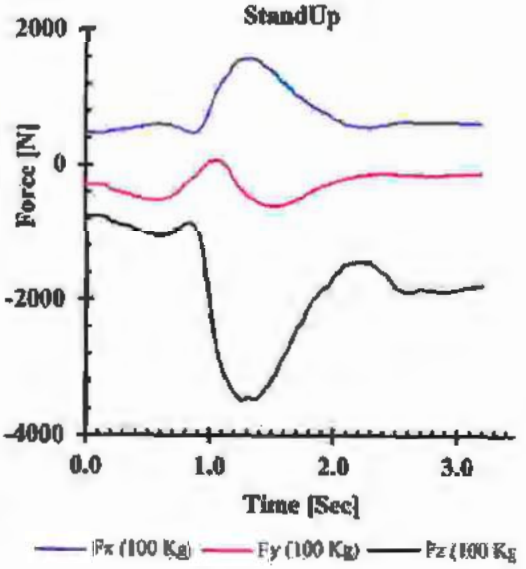

(d) Stand up

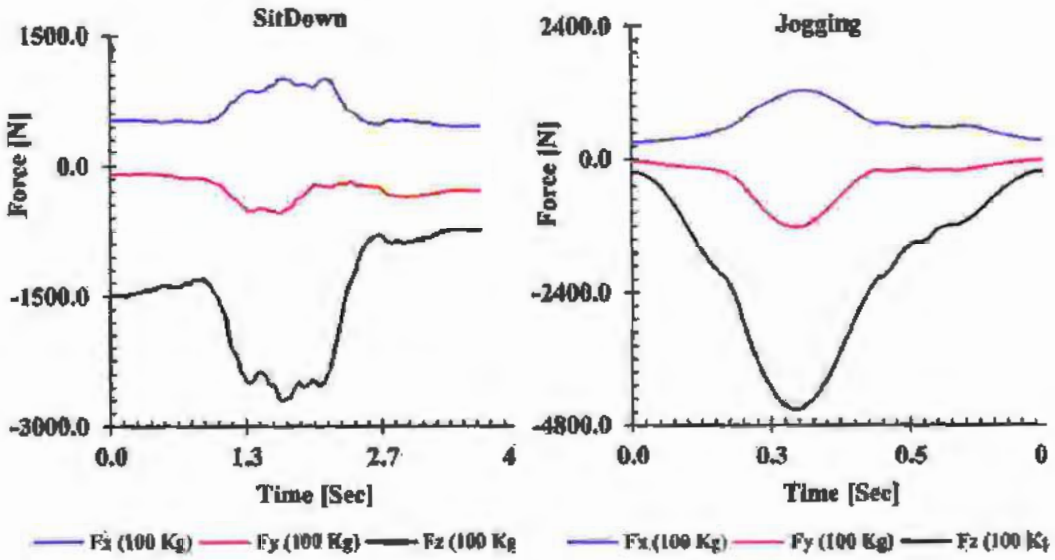

(e) Sit down

(f) Jogging

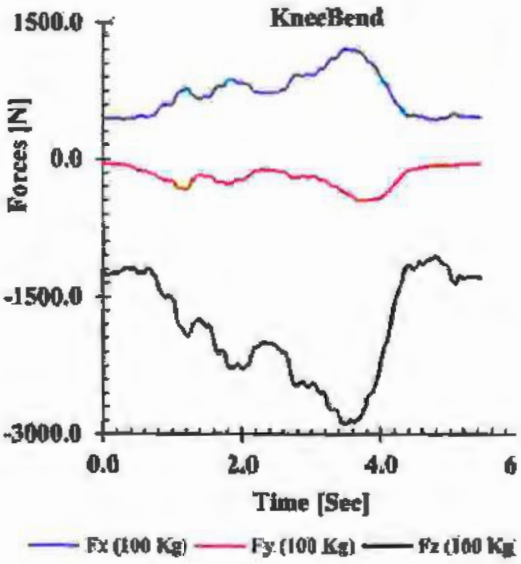

(g) Knee Bend

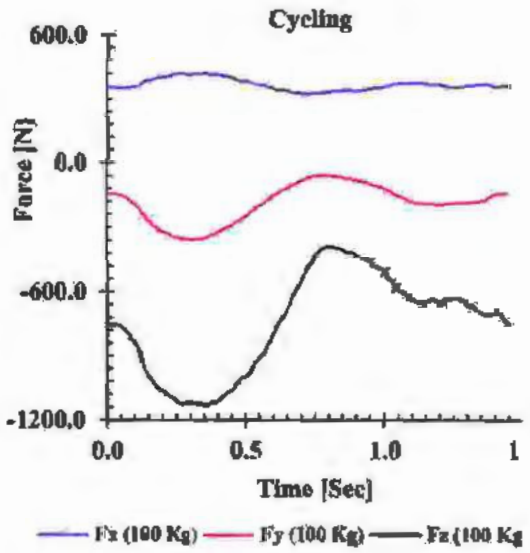

(h) Cycling

Figure 5-6: Measured Forces for 100 kg

5.4 Transient structural analysis results

The contour plot of maximum von Mises stress on the hip implant for Ti-27Nb during different activities for the 75 Kg and 100 Kg body weight subjects is shown in Figure 5-7 and Figure 5-8 respectively.

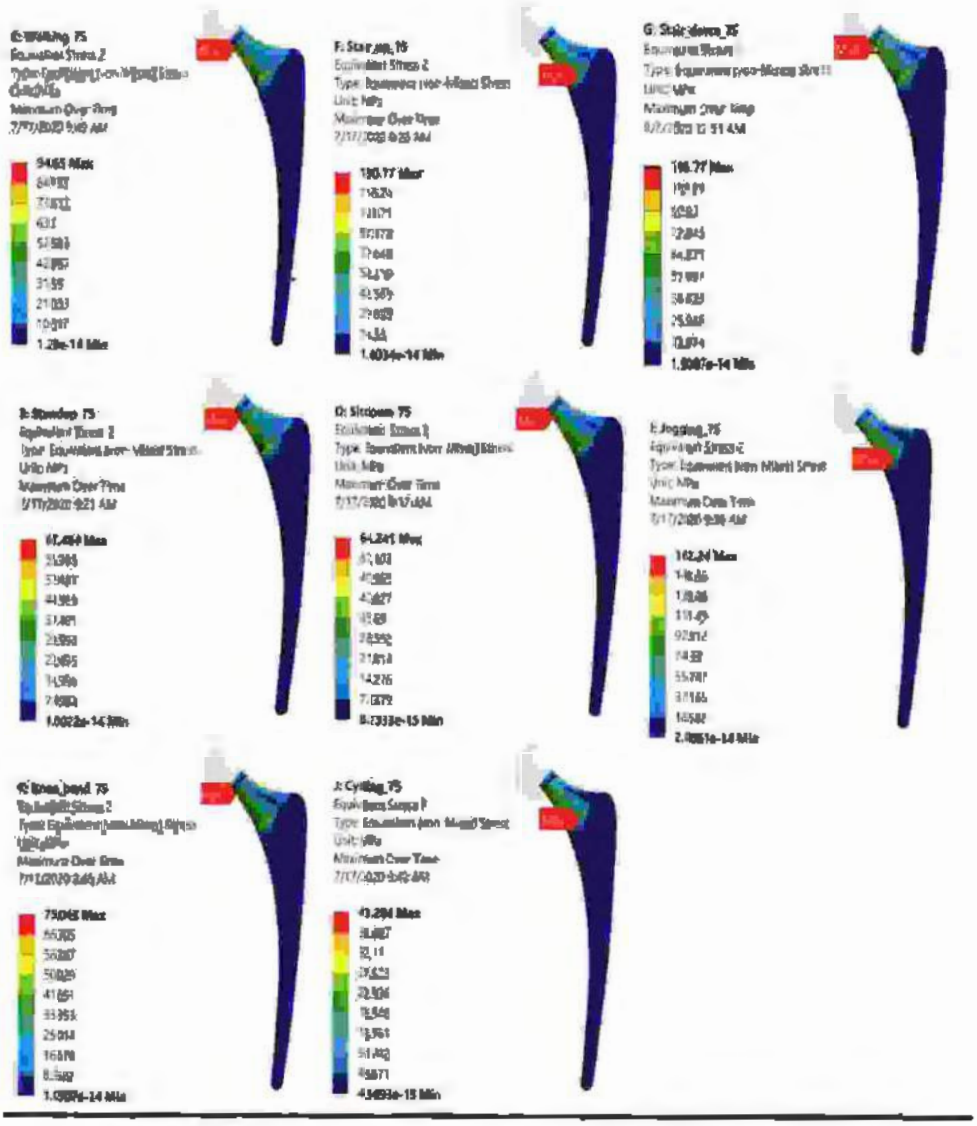

Figure 5-7:Maximum von Mises Stress for all activities (75kg)

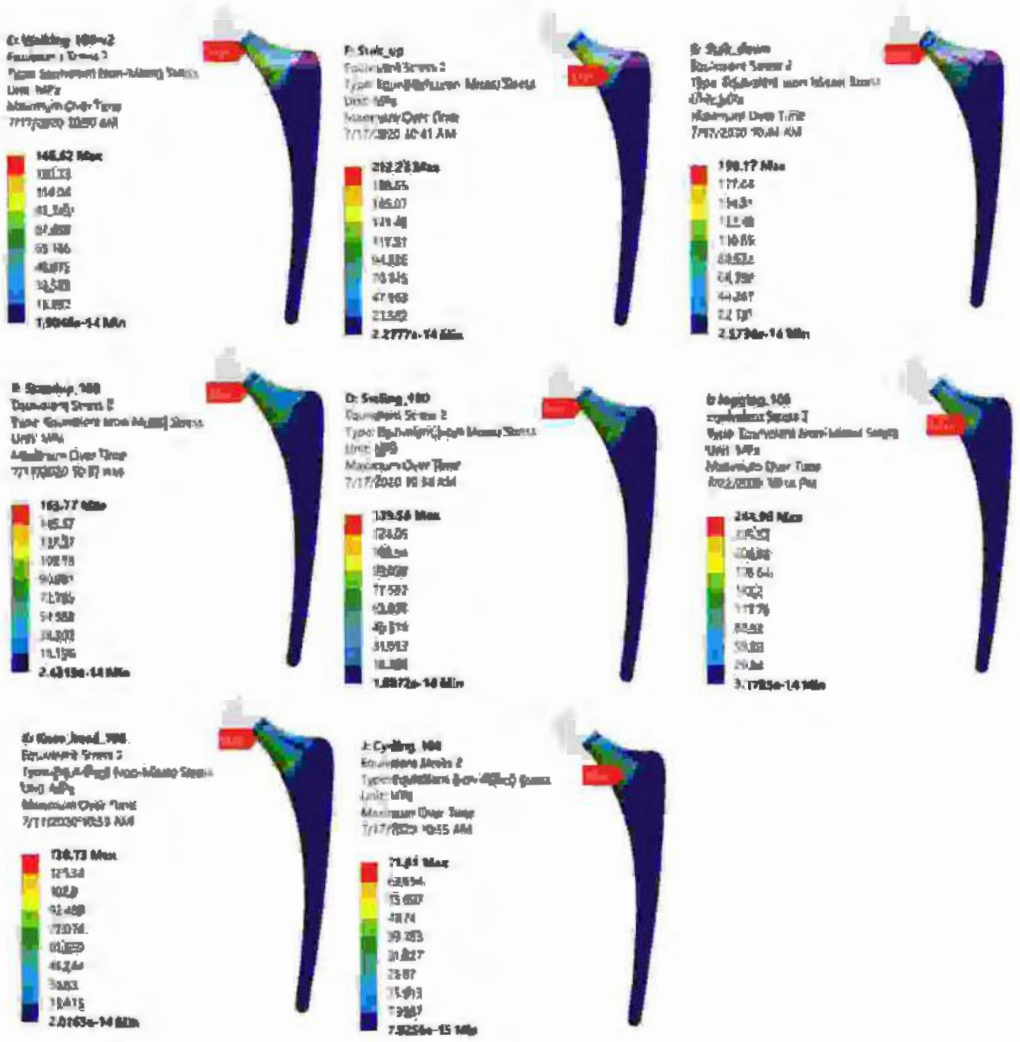

Figure 5-8:Maximum von Mises Stress for all activities (100 Kg)

The maximum value of Von Mises stress occurs in the neck region for both 75 Kg and 100 Kg body weight. Although its position somewhat changes between activities, but it does not cross the neck region. The location of maximum stress is near the circular top portion of the neck region for walking, stair down, stand up, set down and knee bend activities. Whereas for the stair up, jogging and cycling activities the location of maximum stress is shifted to bottom elliptical section of the neck region. This is because the dominant load component for all the activities is the load in z axis. However, the other two load components (i.e. load in x and y axis) also contributes to the overall stress in the implant. The load profiles

shown in Figure 5-7 and Figure 5-8 clearly indicate that for activities where the relative contribution of x and/or y-components of loads is higher, the location of maximum stress is shifted to the bottom elliptical section of neck region and vice versa.

The magnitude of von Mises stress changes between activities and for change in body weights from 75 to 100 Kg as shown in Figure 5-9.

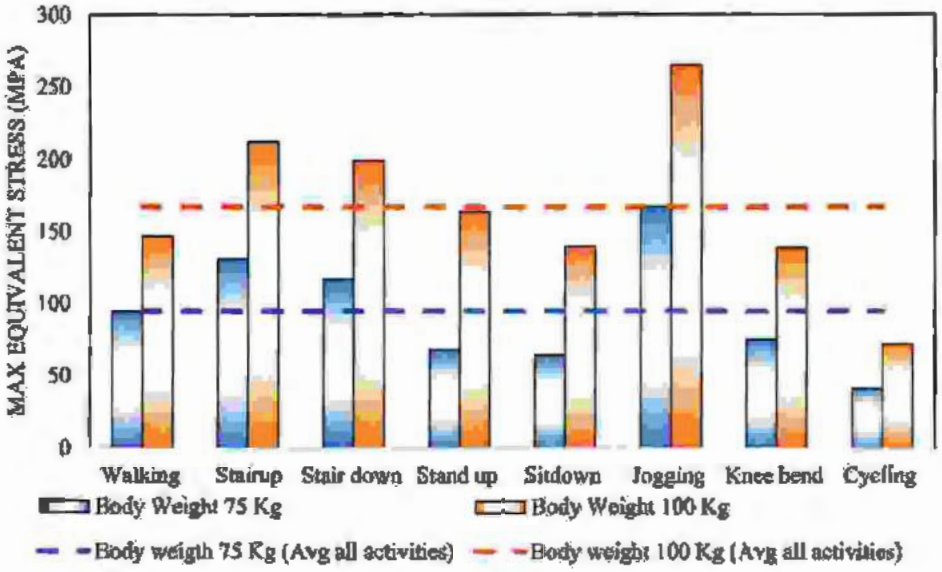

Figure 5-9: Von Mises Stress during different activities of 75 and 100 Kg body weight.

The maximum and minimum values of maximum Von Mises stress is observed for the jogging and cycling activities respectively for both the body weight categories. The values of max Von Mises stress for 100 Kg body load case is significantly higher for all activities. The stair up, stair down and jogging activities produces Von Mises stresses greater than the average value for all activities for both the body weight cases. Whereas, the value of max Von Mises stress for the rest of six activities lie below the average value for all activities.

The von Mises Hencky theory is utilized to evaluate failure of the hip implant against static loads imposed due to various activities. This theory is based on the concept that a combination of principal stresses would cause failure if the maximum equivalent stress exceeds yield

strength of the material (i.e. $\sigma_e/S_y < 1$). Figure 5-10 shows the Factor of Safety (FOS) contours based on maximum equivalent stress theory for various activities of 75 Kg body weight.

Figure 5-10: FOS contours based on maximum equivalent stress theory for all activities (75kg)

Table 5-3: FOS for all activities of 75 and 100 Kg body subject weights (Untreated Sample).

Activity	Factor of Safety		% Reduction in FOS due to weight increase
	75 Kg. Subject	100 Kg. Subject	
Walking	8	5.1	36.3%
Stair up	5.8	3.5	39.7%
Stair down	6.5	3.8	41.5%
Stand up	11.2	4.6	58.9%
Sit down	11.8	5.4	54.2%
Jogging	4.5	2.8	36.7%
Knee bend	10	5.4	46.0%
Cycling	18.3	10.5	30.0%

A quantitative summary of FOS for all activities is provided in Table 5-3. The minimum values of FOS are observed for the case of jogging activity as 4.5 and 2.8 for the body weights of 75 and 100 Kg respectively. The body weight case of 100 Kg gives an indication that this implant design may be vulnerable to failure in the jogging activity with further higher body weights. However, in general the evaluated implant design is found to be safe against all the simulated load cases. Additionally, the values of FOS varies between the simulated activities as well as with change in the subject body weights. For the 75 Kg body weight case the minimum (Min), maximum (Max) and average (Avg) values of FOS are 4.5, 18.3 and 9.5 respectively. Whereas, for the body weight case of 100 Kg the Min, Max and Avg values of FOS are 2.8, 10.5 and 5.13 respectively. The increase in body weight from 75 to 100 Kg reduces the FOS by 42.9% on average for all activities. The Max reduction in FOS is observed for the standup and sit down activities with values of 58.9% and 54.2% respectively when the body weight is increased from 75 to 100 Kg. The simulated time histories of von Mises stress for each activity for 75 kg and 100 kg subjects are shown in Figure 5-11.

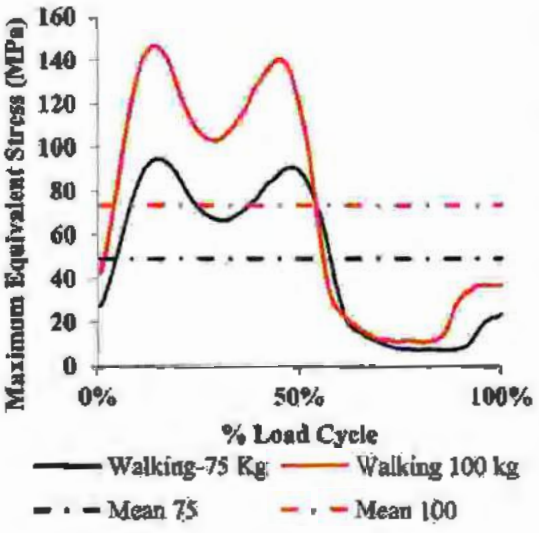

(a) Walking

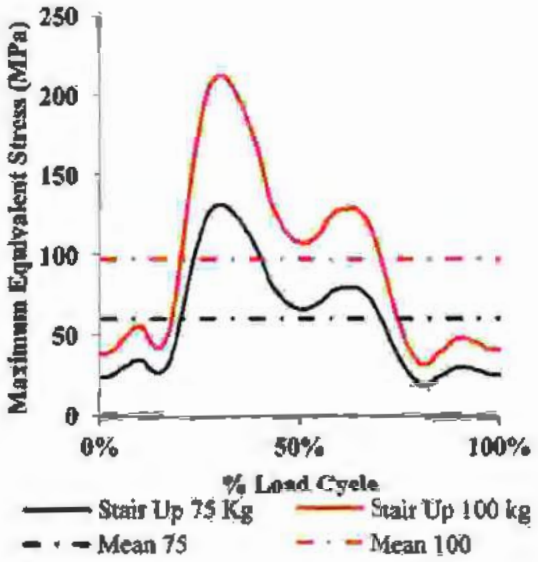

(b) Stair Up

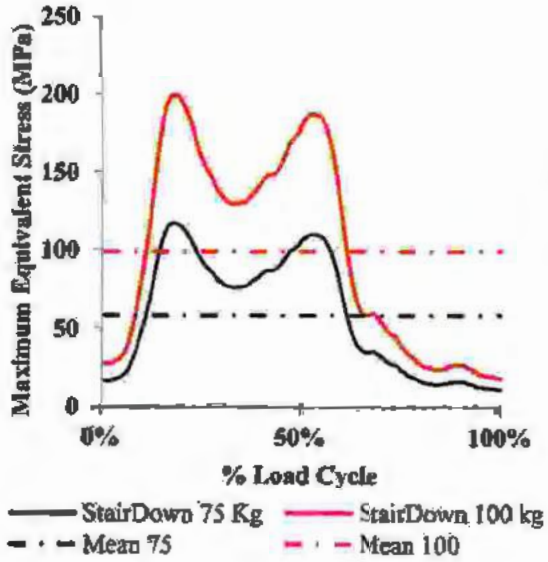

(c) Stair down

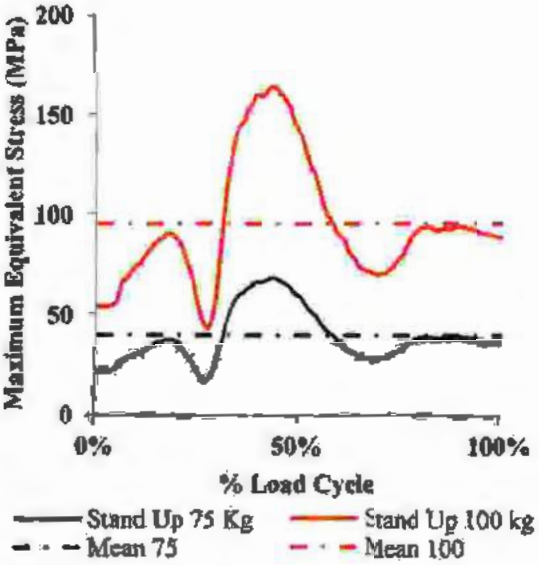

(d) Stand up

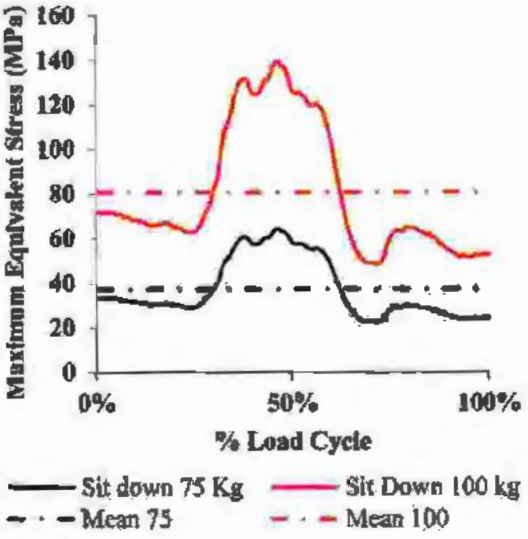

(e) Sit down

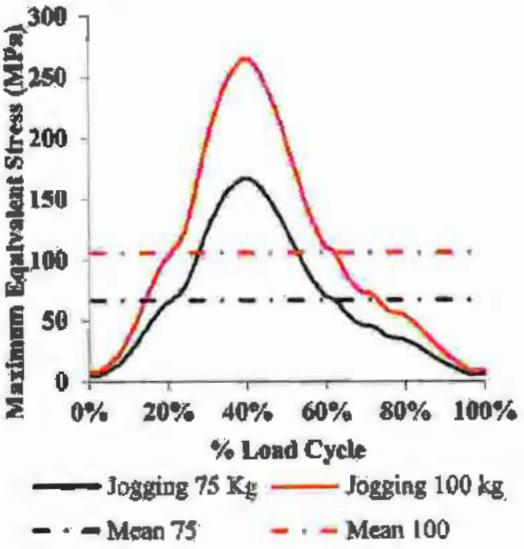

(f) Jogging

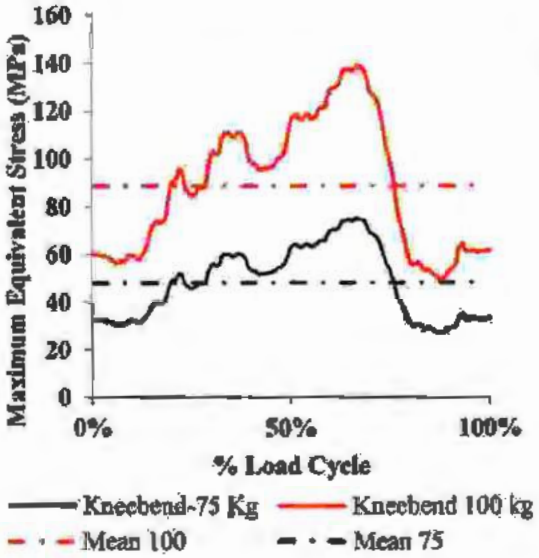

(g) Knee bend

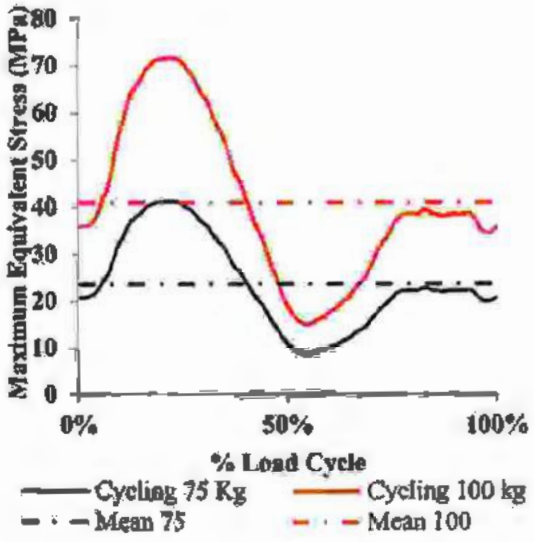

(h) Cycling

Figure 5-11: Cyclic variation in Von Mises Stress for 75kg and 100 kg for different activities

The von Mises stress graphs (Figure 5-11) show that stress on the hip implant during each activity is cyclic in nature. Therefore, the fatigue behavior of the implant should be characterized to establish the influence of stress variation in terms of fatigue parameters. The quantitative representation of mean and alternating stress for all activities for the 75 and 100 subjects is shown in Table 5-4.

Table 5-4: Alternating and mean stresses for 75 and 100 kg subjects for all activities.

Description	Body Weight Kg	Mean Stress (MPa)	Alternating Stress (MPa)	Increase* in Mean Stress (%)	Increase* in Alternating Stress* (%)
Walking	75	48.99	87.55	49.8%	54.9%
	100	73.39	135.61		
Stair up	75	59.8	111.45	62.3%	62.3%
	100	97.05	180.87		
Stair down	75	57.95	106.34	70.6%	70.6%
	100	98.84	181.38		
Stand up	75	39.09	50.16	142.6%	142.7%
	100	94.84	121.72		
Sit down	75	37.24	41.79	117.3%	117.2%
	100	80.91	90.78		
Jogging	75	67.08	162.29	58.4%	58.4%
	100	106.28	257.12		
Knee bend	75	48.02	48.24	84.9%	84.9%
	100	88.77	89.18		
Cycling	75	23.62	32.64	73.4%	73.5%
	100	40.96	56.62		

* Increase denotes the % increase in mean and alternating stresses for the 100 kg body weight with respect to 75 kg body weight.

The increase in subject weight (i.e., from 75 to 100 Kg) considerably increases the mean stress $(\sigma_{Max} + \sigma_{Min}/2)$ and alternating stress $(\sigma_{Max} - \sigma_{Min}/2)$ on the hip implant for all activities. However, the most prominent effect of weight increase on mean and alternating stresses is in the stand up and sits down activities with increases of 142% and 117% respectively. An increase in the tensile mean stress under uniaxial load would decreases fatigue

strength of the hip implant while the fatigue strength would also decrease with increasing alternating stress. From the equivalent stress histories depicted above Figure 5-11, it is clear that increase in the subject weight increases both the mean and alternating stresses. This increase in mean and alternating stress may influence the fatigue life of the implant. Therefore, the subject weight is undoubtedly one of the most dominant parameters to influence the fatigue life of implant. Patients with implanted hip may be educated about this significant influence of increase in body weight on the susceptibility of implants to fatigue failure.

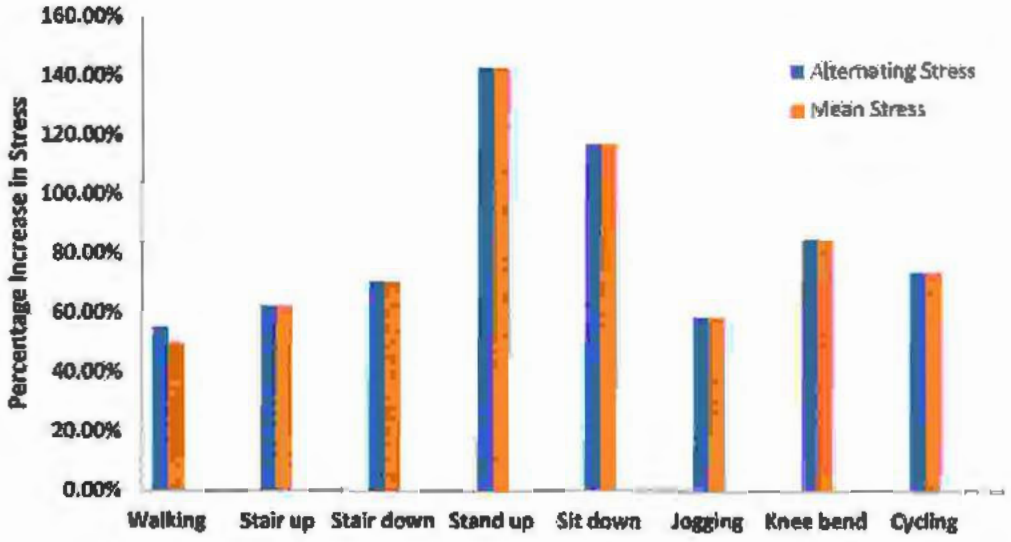

Figure 5-12:Percentage increase in stress due to weight increase

5.5 Fatigue character of the Hip Implant

Stress life fatigue analysis of the selected implant design is conducted to characterize the fatigue behavior of hip implant and quantify the effect of variation in mean and alternating stresses on the fatigue life. Generally, fatigue analysis can be accomplished through (i) Stress Life (ii) Strain Life and (iii) Fracture Mechanics based approaches. The strain life approach computes the fatigue life through the determination of crack initiation. The fracture mechanics approach assumes of predetermined crack of known size and models crack growth to define the crack/fatigue life. The fatigue life is a sum of the component life from crack initiation to crack propagation till a critical size. Although, the strain life approach is

widely used but it is more suited to characterize low cycle fatigue. Contrarily, the stress life approach does not differentiate between the crack initiation and crack growth in determining the fatigue life of components. This approach is based on material S-N curves and is more suited to fatigue situation involving higher number of cycles($i.e. > 10^5\ cycles$). Therefore, in this thesis stress life fatigue analysis approach is adopted for to characterize the fatigue behavior of selected implant design. Figure 5-11 of stress histories plots show that the implant experiences alternating stress, but the mean stress is not zero. This is a case of fluctuating stress subcase tensile stress with tensile mean ($0 < R < 1$). R values for all activities for the conducted simulation is as in Table 5-5

Table 5-5: R-Values for all activities

S.No	Activity	R value	
		75 Kg	100 Kg
1	Walking	0.124711	0.124711
3	Stairup	0.196916	0.196916
4	Stair down	0.136137	0.136137
5	Stand up	0.24377	0.24377
6	Sitdown	0.305329	0.305329
7	Jogging	0.0809	0.080897
8	Knee bend	0.366803	0.366803
9	Cycling	0.410851	0.410851

Load cycles for all the activities Figure 5-11 show that the load is changing randomly, and the load ratio varies at every time step. This implies that the load is of variable amplitude. Additionally, the principal stress axes of the load are not changing with load variation. So, the load is assumed to be proportional load. The loading diagram also show that mean stress is present for all activities as shown in Figure 5-11Therefore, mean stress correction is required to be employed. But the experimental (S-N) data is only available for single mean stress. Therefore, the Gerber empirical relation is employed to account for the mean stress correction. The Gerber empirical relation is mathematically expressed as:

$$\frac{\sigma_{Alternating}}{S_{Endurance\ Limit}} + \left[\frac{\sigma_{Mean}}{S_{Ultimate\ Strength}}\right]^2 = 1 \qquad (5\text{-}3)$$

The Gerber relation is used for analyzing the Ti-27Nb material. The experimental S-N data utilized for analysis in this thesis is obtained using uniaxial loading, while real life loading may be multiaxial. Therefore, multiaxial stress correction is required to be made in such a situation. The Stress state of components in FE analysis is presented through contours of Bi-axiality defined as the ratio of the smallest principal stress to the largest principal stress with principal stress near zero ignored. Biaxiality indication contours of the hip implant analyzed for 75 kg and 100 kg are shown in Figure 5-13 and Figure 5-14 . Biaxiality value of zero represents the case of pure uniaxial stress state, while a value of 1 represents a pure biaxial stress state. The contour plot show that all activities have almost similar maximum value of biaxiality of about 0.9. The maximum value is represented by red color but its part in the overall contour is almost negligible. Majority of the implant is in green yellow color representing biaxiality of (-0.1 to 0.2) to indicate that most part of the implant is in a uniaxial stress state. However, small traces of blue color in a narrow strip near the implant shoulder show areas of shear stress. The lowest value of biaxiality is about -0.9 for all activities to indicate a very small area of shear stress with pure shear stress reaching at a value of -1. Therefore, we can safely assume that the evaluated implant design and activities represent the case of uniaxial stress state.

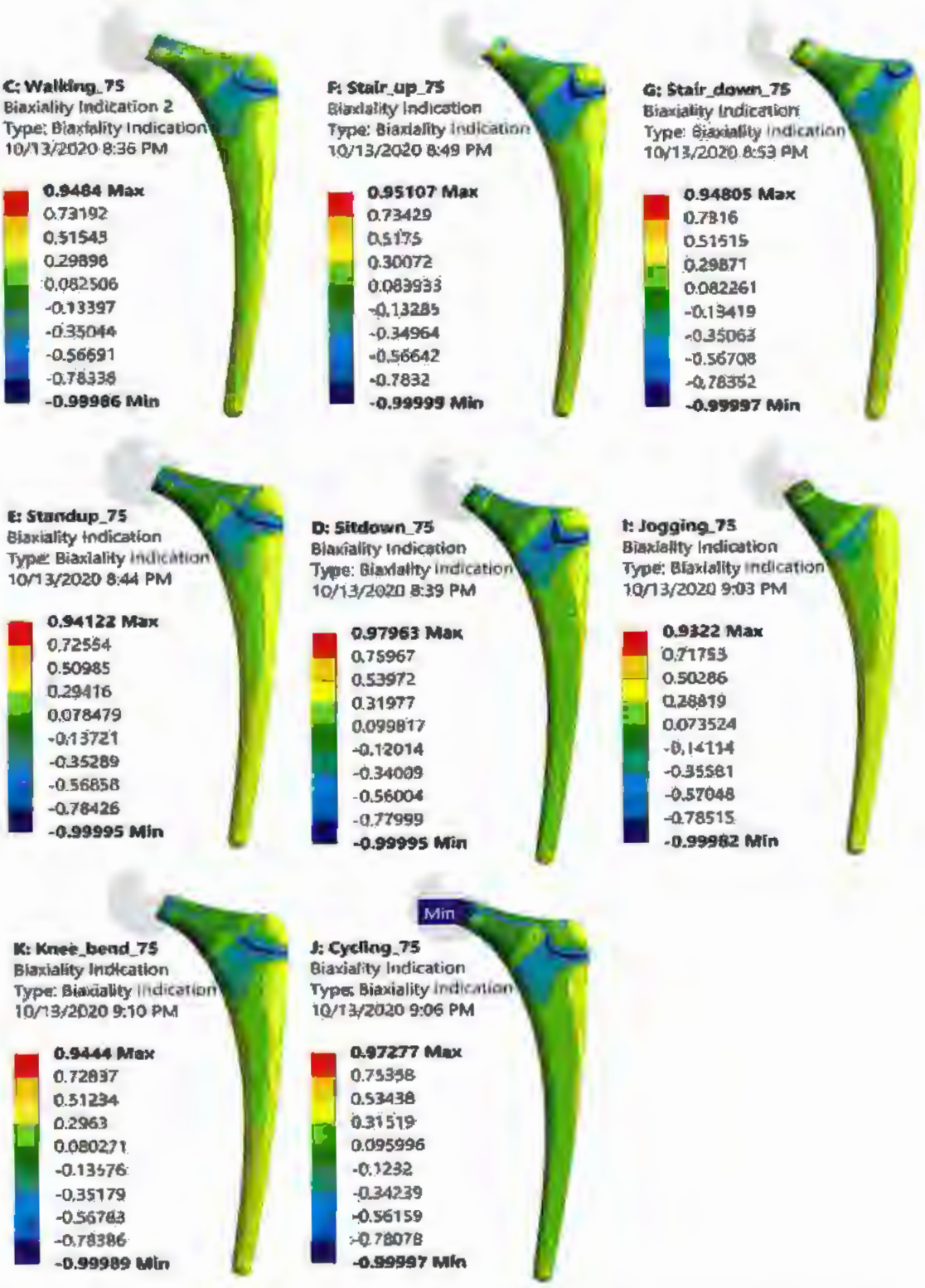

Figure 5-13:Bi axiality Indication contour of different activities for body weight of 75 Kg

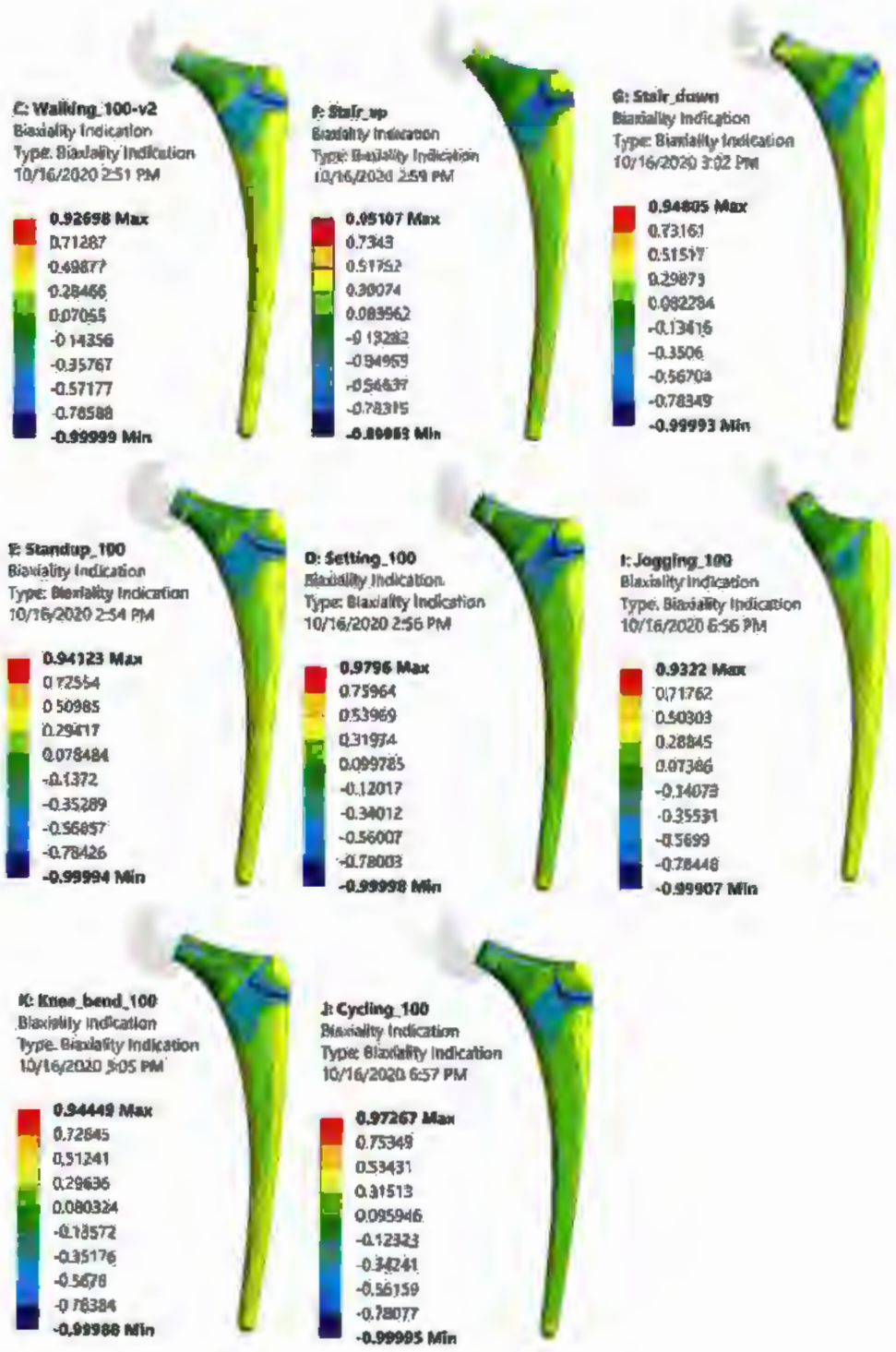

Figure 5-14: Bi axiality Indication contour of different activities for body weight of 100 Kg

Additionally, a combined look into the biaxiality contour and fatigue Factor of Safety. Figure 5-13 and Figure 5-15 show that the critical location relatively more vulnerable to failure is in the area of uniaxial stress.

Table 5-6: Expected load cycles of each activity in 20 years life span.

S.No	Activity	Time for single load cycle [sec]	Total Time of Activity per day [sec]	Cycles per day [sec]	Cycles in 20 years [Number]
1	Walking	1.123	4950	4408	3.2E+07
2	Stair Up	1.505	204	136	9.9E+05
3	Stairs Down	1.489	204	137	1.0E+06
4	Stand UP	3.195	10951	3427	2.5E+07
5	Sit Down	3.628	168	46	3.4E+05
6	Jogging	0.737	7	10	7.1E+04
7	Knee Bend	5.439	240	44	3.2E+05
8	Cycling	1.449	499	344	2.5E+06

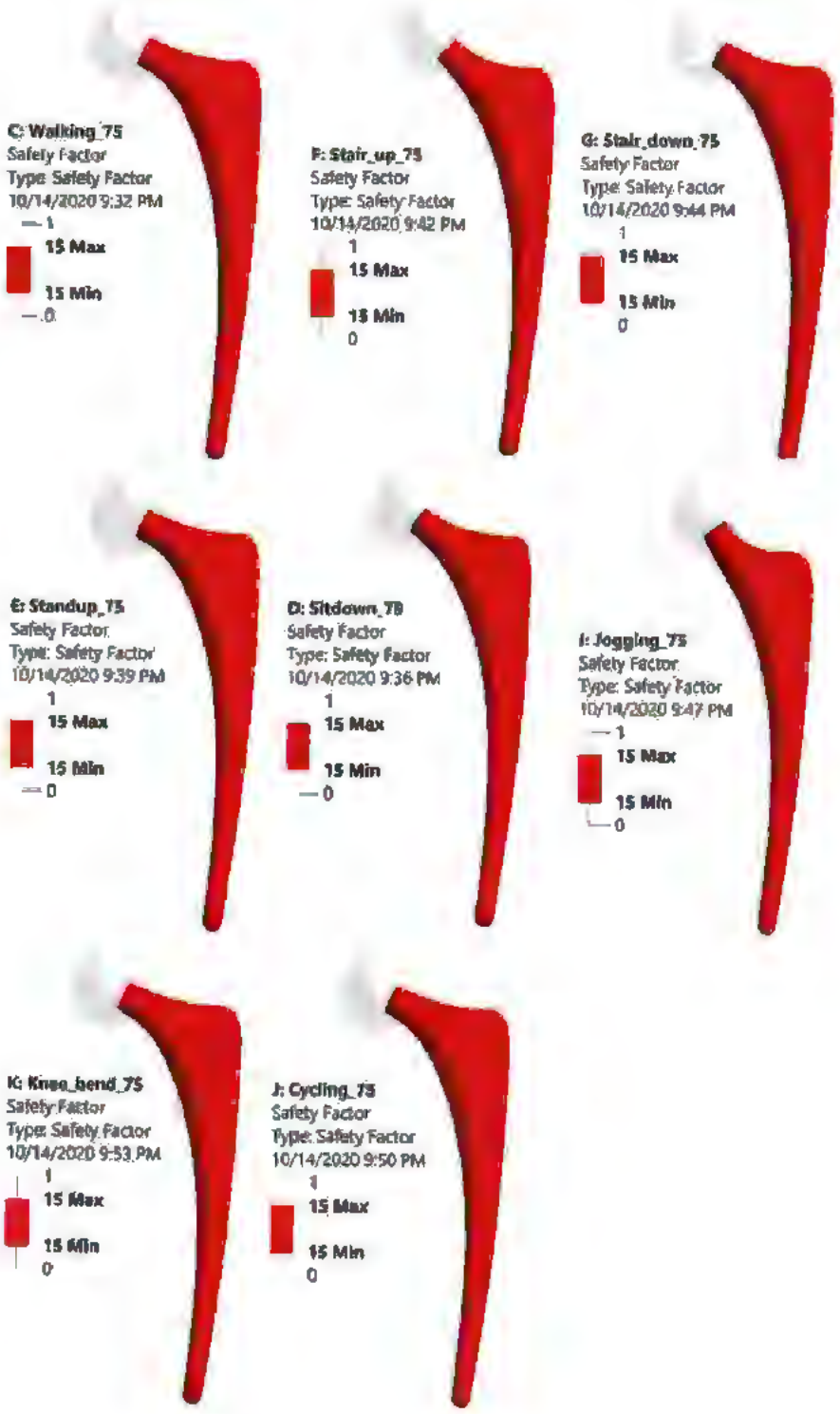

Figure 5-15:Fatigue FOS contour of different activities for body weight of 75 Kg.

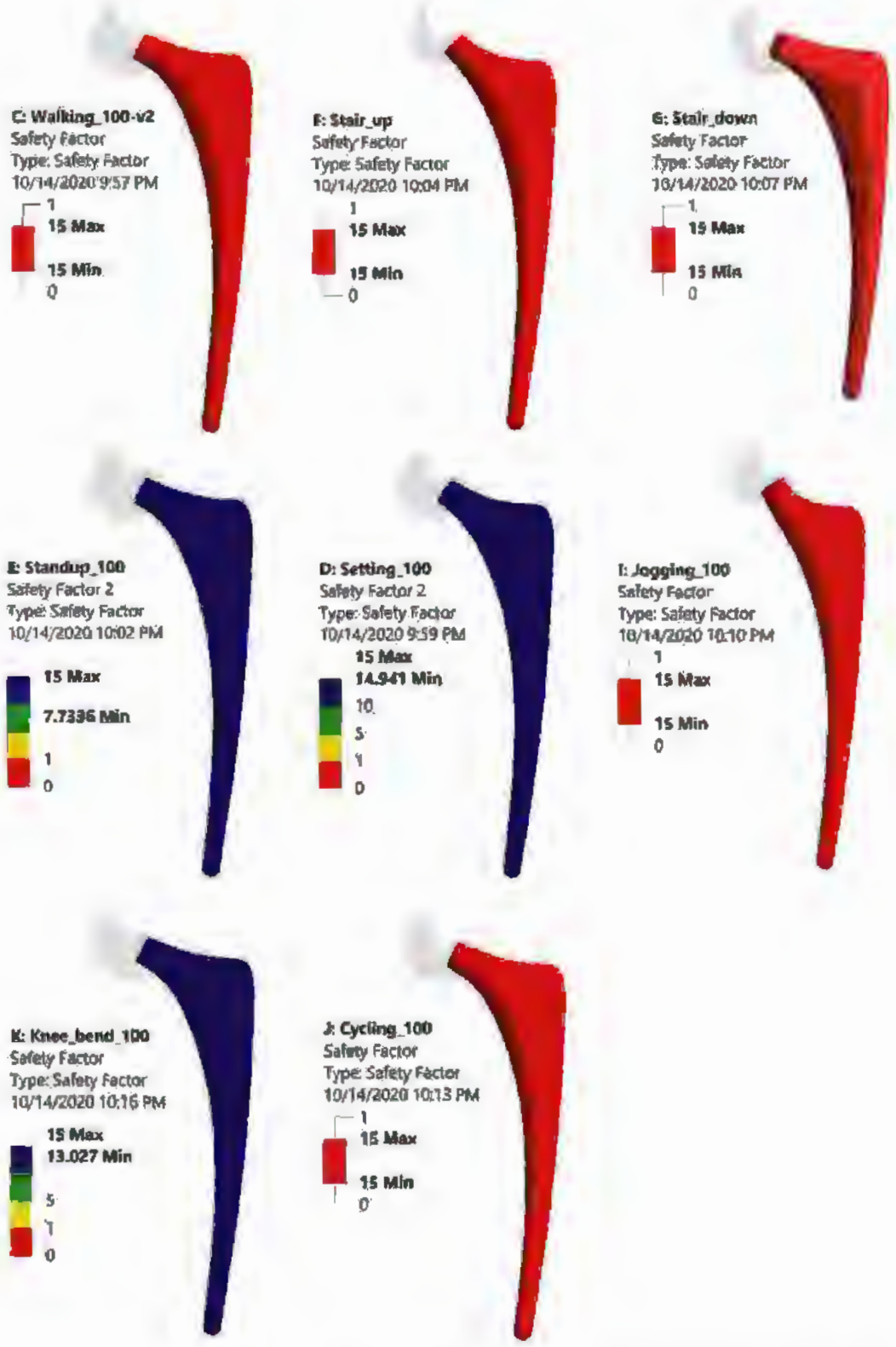

Figure 5-16:Fatigue FOS contour of different activities for body weight of 100 Kg.

The results of the analysis are based on the number of load reversals for each activity in 20 year service life computed from the literature is as shown in Table 5-6 [190].

Therefore, S-N data collected through torsional loading is not required for the analysis presented in this research. Contrarily, if the minimum FOS was located either in the area of shear stress or biaxial stress. Then experimental material S-N data collected through torsional loading and at different load axis would have been required. Figure 5-15 and Figure 5-16 show that the location of minimum FOS is similar to the location of maximum equivalent stress and it is located in the neck region. Table 5-7quantifies the reduction in FOS due to increase in body weight and SBF treatment.

Table 5-7:Reduction in FOS due to body weight and SBF

FOS (Min)						
S.No	**Activity**	**Body weight**	**Un-treated**	**Decrease due to Body weight [%]**	**SBF treated**	**Decrease due to SBF treatment [%]**
1	**Walking**	**75**	15.0	0.0%	15.0	0.00%
		100	15.0		15.0	0.00%
2	**StairUp**	**75**	15.0	0.0%	15.0	0.00%
		100	15.0		15.0	0.00%
3	**StairsDown**	**75**	15.0	0.0%	15.0	0.00%
		100	15.0		15.0	0.00%
4	**StandUP**	**75**	15.0	48.4%	15.0	0.00%
		100	7.7		7.6	2.00%
5	**SitDown**	**75**	15.0	0.4%	15.0	0.00%
		100	14.9		14.7	1.70%
6	**Jogging**	**75**	15.0	0.0%	15.0	0.00%
		100	15.0		15.0	0.00%
7	**KneeBend**	**75**	15.0	13.5%	15.0	0.00%
		100	13.0		12.9	1.30%
8	**Cycling**	**75**	15.0	0.0%	15.0	0.00%
		100	15.0		15.0	0.00%

The minimum value of fatigue FOS is greater than 15 for all activities for 75 Kg body weight subject. Similarly, for the 100 Kg body weight subject the value of fatigue FOS is quite higher except the standup activity with a minimum value of 7.7. this activity also has the maximum reduction in FOS (48 %) due to increase in body weight. Although a reduction of 13.5 % has also been observed for the knee bend activity when the body weight is increased from 75 to 100 Kg. Contrarily the influence of SBF treatment on the fatigue FOS in 20-year life span is not much prominent. Although a reduction of 1-2% has been observed for standup, sit-down and knee bend activities of 100 kg body weight.

Figure 5-17 and Figure 5-18 show the contours of fatigue life obtained from the fatigue analysis of hip implant for subjects having 75 and 100 Kg body weights.

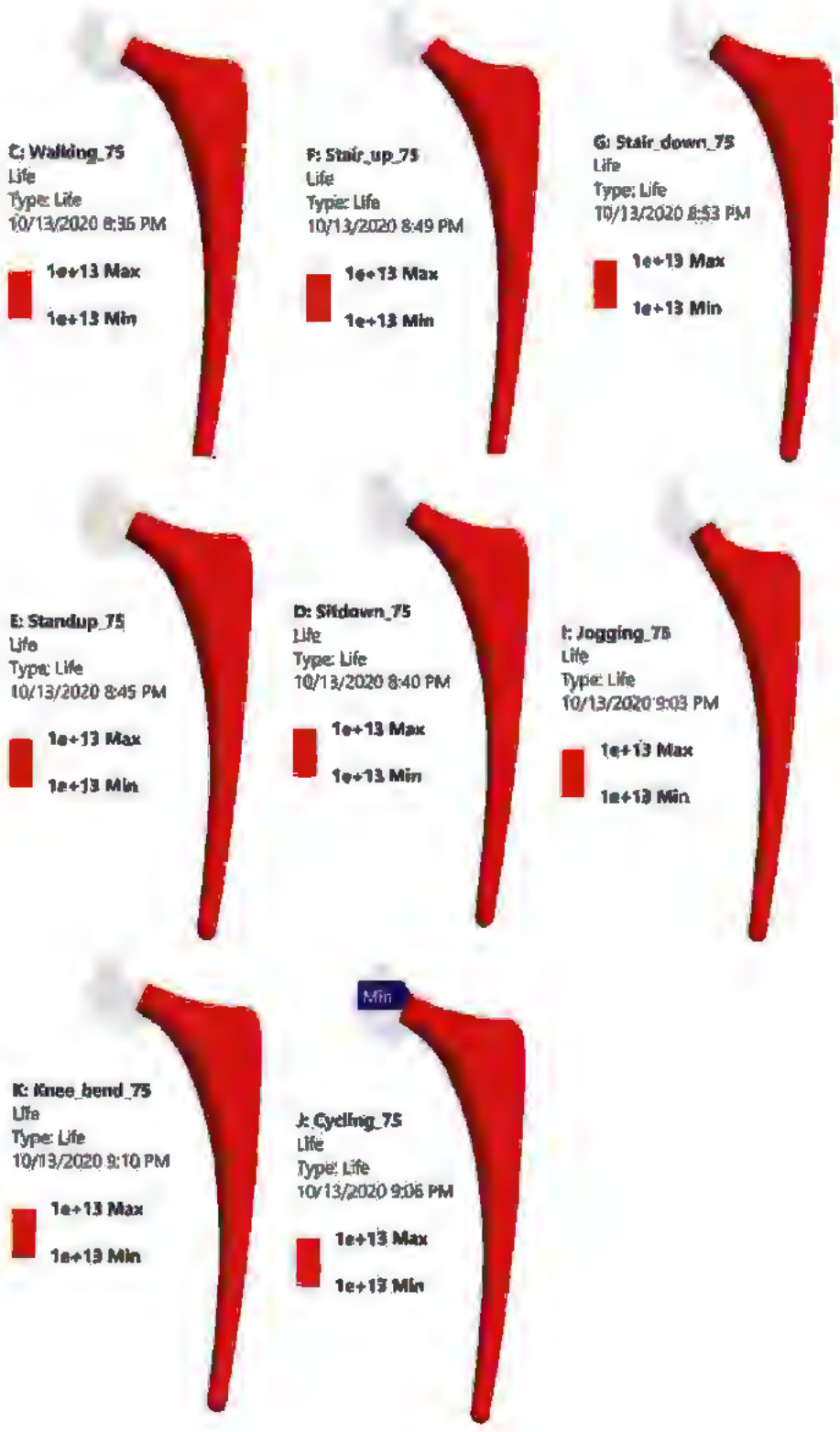

Figure 5-17:Fatigue life contour of different activities for body weight of 75 Kg.

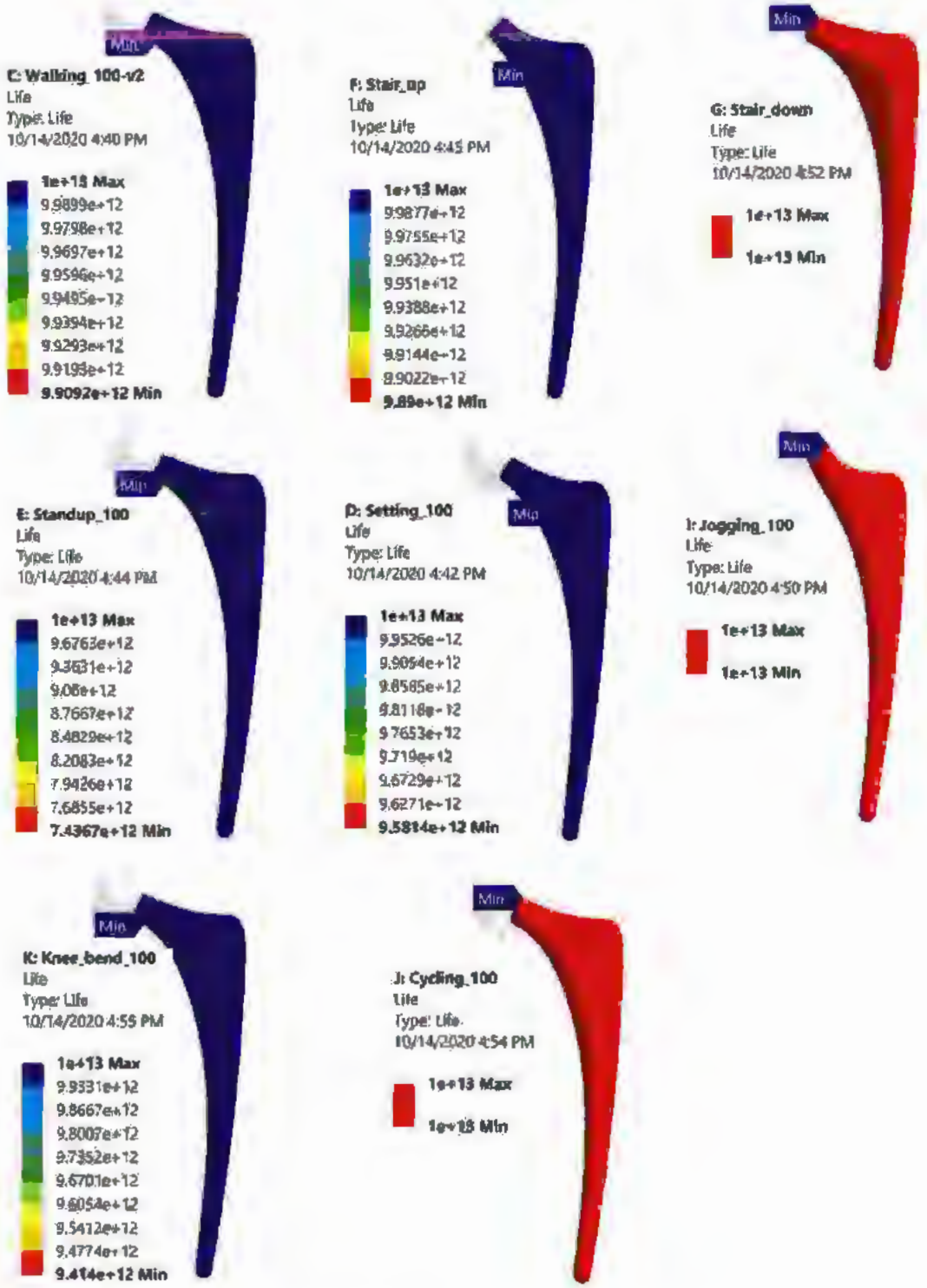

Figure 5-18:Fatigue life contour of different activities for body weight of 100 Kg.

These contours show that the evaluated implant design would sustain significantly higher number of load cycles than the number of load cycles occurring in design life of 20 years.

For the 75 Kg body weight subjects the implant would be safe against more than 1×10^{13} load cycles for all activities. Whereas, for the 100 Kg body weight subjects the implant would exhibit relatively shorter life expectancy for some activities like walking, stair up, standup, sit down and knee bend less fatigue life expectancy with number cycles ranging from $(7 \times 10^{12} - 9 \times 10^{12})$.

Similarly, for the case of SBF treatment for 75kg body weight, the fatigue life has not much varied for almost all the activities except the standup activity, where the fatigue life is reduced to a value of (9×10^{12}). For the case of 100 kg body weight, the SBF treatment has further reduced the fatigue life expectancy in the walking, stair up, standup, sit down and knee bend activities in the range $(5 \times 10^{12} - 9 \times 10^{12})$ load cycles. These results suggest that subject body weight and SBF treatment both have a reducing influence on the fatigue life of hip implant. This influence is significant for the increase in body weight, while not much pronounced for the SBF treatment. In any case the results clearly show that the evaluated implant design can easily withstand a far greater number of load reversal than that could happen in the design life expectancy of 20 years.

Figure 5-19 and Figure 5-20 show the contour plot of fatigue damage for all activities for 75 and 100 Kg body weight subjects.

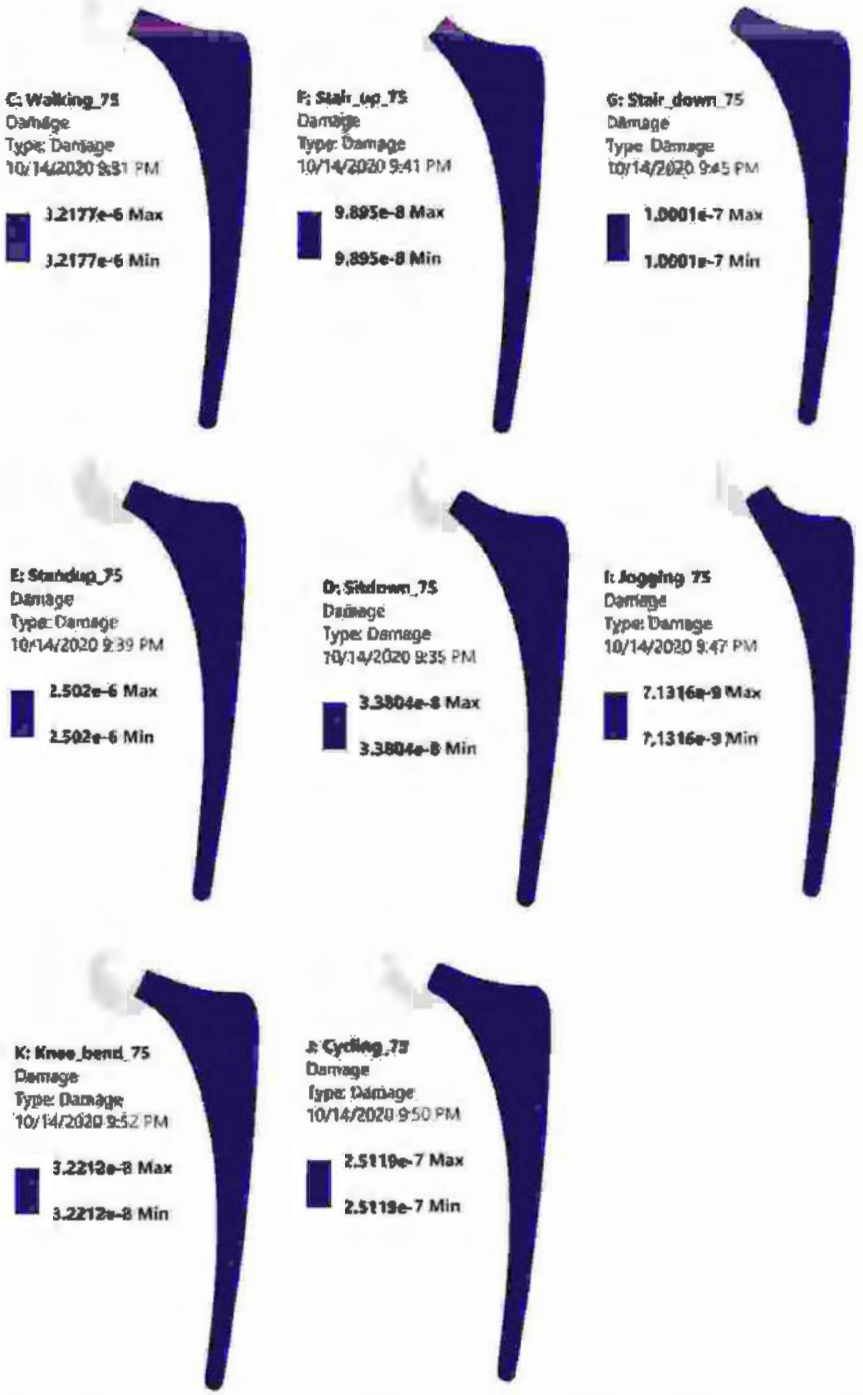

Figure 5-19:Fatigue damage contour of different activities for body weight of 75 Kg

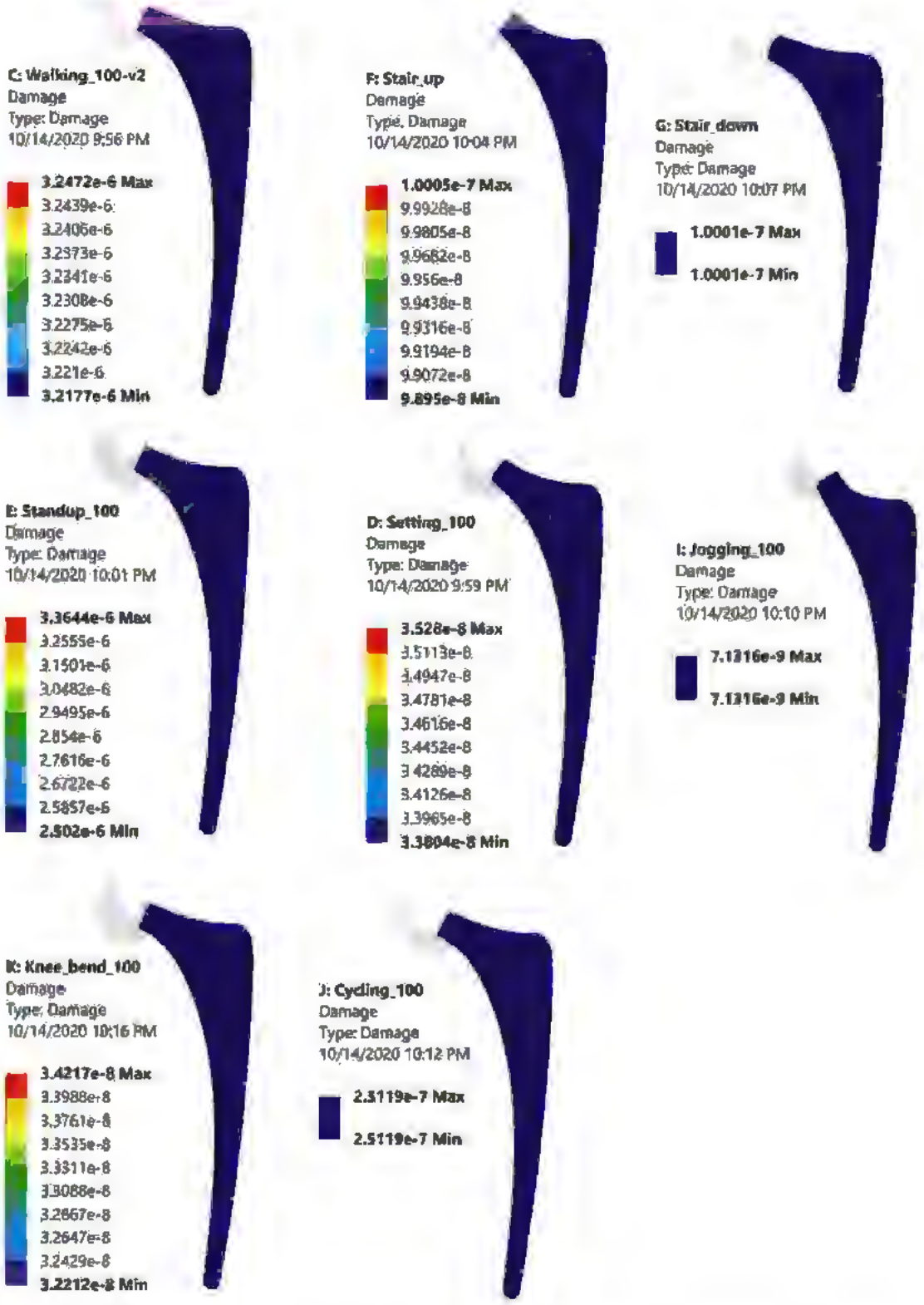

Figure 5-20: Fatigue damage contour of different activities for body weight of 100 Kg.

Damage (Max)						
S.No	Activity	Body Weight	Un-treated	Increase due to Body weight [%]	HBF treated	increase due to SBF treatment [%]
1	Walking	75	3.2E-06	1.0%	3.2E-06	0.6%
		100	3.2E-06		3.3E-06	1.7%
2	StairUp	75	9.9E-08	1.1%	9.9E-08	0.1%
		100	1.0E-07		1.0E-07	2.8%
3	StairsDown	75	1.0E-07	0.0%	1.0E-07	0.0%
		100	1.0E-07		1.0E-07	0.0%
4	StandUP	75	2.5E-06	25.6%	2.5E-06	0.9%
		100	3.4E-06		4.9E-06	45.4%
5	SitDown	75	3.4E-08	4.2%	3.4E-08	0.6%
		100	3.5E-08		3.8E-08	8.4%
6	Jogging	75	7.1E-09	0.0%	7.1E-09	0.4%
		100	7.1E-09		7.1E-09	0.4%
7	KneeBend	75	3.2E-08	5.9%	3.2E-08	0.7%
		100	3.4E-08		3.8E-08	9.9%
8	Cycling	75	2.5E-07	0.0%	2.5E-07	0.5%
		100	2.5E-07		2.5E-07	0.5%

The percentage increase in damage due to weight increase from 75 to 100 kg for individual activity is plotted in the Figure 5-21. It has been observed that walking activity will increase 1 % damage however the standup activity significantly increases the damage value up to 25.6 %. Sit down activity stair up and knee bend activity contributes individually in damage less than 6 %. The sit down activity contributes in the damage increase with a 4.2 %. The stair up activity increases the damage value with 1.1 %. Similarly, the knee bend activity adds up damage value to 5.9 %. The remaining activities like stair down, jogging and cycling do not increase the damage value. The increase of weight rises the accumulated damage value for all the activities up to 14.4 %. This value shows the dependence of weight on the design life of implant. For the 75 kg body weight subjects the increase in activity base and cumulative fatigue damage due to SBF treatment is almost negligible. However, for the 100 kg body weight

subject, the increase in fatigue damage is significant for activities of stand up, sit down and knee bend with percentage increases of 45, 8.4 and 9.9 respectively. Similarly, for the 100 kg body weight subject the cumulative fatigue damage increases by 22.3%. These results indicate that for higher stress levels due to increased body weights the influence of SBF may become more significant. It is therefore suggested that this research may be extended to subjects with higher body to fully ascertain this influence.

In the total cumulative damage the major contribution in the implant damage parameter is due to the equivalent alternating stress of the standup activity that is 145 % for increase of 75 Kg to 100 Kg body weight.

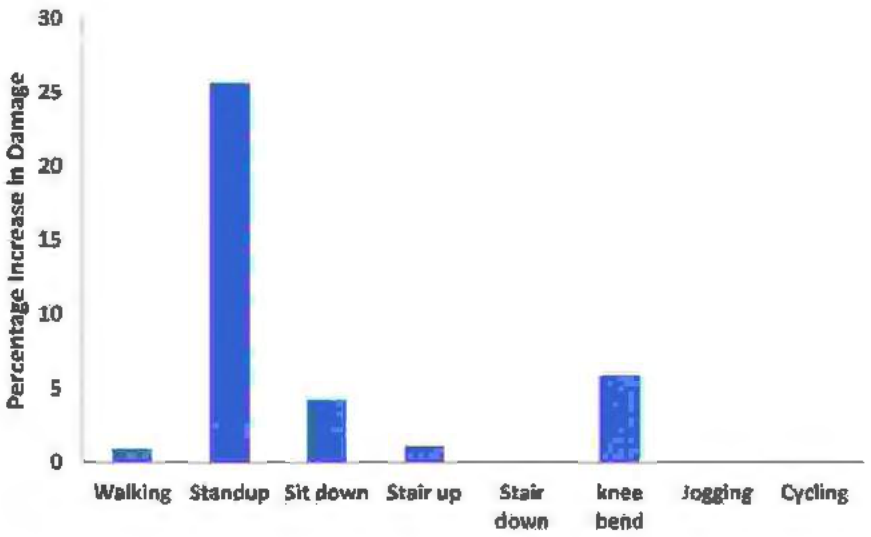

Figure 5-21: Percentage Increase of Damage due to Increase in Weight

In the preceding paragraph the percentage increase in damage was observed for each activity. The reason of increase in damage is due to the increase of alternating stress at the local neck region. The percentage increase of damage is plotted against the percentage increase of alternating stress due to increase in weight from 75 Kg to 100 Kg for each activity.

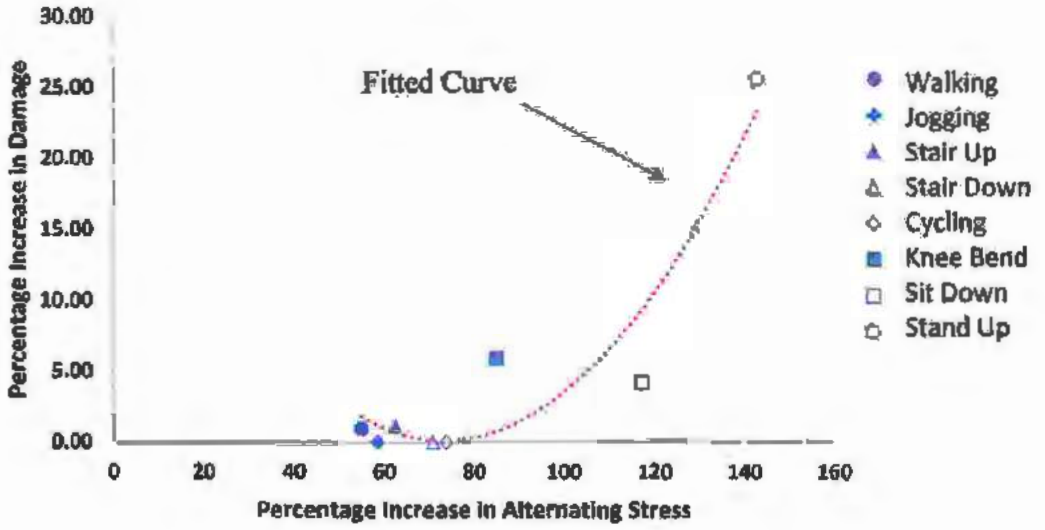

Figure 5-22 : Percentage Increase in Damage vs Percentage Increase in Alternating Stress

The line fitted in the data points is not linear rather it is two-degree polynomial. For the sit-down activity the percentage increase in alternating stress is 117 % and percentage increase in damage is 4.18 %. Further increasing the alternating stress to 140 % the damage increases significantly to 25.6 %. The polynomial relating the percentage of damage and alternating stress is as under:

$$\Delta D = 0.49\Delta\sigma_a^2 - 0.7132\Delta\sigma_a + .26241 \qquad (5\text{-}4)$$

In this equation ΔD is the percent increase in damage, $\Delta\sigma_a$ is the percent increase in alternating stress whereas the 0.49, 0.7132 and 0.26241 are the curve fitting parameters.

6 Conclusions and future directions

6.1 Conclusions

In this research the utilization of Ti-27Nb and Ti-25Ta as hip implant have been investigated using experimental and finite element analysis approaches. The mechanical behavior of the above materials were analyzed using tensile, fatigue life, fracture toughness, fatigue crack growth and hardness testing. All these tests were carried out using untreated and SBF treated samples. These tests results are used for FEA analysis of both the alloys for different routine activities for 75 kg and 100 kg body weights.

Following conclusions are drawn from the research.

1. The SBF treatment form an oxide layer on both Ti-27Nb and Ti-25Ta. The thickness of the oxide layers strongly depends upon the exposure time to the SBF. Therefore, the increase in the thickness of oxide layer is about twice the thickness of untreated specimen for SBF treatment of 504 Hrs and more than three times thick for 816 Hrs treatment of Ti27Nb. Similarly, for Ti-25Ta the increase in thickens for 504 Hrs is one times and two times for 816 Hrs.
2. The simulated body fluid changes the surface morphology, which is demonstrated in the formation of layers and loss of ductility. Transgranular faceted fractures as well as intergranular fracture mode for SBF specimens are observed, which is mainly related to the brittle failure. This intergranular fracture is ascribed to the corrosion fatigue, which occurs due to chemical dissolution along the grain boundaries when placed in body fluids.
3. The SBF treatment affected tensile strength, young modulus and fatigue life of the Ti27Nb and Ti-25Ta. The test results show slight decrease due to treatment which is negligible.

4. The crack growth rate increased in the treated specimen significantly. The increase is attributed to the formation of oxide layer on newly generated fracture surfaces.
5. The fatigue crack fracture surfaces of untreated specimens demonstrate striation marks, implying ductile fracture and consumption of higher energy and slow growth.
6. The crack growth curve for the untreated case has a typical sigmoidal shape, demonstrating the threshold and critical crack growth regions, whereas the SBF-treated specimens do not have specific threshold regions, implying fast growth at even lower energies.
7. The fatigue life models for untreated and SBF treated implant alloy are following the non-linear relation given by following equation

$$N = \left(\frac{\sigma_a}{900.46}\right)^{-1/0.062}$$

$$N = \left(\frac{\sigma_a}{885.45}\right)^{-1/0.06}$$

8. The weight contribution in stress damage and factor of safety is different for different activities. In walking and standup activities the stress and damage is sharply increased with weight, however the factor of safety is decreased for above activities due to weight increase.
9. The fatigue damage strongly depends on the weight of the body. The relation of fatigue damage and applied stress is not linear rather a two-degree polynomial. The change in increase of 120 % to 140 % in applied alternating stress change the damage value from 4.18 % to 25.6 %. This shows the strong influence of weight on the design life of implant. The fitted curve model established from FE simulation for all activities is reproduced here;

$$\Delta D = 0.49\Delta\sigma_a^2 - 0.7132\Delta\sigma_a + 0.26241$$

The equation enables to predict the percentage increase in damage. The static FE analysis through which alternating stress can be determined is enough to predict the damage instead of doing the fatigue analysis.

6.2 Future directions

1. The analysis may be extended to evaluate further body weights to ascertain the effect of subject body weights on the fatigue character of hip implants.
2. Load histories utilized for the structural and fatigue analysis in this research are recorded for only a few cycles. Additionally, data regarding the shares of activities in daily routines for subjects is also limited. It is therefore suggested that detailed load histories may be recorded for the entire duration of the day and repeated for several days.
3. Impact analysis of hip implants made from Ti-27Nb and Ti-25Ta alloys may be conducted.
4. The effect of SBF on the implant material should be tested for the long periods to correlate the degradation characteristics of implant with time and also to find the effect of SBF on the modulus and its correlation with the stress shielding.
5. Experimental analysis of hip implant is required to be conducted using TI-27Nb and Ti-25Ta alloys.

7 References

[1] D. Shi, *Introduction to biomaterials*. World Scientific, 2005.

[2] J. Enderle and J. Bronzino, *Introduction to biomedical engineering*. Academic press, 2012.

[3] S. Ramakrishna, J. Mayer, E. Wintermantel, and K. W. Leong, "Biomedical applications of polymer-composite materials: a review," *Composites science and technology*, vol. 61, no. 9, pp. 1189-1224, 2001.

[4] D. L. Wise, D. J. Trantolo, K.-U. Lewandrowski, J. D. Gresser, M. V. Cattaneo, and M. J. Yaszemski, "Biomaterials engineering and devices: human applications," 2000.

[5] J. B. Park and J. D. Bronzino, *Biomaterials: principles and applications*. crc press, 2002.

[6] M. Niinomi, "Recent metallic materials for biomedical applications," *Metallurgical and materials transactions A*, vol. 33, no. 3, p. 477, 2002.

[7] M. J. Donachie, "Titanium," *A Technical Guide. Second edition. ASM International*, 2000.

[8] G. He and M. Hagiwara, "Bimodal structured Ti-base alloy with large elasticity and low Young's modulus," *Materials Science and Engineering: C*, vol. 25, no. 3, pp. 290-295, 2005.

[9] B. Venkataraman and S. Sudha, "Vanadium toxicity," *Asian J Exp Sci*, vol. 19, no. 2, pp. 127-134, 2005.

[10] W. A. Banks and A. J. Kastin, "Aluminum-induced neurotoxicity: alterations in membrane function at the blood-brain barrier," *Neuroscience & Biobehavioral Reviews*, vol. 13, no. 1, pp. 47-53, 1989.

[11] R. Barbucci, *Integrated biomaterials science*. Springer Science & Business Media, 2002.

[12] P. Fratzl and R. Weinkamer, "Nature's hierarchical materials," *Progress in materials Science*, vol. 52, no. 8, pp. 1263-1334, 2007.

[13] M. C. Pierce, G. E. Bertocci, E. Vogeley, and M. S. Moreland, "Evaluating long bone fractures in children: a biomechanical approach with illustrative cases," *Child abuse & neglect*, vol. 28, no. 5, pp. 505-524, 2004.

[14] M. F. Ashby, L. Gibson, U. Wegst, and R. Olive, "The mechanical properties of natural materials. I. Material property charts," *Proceedings of the Royal Society of London. Series A: Mathematical and Physical Sciences*, vol. 450, no. 1938, pp. 123-140, 1995.

[15] P. Townsend, P. Raux, R. Rose, R. Miegel, and E. Radin, "The distribution and anisotropy of the stiffness of cancellous bone in the human patella," *Journal of biomechanics*, vol. 8, no. 6, pp. 363-367, 1975.

[16] W. Jee, "Integrated bone tissue physiology: anatomy and physiology," *Bone mechanics handbook*, 2001.

[17] Y. Fung, "1993, Biomechanics: Mechanical Properties of Living Tissues, Springer-Verlag, New York."

[18] B. M. Nigg and W. Herzog, *Biomechanics of the musculo-skeletal system*. Wiley, 2007.

[19] https://www.ncbi.nlm.nih.gov/books/NBK45515/, "Osteoporosis."

[20] https://boneandspine.com/hip-osteoarthritis/, "Osteoarthritis."

[21] l. C. h. a. b. v. https://www.mayoclinic.org/diseases-conditions/rheumatoid-arthritis/symptoms-causes/syc-20353648#:~:text=Rheumatoid%20arthritis%20is%20a%20chronic, "Rheumatiod arthristis."

[22] https://www.shutterstock.com/image-vector/rheumatoid-arthritis-hip-joint-87959149, "Rheumatoid fig."

[23] https://en.wikipedia.org/wiki/Juvenile_idiopathic_arthritis, "Juvenile arthritis."

[24] https://en.wikipedia.org/wiki/Ankylosing_spondylitis, "Ankylosing spondylitis."

[25] https://www.ncbi.nlm.nih.gov/pmc/articles/PMC4443866/, "Lyme Arthritis."

[26] https://en.wikipedia.org/wiki/Lupus, "wikipedia."

[27] https://en.wikipedia.org/wiki/Gout, "wikipedia."

[28] b. b. s. p. a. https://www.mayoclinic.org/diseases-conditions/psoriatic-arthritis/symptoms-causes/ syc-20354076#:~:text=Psoriatic%20arthritis%20is%20a%20form, "Psoriatic arthritis."

[29] o. w. o. a. i. https://www.arthritis.org/diseases/infectious-arthritis#:~:text=Infectious%20arthritis%2C%20also%20called%20septic, "Infectious arthritis."

[30] i. p. y. r. https://www.arthritis.org/diseases/polymyalgia-rheumatica#:~:text=Polymyalgia%20rheumatica%20(PMR)%20is%20an, "Polymyalgia rheumatic."

[31] c. m. e. n. b. https://medlineplus.gov/osteonecrosis.html#:~:text=Osteonecrosis%20is%20a%20disease%20caused, "Osteonecrosis."

[32] o. o. o. m. b. https://en.wikipedia.org/wiki/Paget%27s_disease_of_bone#:~:text=Paget's%20disease%20of%20bone%20(commonly, "Paget's disease of the bone."

[33] o. s. o. y. b. https://www.mayoclinic.org/diseases-conditions/sciatica/symptoms-causes/syc-20377435#:~:text=Sciatica%20refers%20to%20pain%20that, "Sciatica."

[34] M. Geetha, A. K. Singh, R. Asokamani, and A. K. Gogia, "Ti based biomaterials, the ultimate choice for orthopaedic implants–a review," *Progress in materials science*, vol. 54, no. 3, pp. 397-425, 2009.

[35] Y. Jun and K. Choi, "Design of patient-specific hip implants based on the 3D geometry of the human femur," *Adv. Eng. Softw.*, vol. 41, no. 4, pp. 537–547, 2010.

[36] S. M. Kurtz *et al.*, "Future clinical and economic impact of revision total hip and knee arthroplasty," *JBJS*, vol. 89, no. suppl_3, pp. 144-151, 2007.

[37] S. Savilahti, I. Myllyneva, T. S. Lindholm, K. Pajamaki, J. Nevalainen, and P. Laippala, "Clinical outcome and survival of Link RS total hip prosthesis," *The Journal of bone and joint surgery. British volume*, vol. 77, no. 3, pp. 369-373, 1995.

[38] T. Jinno, S. K. Kirk, S. Morita, and V. M. Goldberg, "Effects of calcium ion implantation on osseointegration of surface-blasted titanium alloy femoral implants in a canine total hip arthroplasty model," *The Journal of arthroplasty*, vol. 19, no. 1, pp. 102-109, 2004.

[39] A. F. von Recum, *Handbook of biomaterials evaluation: scientific, technical and clinical testing of implant materials*. CRC Press, 1998.

[40] A. Ravaglioli and A. Krajewski, *Bioceramics: Materials· Properties· Applications*. Springer Science & Business Media, 1991.

[41] M. Long and H. Rack, "Titanium alloys in total joint replacement—a materials science perspective," *Biomaterials*, vol. 19, no. 18, pp. 1621-1639, 1998.

[42] S. Zhang, "State-of-the-art of polymer tribology," *Tribology International*, vol. 31, no. 1-3, pp. 49-60, 1998.

[43] C. L. Nelson, "Cemented femoral revision: technique and outcome," *American journal of orthopedics (Belle Mead, NJ)*, vol. 31, no. 4, pp. 187-189, 2002.

[44] J. Callaghan, S. Dysart, and C. Savory, "The uncemented porous-coated anatomic total hip prosthesis. Two-year results of a prospective consecutive series," *JBJS*, vol. 70, no. 3, pp. 337-346, 1988.

[45] H.-G. Willert, H. Bertram, and G. H. Buchhorn, "Osteolysis in alloarthroplasty of the hip. The role of bone cement fragmentation," *Clinical orthopaedics and related research*, no. 258, pp. 108-121, 1990.

[46] https://bonesmart.org/hip/types-of-total-hip-implants/, "cemented picture."

[47] r. s. r. s. https://www.arthritis-health.com/surgery/shoulder-surgery/cemented-vs-cementless-alternatives-joint-replacement#:~:text=The%20drawback%20to%20using%20bone, "cemented implant disadvantage."

[48] A. O. El-Warrak *et al.*, "An experimental animal model of aseptic loosening of hip prostheses in sheep to study early biochemical changes at the interface membrane," *BMC musculoskeletal disorders*, vol. 5, no. 1, pp. 1-13, 2004.

[49] C. A. Engh and J. D. Bobyn, "The influence of stem size and extent of porous coating on femoral bone resorption after primary cementless hip arthroplasty," *Clinical orthopaedics and related research*, no. 231, pp. 7-28, 1988.

[50] C. A. Engh, J. Bobyn, and A. H. Glassman, "Porous-coated hip replacement. The factors governing bone ingrowth, stress shielding, and clinical results," *The Journal of bone and joint surgery. British volume*, vol. 69, no. 1, pp. 45-55, 1987.

[51] J. Sanchez-Sotelo, D. J. Berry, and S. Harmsen, "Long-term results of use of a collared matte-finished femoral component fixed with second-generation cementing techniques: a fifteen-year-median follow-up study," *JBJS*, vol. 84, no. 9, pp. 1636-1641, 2002.

[52] R. L. Barrack, R. D. Mulroy Jr, and W. H. Harris, "Improved cementing techniques and femoral component loosening in young patients with hip arthroplasty. A 12-year radiographic review," *The Journal of bone and joint surgery. British volume*, vol. 74, no. 3, pp. 385-389, 1992.

[53] J. E. Gough and S. Downes, "Osteoblast cell death on methacrylate polymers involves apoptosis," *Journal of Biomedical Materials Research: An Official Journal of The Society for Biomaterials, The Japanese Society for Biomaterials, and The Australian Society for Biomaterials and the Korean Society for Biomaterials*, vol. 57, no. 4, pp. 497-505, 2001.

[54] M. F. Moreau, D. Chappard, M. Lesourd, J. Montheard, and M. F. Baslé, "Free radicals and side products released during methylmethacrylate polymerization are cytotoxic for osteoblastic cells," *Journal of Biomedical Materials Research: An Official Journal of The Society for Biomaterials, The Japanese Society for Biomaterials, and the Australian Society for Biomaterials*, vol. 40, no. 1, pp. 124-131, 1998.

[55] D. S. Hungerford and L. C. Jones, "The rationale for cementless total hip replacement," *The Orthopedic clinics of North America*, vol. 24, no. 4, pp. 617-626, 1993.

[56] R. M. Urban, J. J. Jacobs, D. R. Sumner, C. L. Peters, F. R. Voss, and J. O. Galante, "The bone-implant interface of femoral stems with non-circumferential porous coating. A study of specimens retrieved at autopsy," *JBJS*, vol. 78, no. 7, pp. 1068-81, 1996.

[57] D. M. LaPorte, M. A. Mont, and D. S. Hungerford, "Proximally porous-coated ingrowth prostheses: limits of use," *Orthopedics*, vol. 22, no. 12, pp. 1154-1160, 1999.

[58] Y. Higuchi, T. Seki, D. Morita, D. Komatsu, Y. Takegami, and N. Ishiguro, "Comparison of wear rate between ceramic-on-ceramic, metal on highly cross-linked

polyethylene, and metal-on-metal bearings," *Revista brasileira de ortopedia*, vol. 54, no. 3, pp. 295-302, 2019.

[59] C. Fleck and D. Eifler, "Corrosion, fatigue and corrosion fatigue behaviour of metal implant materials, especially titanium alloys," *International journal of fatigue*, vol. 32, no. 6, pp. 929-935, 2010.

[60] M. J. Donachie, *Titanium: a technical guide*. ASM international, 2000.

[61] M. WALCZAK, D. GĄSKA, and J. SIDOR, "Properties and application titanium and titanium alloys in aerospace systems," *MODERN TECHNIQUES IN MECHANICAL ENGINEERING*, p. 125.

[62] M. Niinomi, M. Nakai, and J. Hieda, "Development of new metallic alloys for biomedical applications," *Acta biomaterialia*, vol. 8, no. 11, pp. 3888-3903, 2012.

[63] M. Niinomi *et al.*, "Development of low rigidity β-type titanium alloy for biomedical applications," *Materials Transactions*, vol. 43, no. 12, pp. 2970-2977, 2002.

[64] K. Takahashi *et al.*, "Biomechanical evaluation of Ti-Nb-Sn alloy implants with a low Young's modulus," *International journal of molecular sciences*, vol. 16, no. 3, pp. 5779-5788, 2015.

[65] Y. Daimatsu, A. Yamamoto, H. Hosoda, and S. Miyazaki, "Shape memory characteristics of Ti–Mo–Ga for biomedical applications," *Proc. Fall Meet. Jpn Inst. Met*, vol. 401, 2001.

[66] H. Hosoda, A. Yamamoto, and S. Miyazaki, "Mechanical properties of Ti–Mo–Ge shape memory alloy for biomedical applications," *Proc. Fall Meet. Jpn Inst. Met*, vol. 401, 2001.

[67] H. Hiromoto *et al.*, "Polarization behavior of Ti–Mo–Al shape memory alloy in simulated body liquid," *Proc. Annu. Meet. Jpn Inst. Met*, vol. 443, 2002.

[68] M. Ikeda, Y. Nakamura, and N. Takahama, "Effect of Zr contents on heat treatment behaviors and phase constitution of Ti-50 mass% Ta–Zr alloy," *Proc. Annu. Meet. JIM*, vol. 130, 2003.

[69] T. Maeshima, T. Eto, H. Uchiyama, K. Uchiyama, and M. Nishida, "Development of Ti–Sc–Mo shape memory alloy," *Annu. Meet. JIM*, p. 134, 2003.

[70] M. Niinomi, "Recent titanium R&D for biomedical applications in Japan," *Jom*, vol. 51, no. 6, pp. 32-34, 1999.

[71] Y.-L. Zhou and M. Niinomi, "Ti–25Ta alloy with the best mechanical compatibility in Ti–Ta alloys for biomedical applications," *Materials Science and Engineering: C*, vol. 29, no. 3, pp. 1061-1065, 2009.

[72] M. A.-H. Gepreel and M. Niinomi, "Biocompatibility of Ti-alloys for long-term implantation," *Journal of the mechanical behavior of biomedical materials*, vol. 20, pp. 407-415, 2013.

[73] R. Banerjee, S. Nag, J. Stechschulte, and H. L. Fraser, "Strengthening mechanisms in Ti–Nb–Zr–Ta and Ti–Mo–Zr–Fe orthopaedic alloys," *Biomaterials*, vol. 25, no. 17, pp. 3413-3419, 2004.

[74] G. He and M. Hagiwara, "Ti alloy design strategy for biomedical applications," *Materials Science and Engineering: C*, vol. 26, no. 1, pp. 14-19, 2006.

[75] L. Elias, S. Schneider, S. Schneider, H. Silva, and F. Malvisi, "Microstructural and mechanical characterization of biomedical Ti–Nb–Zr (–Ta) alloys," *Materials Science and Engineering: A*, vol. 432, no. 1-2, pp. 108-112, 2006.

[76] M. Balazic, J. Kopac, M. J. Jackson, and W. Ahmed, "Titanium and titanium alloy applications in medicine," *International Journal of Nano and Biomaterials*, vol. 1, no. 1, pp. 3-34, 2007.

[77] G. Lütjering and J. C. Williams, *Titanium*. Springer Science & Business Media, 2007.

[78] V. A. Joshi, *Titanium alloys: an atlas of structures and fracture features*. Crc Press, 2006.

[79] C. Veiga, J. Davim, and A. Loureiro, "Properties and applications of titanium alloys: a brief review," *Rev. Adv. Mater. Sci*, vol. 32, no. 2, pp. 133-148, 2012.

[80] C. Leyens and M. Peters, *Titanium and titanium alloys: fundamentals and applications*. John Wiley & Sons, 2003.

[81] I. Gotman, "Characteristics of metals used in implants," *Journal of endourology*, vol. 11, no. 6, pp. 383-389, 1997.

[82] A. Biesiekierski, J. Wang, M. A.-H. Gepreel, and C. Wen, "A new look at biomedical Ti-based shape memory alloys," *Acta biomaterialia*, vol. 8, no. 5, pp. 1661-1669, 2012.

[83] R. Köster *et al.*, "Nickel and molybdenum contact allergies in patients with coronary in-stent restenosis," *The Lancet*, vol. 356, no. 9245, pp. 1895-1897, 2000.

[84] D. B. Burr, "The Human Skeleton, Pat Shipman, Alan Walker, David Bichell, Harvard University Press, Cambridge, Mass (1985), 360 pp. $23. 50, ISBN: 0-674-41610-4," ed: Academic Press, 1986.

[85] https://www.doitpoms.ac.uk/tlplib/bones/bone_mechanical.php, "tensile and compressive stregth of bone."

[86] M. Abdel-Hady, K. Hinoshita, and M. Morinaga, "General approach to phase stability and elastic properties of β-type Ti-alloys using electronic parameters," *Scripta Materialia*, vol. 55, no. 5, pp. 477-480, 2006.

[87] M. Semlitsch, "Classic and new titanium alloys for production of artificial hip joints," *Titanium Development Association*, pp. 721-740, 1987.

[88] Y. Okazaki, K. Kyo, Y. Ito, and T. Tateishi, "Mechanical properties and corrosion fatigue of new titanium alloys for medical implants in physiological saline solution," *Nippon Kinzoku Gakkaishi (1952)*, vol. 59, no. 10, pp. 1078-1083, 1995.

[89] J. Davidson and F. Georgette, *State of the art materials for orthopedic prosthetic devices*. Society of Manufacturing Engineers, 1987.

[90] K.-H. Borowy and K.-H. Kramer, "On the Properties of a New Titanium Alloy(TiAl 5 Fe 2. 5) as Implant Material," *Titanium--Science and Technology.*, vol. 2, pp. 1381-1386, 1984.

[91] R. Allen, N. Baldini, P. Donofrio, E. Gutman, E. Keefe, and J. Kramer, "Annual book of ASTM standards, medical devices and services," *ASTM International*, 1998.

[92] D. Kuroda, M. Niinomi, M. Morinaga, Y. Kato, and T. Yashiro, "Design and mechanical properties of new β type titanium alloys for implant materials," *Materials Science and Engineering: A*, vol. 243, no. 1-2, pp. 244-249, 1998.

[93] K. Wang, "The Characterization of Ti-12Mo-6Zr-2Fe A New Biocompatible Titanium Alloy Developed for Surgical Implant," *Beta Titanium Alloys in the 1990's*, pp. 49-60, 1993.

[94] S. A. Brown and J. E. Lemons, "Medical applications of titanium and its alloys: the material and biological issues," 1996: ASTM West Conshohocken, PA.

[95] Y. Hao *et al.*, "Young's modulus and mechanical properties of Ti-29Nb-13Ta-4.6 Zr in relation to α "martensite," *Metallurgical and Materials Transactions A*, vol. 33, no. 10, pp. 3137-3144, 2002.

[96] M. Nakai, M. Niinomi, K. Cho, and K. Narita, "Enhancing functionalities of metallic materials by controlling phase stability for use in orthopedic implants," in *Interface Oral Health Science 2014*: Springer, Tokyo, 2015, pp. 79-91.

[97] R. Narayan, *Biomedical materials*. Springer Science & Business Media, 2009.

[98] M. Niinomi, "Mechanical properties of biomedical titanium alloys," *Materials Science and Engineering: A*, vol. 243, no. 1-2, pp. 231-236, 1998.

[99] L. S. Kubie and G. M. Shults, "Studies on the relationship of the chemical constituents of blood and cerebrospinal fluid," *The Journal of experimental medicine*, vol. 42, no. 4, p. 565, 1925.

[100] J. J. Jacobs, J. L. Gilbert, and R. M. Urban, "Current concepts review-corrosion of metal orthopaedic implants," *Jbjs*, vol. 80, no. 2, pp. 268-82, 1998.

[101] B. Kasemo and J. Lausmaa, "Surface science aspects on inorganic biomaterials," *CRC Crit. Rev. Clin. Neurobiol.;(United States)*, vol. 4, 1986.

[102] Y. Okazaki and E. Gotoh, "Implant applications of highly corrosion-resistant Ti-15Zr-4Nb-4Ta alloy," *Materials Transactions*, vol. 43, no. 12, pp. 2943-2948, 2002.

[103] S. Barril, N. Debaud, S. Mischler, and D. Landolt, "A tribo-electrochemical apparatus for in vitro investigation of fretting–corrosion of metallic implant materials," *Wear*, vol. 252, no. 9-10, pp. 744-754, 2002.

[104] J. Komotori, N. Hisamori, and Y. Ohmori, "The corrosion/wear mechanisms of Ti–6Al–4V alloy for different scratching rates," *Wear*, vol. 263, no. 1-6, pp. 412-418, 2007.

[105] P. Aragon and S. Hulbert, "Corrosion of Ti-6Al-4V in simulated body fluids and bovine plasma," *Journal of biomedical materials research*, vol. 6, no. 3, pp. 155-164, 1972.

[106] E. Kobayashi, T. Wang, H. Doi, T. Yoneyama, and H. Hamanaka, "Mechanical properties and corrosion resistance of Ti–6Al–7Nb alloy dental castings," *Journal of Materials Science: Materials in Medicine*, vol. 9, no. 10, pp. 567-574, 1998.

[107] Y. L. Zhou, M. Niinomi, T. Akahori, H. Fukui, and H. Toda, "Corrosion resistance and biocompatibility of Ti–Ta alloys for biomedical applications," *Materials Science and Engineering: A*, vol. 398, no. 1-2, pp. 28-36, 2005.

[108] G. Bergmann, F. Graichen, and A. Rohlmann, "Hip joint loading during walking and running, measured in two patients," *Journal of biomechanics*, vol. 26, no. 8, pp. 969-990, 1993.

[109] G. Bergmann, H. Kniggendorf, F. Graichen, and A. Rohlmann, "Influence of shoes and heel strike on the loading of the hip joint," *Journal of biomechanics*, vol. 28, no. 7, pp. 817-827, 1995.

[110] G. Bergmann, F. Graichen, A. Rohlmann, and H. Linke, "Hip joint forces during load carrying," *Clinical orthopaedics and related research*, no. 335, pp. 190-201, 1997.

[111] G. Bergmann *et al.*, "Hip contact forces and gait patterns from routine activities," *Journal of biomechanics*, vol. 34, no. 7, pp. 859-871, 2001.

[112] G. Bergmann, F. Graichen, and A. Rohlmann, "HIP98 (2001 Version). Biomechanics Lab," ed: Benjamin Franklin School of Medicine, Free University of Berlin, Germany.

[113] G. Bergmann, F. Graichen, and A. a. Rohlmann, "Is staircase walking a risk for the fixation of hip implants?," *Journal of biomechanics*, vol. 28, no. 5, pp. 535-553, 1995.

[114] B. Stansfield and A. Nicol, "Hip joint contact forces in normal subjects and subjects with total hip prostheses: walking and stair and ramp negotiation," *Clinical Biomechanics*, vol. 17, no. 2, pp. 130-139, 2002.

[115] D. E. Hurwitz, K. C. Foucher, and T. P. Andriacchi, "A new parametric approach for modeling hip forces during gait," *Journal of biomechanics*, vol. 36, no. 1, pp. 113-119, 2003.

[116] B. MavČiČ, B. Pompe, V. Antolič, M. Daniel, A. Iglič, and V. Kralj-Iglič, "Mathematical estimation of stress distribution in normal and dysplastic human hips," *Journal of Orthopaedic Research*, vol. 20, no. 5, pp. 1025-1030, 2002.

[117] A. Vora, J. C. Kudrna, V. S. Harder, and B. Mazahery, "Early failure of a proximally cemented, distally uncemented total hip arthroplasty," *The Journal of arthroplasty*, vol. 18, no. 7, pp. 889-896, 2003.

[118] R. Huiskes and C. O. R. Res, "The various stress patterns of press-fit, ingrown, and cemented femoral stems," *Clin Orthop*, vol. 2612738, 1990.

[119] C. H. Turner, V. Anne, and R. M. Pidaparti, "A uniform strain criterion for trabecular bone adaptation: do continuum-level strain gradients drive adaptation?," *Journal of Biomechanics*, vol. 30, no. 6, pp. 555-563, 1997.

[120] C. F. Scifert, T. D. Brown, and J. D. Lipman, "Finite element analysis of a novel design approach to resisting total hip dislocation," *Clinical Biomechanics*, vol. 14, no. 10, pp. 697-703, 1999.

[121] S. Gross and E. Abel, "A finite element analysis of hollow stemmed hip prostheses as a means of reducing stress shielding of the femur," *Journal of Biomechanics*, vol. 34, no. 8, pp. 995-1003, 2001.

[122] A. Philips, "Finite element analysis of the acetabulum after impaction grafting," *The University of Edinburgh.—2001*, 2001.

[123] P. B. Chang *et al.*, "Design and analysis of robust total joint replacements: finite element model experiments with environmental variables," *J. Biomech. Eng.*, vol. 123, no. 3, pp. 239-246, 2001.

[124] P. B. Chang, B. J. Williams, T. J. Santner, W. I. Notz, and D. L. Bartel, "Robust optimization of total joint replacements incorporating environmental variables," 1999.

[125] S. Senapati and S. Pal, "Uhmwpe-Alumina Ceramic Composite, An Improved Prosthesis Materials For An Artificial Cemented Hip Joint," *Trends in Biomaterials & Artificial Organs*, vol. 16, no. 1, 2002.

[126] H. Katoozian, D. T. Davy, A. Arshi, and U. Saadati, "Material optimization of femoral component of total hip prosthesis using fiber reinforced polymeric composites," *Medical engineering & physics*, vol. 23, no. 7, pp. 505-511, 2001.

[127] H. Katoozian, "Three-dimensional shape optimization of femoral components of total hip prostheses," in *Bioengineering Conference ASME, BED*, 1993, vol. 24, p. 552.

[128] H. Katoozian and D. T. Davy, "Effects of loading conditions and objective function on three-dimensional shape optimization of femoral components of hip endoprostheses," *Medical Engineering & Physics*, vol. 22, no. 4, pp. 243-251, 2000.

[129] D. P. Nicolella, B. H. Thacker, H. Katoozian, and D. T. Davy, "Probabilistic risk analysis of a cemented hip implant," *ASME-PUBLICATIONS-BED*, vol. 50, pp. 427-428, 2001.

[130] R. Shirandami and I. Esat, "New design of hip prosthesis using carbon fibre reinforced composite," *Journal of biomedical engineering*, vol. 12, no. 1, pp. 19-22, 1990.

[131] B. Weisse, M. Zahner, W. Weber, and W. Rieger, "Improvement of the reliability of ceramic hip joint implants," *Journal of Biomechanics*, vol. 36, no. 11, pp. 1633-1639, 2003.

[132] P. Prendergast, "Finite element models in tissue mechanics and orthopaedic implant design," *Clinical Biomechanics*, vol. 12, no. 6, pp. 343-366, 1997.

[133] J. Simoes, A. Marques, and G. Jeronimidis, "Design of a controlled-stiffness composite proximal femoral prosthesis," *Composites Science and Technology*, vol. 60, no. 4, pp. 559-567, 2000.

[134] J. de Oliveira Simões and A. Marques, "Determination of stiffness properties of braided composites for the design of a hip prosthesis," *Composites Part A: Applied Science and Manufacturing*, vol. 32, no. 5, pp. 655-662, 2001.

[135] H. Hedia, D. Barton, J. Fisher, and T. Elmidany, "A method for shape optimization of a hip prosthesis to maximize the fatigue life of the cement," *Medical engineering & physics*, vol. 18, no. 8, pp. 647-654, 1996.

[136] K. Tanner, P. Reed, W. Bonfield, G. L. Rasmussen, and M. Freeman, "A system for modelling forces on the hip joint in one-legged stance," *Journal of biomedical engineering*, vol. 10, no. 3, pp. 289-290, 1988.

[137] J. Howell, L. Blunt, C. Doyle, R. Hooper, A. Lee, and R. Ling, "In vivo surface wear mechanisms of femoral components of cemented total hip arthroplasties: the influence of wear mechanism on clinical outcome," *The Journal of arthroplasty*, vol. 19, no. 1, pp. 88-101, 2004.

[138] P. Scannell and P. Prendergast, "Simulation of changes in bone around hip replacement implants," *The Engineers Journal*, vol. 59, pp. 372-377, 2005.

[139] C. Li, C. Granger, H. Del Schutte Jr, S. B. Biggers Jr, J. M. Kennedy, and R. A. Latour Jr, "Progressive failure analysis of laminated composite femoral prostheses for total hip arthroplasty," *Biomaterials*, vol. 23, no. 21, pp. 4249-4262, 2002.

[140] C. Li, C. Granger, H. Del Schutte, S. B. Biggers, J. M. Kennedy, and R. A. Latour, "Failure analysis of composite femoral components for hip arthroplasty," *Journal of rehabilitation research and development*, vol. 40, no. 2, pp. 131-146, 2003.

[141] Y. Zhou, C. Li, and J. J. Mason, "Shape optimization of randomly oriented short fibers for bone cement reinforcements," *Materials Science and Engineering: A*, vol. 393, no. 1-2, pp. 374-381, 2005.

[142] C. L. Peters, K. N. Bachus, M. A. Craig, and T. O. Higginbotham, "The effect of femoral prosthesis design on cement strain in cemented total hip arthroplasty," *The Journal of Arthroplasty*, vol. 16, no. 2, pp. 216-224, 2001.

[143] M. Pérez, J. García-Aznar, M. Doblaré, B. Seral, and F. Seral, "A comparative FEA of the debonding process in different concepts of cemented hip implants," *Medical engineering & physics*, vol. 28, no. 6, pp. 525-533, 2006.

[144] M. G. Joshi, S. G. Advani, F. Miller, and M. H. Santare, "Analysis of a femoral hip prosthesis designed to reduce stress shielding," *Journal of biomechanics*, vol. 33, no. 12, pp. 1655-1662, 2000.

[145] R. Sakai, M. Itoman, and K. Mabuchi, "Assessments of different kinds of stems by experiments and FEM analysis: appropriate stress distribution on a hip prosthesis," *Clinical Biomechanics*, vol. 21, no. 8, pp. 826-833, 2006.

[146] C.-C. Hu, J.-J. Liau, C.-Y. Lung, C.-H. Huang, and C.-K. Cheng, "A two-dimensional finite element model for frictional heating analysis of total hip prosthesis," *Materials Science and Engineering: C*, vol. 17, no. 1-2, pp. 11-18, 2001.

[147] M. Baleani, M. Viceconti, R. Muccini, and M. Ansaloni, "Endurance verification of custom-made hip prostheses," *International journal of fatigue*, vol. 22, no. 10, pp. 865-871, 2000.

[148] Y. San Yoon, G. H. Jang, and Y. Y. Kim, "Shape optimal design of the stem of a cemented hip prosthesis to minimize stress concentration in the cement layer," *Journal of biomechanics*, vol. 22, no. 11-12, pp. 1279-1284, 1989.

[149] M. Taylor, K. Tanner, M. Freeman, and A. Yettram, "Cancellous bone stresses surrounding the femoral component of a hip prosthesis: an elastic-plastic finite element analysis," *Medical engineering & physics*, vol. 17, no. 7, pp. 544-550, 1995.

[150] C. Zannoni, M. Viceconti, L. Pierotti, and A. Cappello, "Analysis of titanium induced CT artifacts in the development of biomechanical finite element models," *Medical engineering & physics*, vol. 20, no. 9, pp. 653-659, 1998.

[151] P. Prendergast and D. Taylor, "Stress analysis of the proximo-medial femur after total hip replacement," *Journal of biomedical engineering*, vol. 12, no. 5, pp. 379-382, 1990.

[152] B. P. McNamara, L. Cristofolini, A. Toni, and D. Taylor, "Relationship between bone-prosthesis bonding and load transfer in total hip reconstruction," *Journal of biomechanics*, vol. 30, no. 6, pp. 621-630, 1997.

[153] P. Prendergast, J. Monaghan, and D. Taylor, "Materials selection in the artificial hip joint using finite element stress analysis," *Clinical Materials*, vol. 4, no. 4, pp. 361-376, 1989.

[154] J. Hertzler, M. A. Miller, and K. A. Mann, "Fatigue crack growth rate does not depend on mantle thickness: an idealized cemented stem construct under torsional loading," *Journal of Orthopaedic Research*, vol. 20, no. 4, pp. 676-682, 2002.

[155] D.-G. Kim, M. A. Miller, and K. A. Mann, "A fatigue damage model for the cement–bone interface," *Journal of biomechanics*, vol. 37, no. 10, pp. 1505-1512, 2004.

[156] P. Colombi, "Fatigue analysis of cemented hip prosthesis: damage accumulation scenario and sensitivity analysis," *International Journal of Fatigue*, vol. 24, no. 7, pp. 739-746, 2002.

[157] P. Colombi, "Fatigue analysis of cemented hip prosthesis: model definition and damage evolution algorithms," *International journal of fatigue*, vol. 24, no. 8, pp. 895-901, 2002.

[158] M. T. Raimondi and R. Pietrabissa, "Modelling evaluation of the testing condition influence on the maximum stress induced in a hip prosthesis during ISO 7206 fatigue testing," *Medical engineering & physics*, vol. 21, no. 5, pp. 353-359, 1999.

[159] J.-P. Hung, J.-H. Chen, H.-L. Chiang, and J. S.-S. Wu, "Computer simulation on fatigue behavior of cemented hip prostheses: a physiological model," *Computer methods and programs in biomedicine*, vol. 76, no. 2, pp. 103-113, 2004.

[160] P. Ortega, W. Medeiros Jr, A. Moré, R. Vasconcelos, E. da Rosa, and C. Roesler, "Failure analysis of a modular revision total HIP arthroplasty femoral stem fractured in vivo," *Engineering Failure Analysis*, p. 104591, 2020.

[161] J. Stolk, N. Verdonschot, and R. Huiskes, "Sensitivity of failure criteria of cemented total hip replacements to finite element mesh density," *Journal of Biomechanics*, vol. 1001, no. 31, p. 165, 1998.

[162] A. Ramos and J. Simoes, "Tetrahedral versus hexahedral finite elements in numerical modelling of the proximal femur," *Medical engineering & physics*, vol. 28, no. 9, pp. 916-924, 2006.

[163] P. Aspenberg and P. Herbertsson, "Periprosthetic bone resorption: particles versus movement," *The Journal of bone and joint surgery. British volume*, vol. 78, no. 4, pp. 641-646, 1996.

[164] M. Bernakiewicz and M. Viceconti, "The role of parameter identification in finite element contact analyses with reference to orthopaedic biomechanics applications," *Journal of biomechanics*, vol. 35, no. 1, pp. 61-67, 2002.

[165] G. N. Duda, E. Schneider, and E. Y. Chao, "Internal forces and moments in the femur during walking," *Journal of biomechanics*, vol. 30, no. 9, pp. 933-941, 1997.

[166] L. Cristofolini, M. Viceconti, A. Toni, and A. Giunti, "Influence of thigh muscles on the axial strains in a proximal femur during early stance in gait," *Journal of biomechanics*, vol. 28, no. 5, pp. 617-624, 1995.

[167] J. Stolk, N. Verdonschot, and R. Huiskes, "Hip-joint and abductor-muscle forces adequately represent in vivo loading of a cemented total hip reconstruction," *Journal of Biomechanics*, vol. 34, no. 7, pp. 917-926, 2001.

[168] T. Kokubo and H. Takadama, "How useful is SBF in predicting in vivo bone bioactivity?," *Biomaterials*, vol. 27, no. 15, pp. 2907-2915, 2006.

[169] E. ASTM, "Standard test methods for tension testing of metallic materials," *Annual book of ASTM standards. ASTM*, 2001.

[170] I. ASTM, "Standard test methods and definitions for mechanical testing of steel products," *ASTM A370*, 2012.

[171] A. Standard, "E399," *Standard Test Method for Linear-Elastic Plane-Strain Fracture Toughness KIC of Metallic Materials," in ASTM Book of Standards, West Conshohocken, PA: ASTM International*, 2012.

[172] A. Standard, "ASTM-E647-11," *Standard test method for measurement of fatigue crack growth rates.*

[173] Y.-w. Gui, J.-M. Oh, and J.-W. Lim, "Sintering properties of Ti-27Nb alloys prepared by using Ti/TiH2 powders under argon and hydrogen sintering processes," *Powder technology,* vol. 339, pp. 775-780, 2018.

[174] E. Brodie, A. Medvedev, J. Frith, M. Dargusch, H. Fraser, and A. Molotnikov, "Remelt processing and microstructure of selective laser melted Ti25Ta," *Journal of Alloys and Compounds,* vol. 820, p. 153082, 2020.

[175] D. Zhao *et al.*, "Improvement on mechanical properties and corrosion resistance of titanium-tantalum alloys in-situ fabricated via selective laser melting," *Journal of Alloys and Compounds,* vol. 804, pp. 288-298, 2019.

[176] G. Zeng *et al.*, "A comparative study of cell growth on a cold sprayed Ti–Ta composite," *Journal of Alloys and Compounds,* vol. 826, p. 154014, 2020.

[177] M. Amjad, S. Badshah, M. A. Khattak, R. U. Khan, and M. Mujahid, "Characterization of Nickle Free Titanium Alloy TI-27Nb for Biomedical Applications," *JOURNAL OF ENGINEERING AND APPLIED SCIENCES,* vol. 36, no. 2, 2017.

[178] M. Janeček *et al.*, "The Very High Cycle Fatigue Behaviour of Ti-6Al-4V Alloy," *Acta Physica Polonica, A.,* vol. 128, no. 4, 2015.

[179] M. Niinomi, "Mechanical biocompatibilities of titanium alloys for biomedical applications," *Journal of the mechanical behavior of biomedical materials,* vol. 1, no. 1, pp. 30-42, 2008.

[180] X. Shi, W. Zeng, and Q. Zhao, "The effects of lamellar features on the fracture toughness of Ti-17 titanium alloy," *Materials Science and Engineering: A,* vol. 636, pp. 543-550, 2015.

[181] R. Stephens, R. Stephens, A. Veit, and T. Albertson, "Fatigue crack growth of Ti-62222 titanium alloy under constant amplitude and miniTWIST flight spectra at 25° C and 175° C," *International journal of fatigue*, vol. 19, no. 4, pp. 301-308, 1997.

[182] T. H. Courtney, *Mechanical behavior of materials*. Waveland Press, 2005.

[183] R. W. Hertzberg and F. E. Hauser, "Deformation and fracture mechanics of engineering materials," 1977.

[184] M. Niinomi, T. Kobayashi, O. Toriyama, N. Kawakami, Y. Ishida, and Y. Matsuyama, "Fracture characteristics, microstructure, and tissue reaction of Ti-5Al-2.5 Fe for orthopedic surgery," *Metallurgical and Materials Transactions A*, vol. 27, no. 12, pp. 3925-3935, 1996.

[185] Y.-j. Liu, S.-m. Cui, C. He, J.-k. Li, and Q.-y. Wang, "High cycle fatigue behavior of implant Ti-6Al-4V in air and simulated body fluid," *Bio-medical materials and engineering*, vol. 24, no. 1, pp. 263-269, 2014.

[186] N. Verdhan, D. Bhende, R. Kapoor, and J. Chakravartty, "Effect of microstructure on the fatigue crack growth behaviour of a near-α Ti alloy," *International Journal of Fatigue*, vol. 74, pp. 46-54, 2015.

[187] S. Samsami, P. Augat, and G. Rouhi, "Stability of femoral neck fracture fixation: A finite element analysis," *Proceedings of the Institution of Mechanical Engineers, Part H: Journal of Engineering in Medicine*, vol. 233, no. 9, pp. 892-900, 2019.

[188] M. Babić, O. Verić, Ž. Božić, and A. Sušić, "Finite element modelling and fatigue life assessment of a cemented total hip prosthesis based on 3D scanning," *Engineering Failure Analysis*, p. 104536, 2020.

[189] G. Bergmann, A. Bender, J. Dymke, G. Duda, and P. Damm, "Standardized loads acting in hip implants," *PloS one*, vol. 11, no. 5, p. e0155612, 2016.

[190] M. S. Johansson *et al.*, "Time spent cycling, walking, running, standing and sedentary: a cross-sectional analysis of accelerometer-data from 1670 adults in the Copenhagen City Heart Study," *BMC public health*, vol. 19, no. 1, p. 1370, 2019.

Appendix A: Ti-27Nb Results

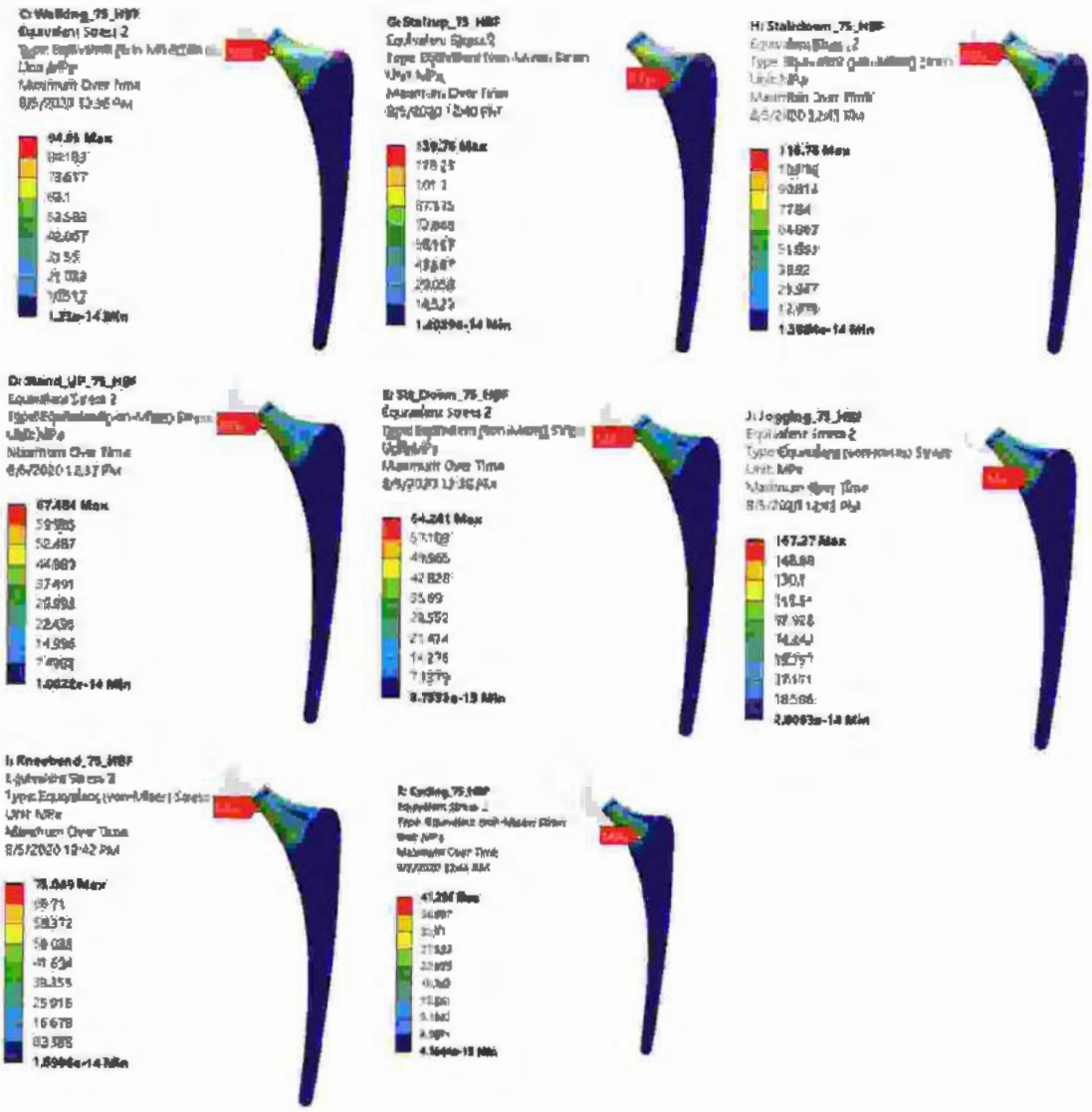

Figure_Apx A-1:Maximum Von Mises Stress all activities of 75kg body weight SBF Treated Ti-27Nb.

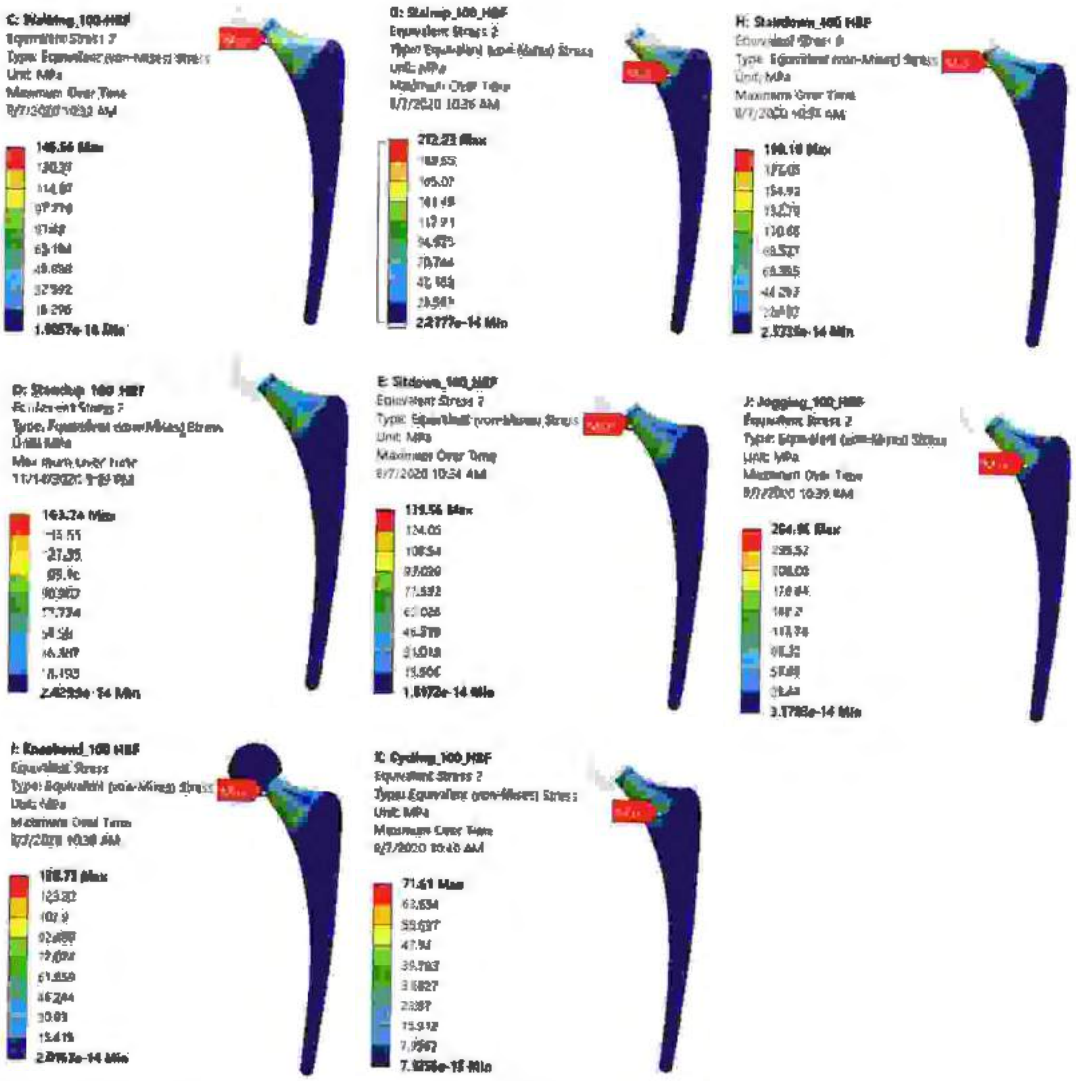

Figure_Apx A-2:Maximum Von Mises Stress all activities of 100kg body weight SBF Treated Ti-27Nb.

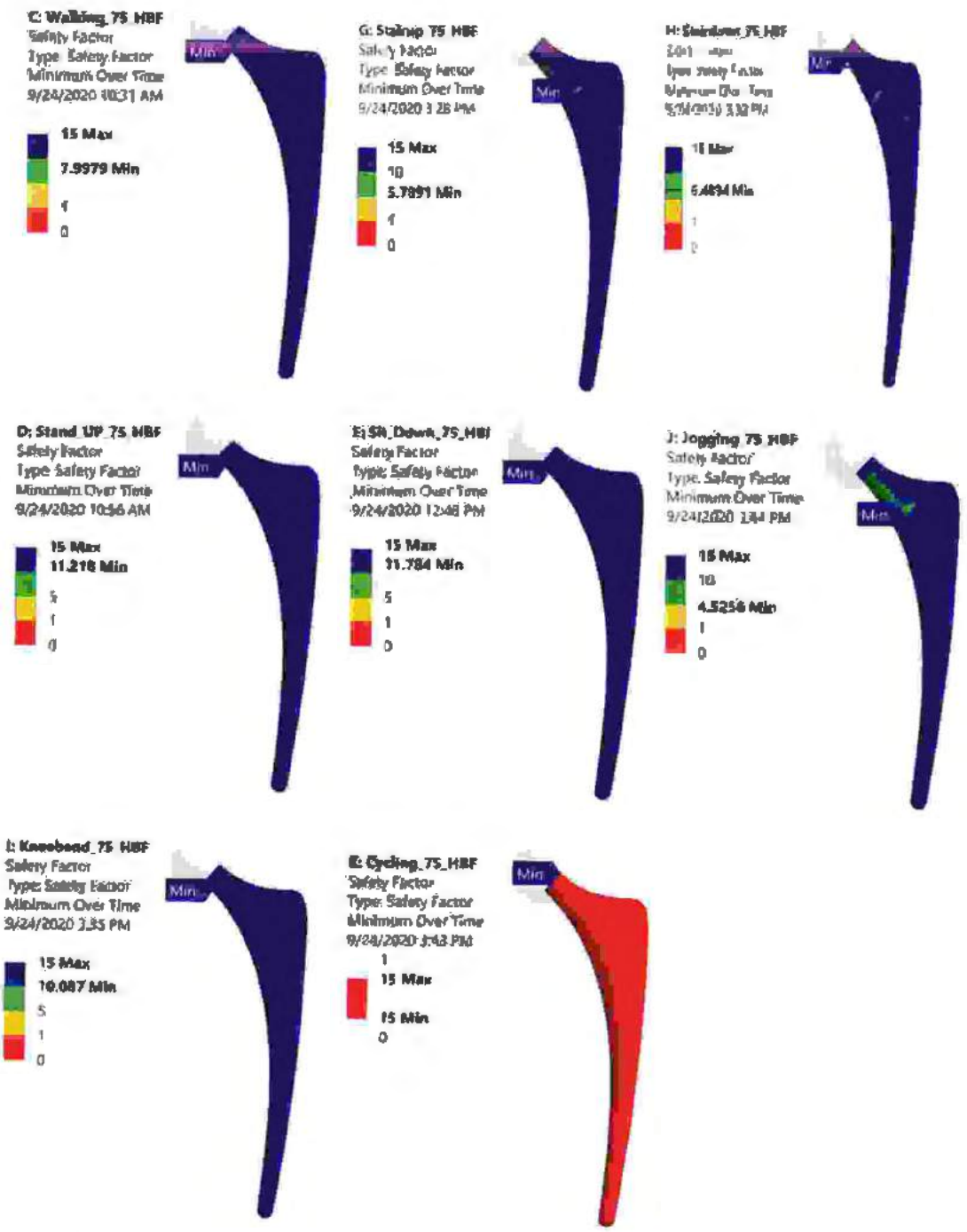

Figure_Apx A- 3:Factor of Safety all activities of 75kg body weight SBF Treated Ti-27Nb.

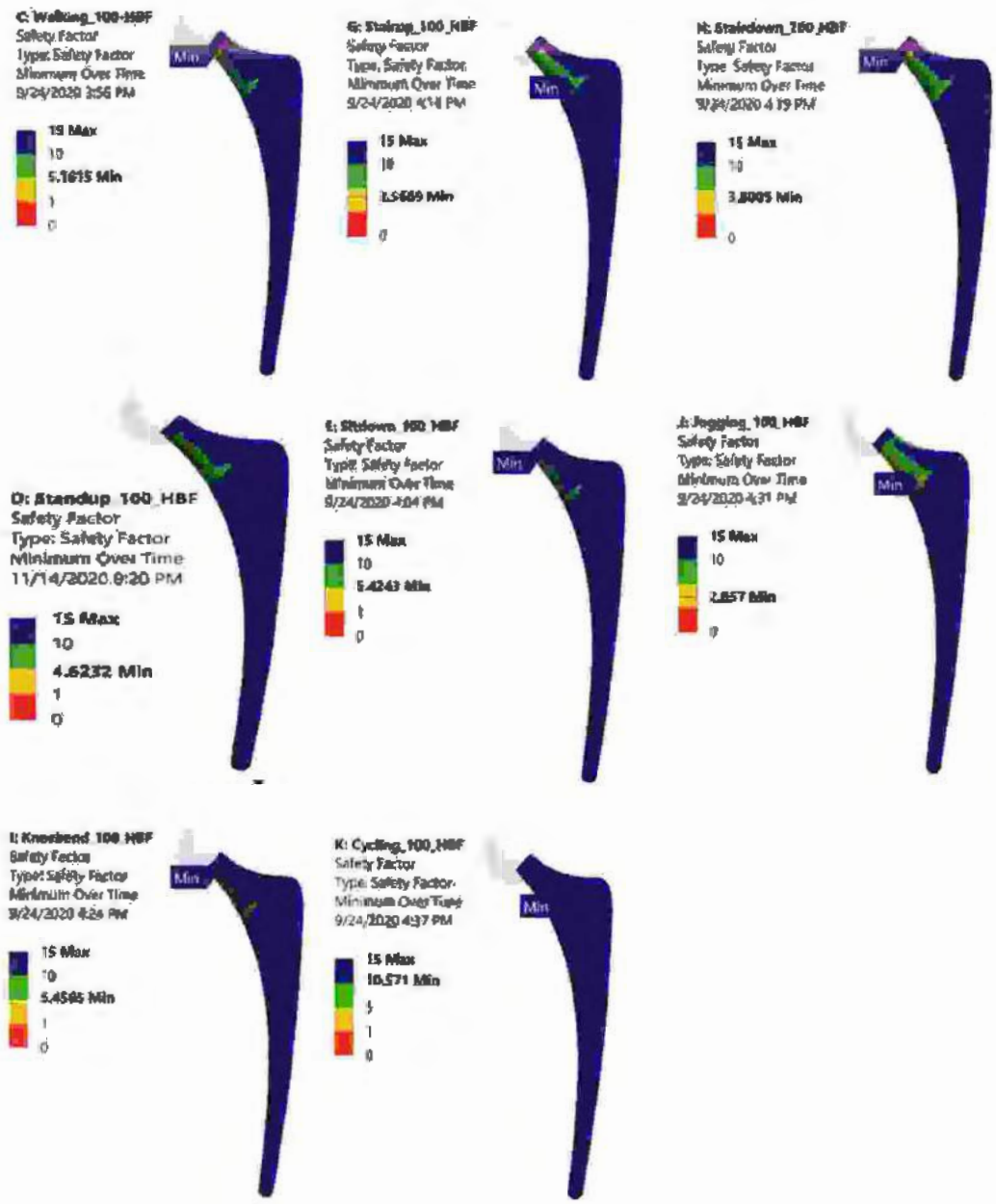

Figure_Apx A- 4: Factor of Safety all activities of 100kg body weight SBF Treated Ti-27Nb.

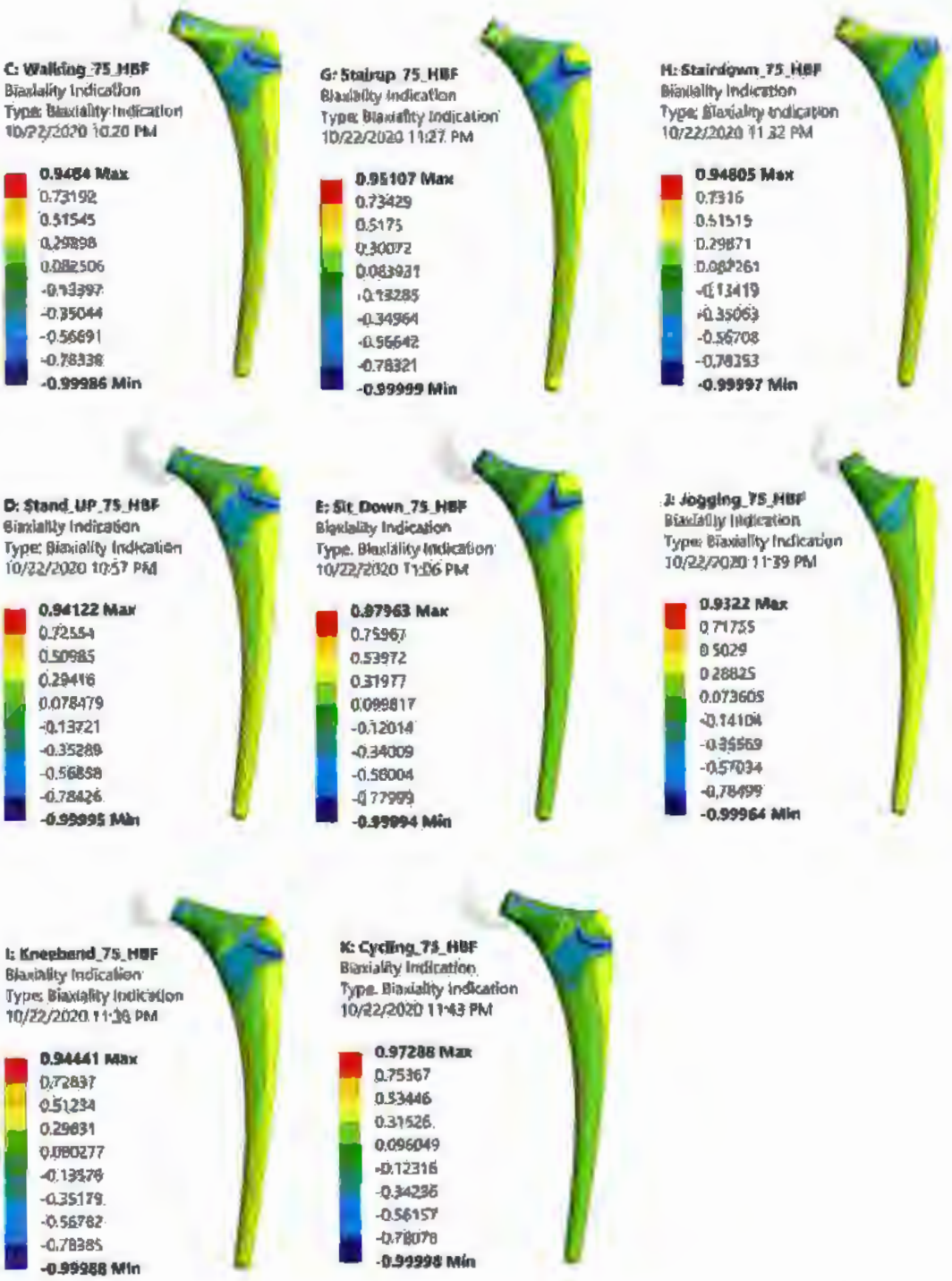

Figure_Apx A- 5: Bi axiality Indication contour of different activities for body weight of 75 Kg SBF Treated Ti-27Nb.

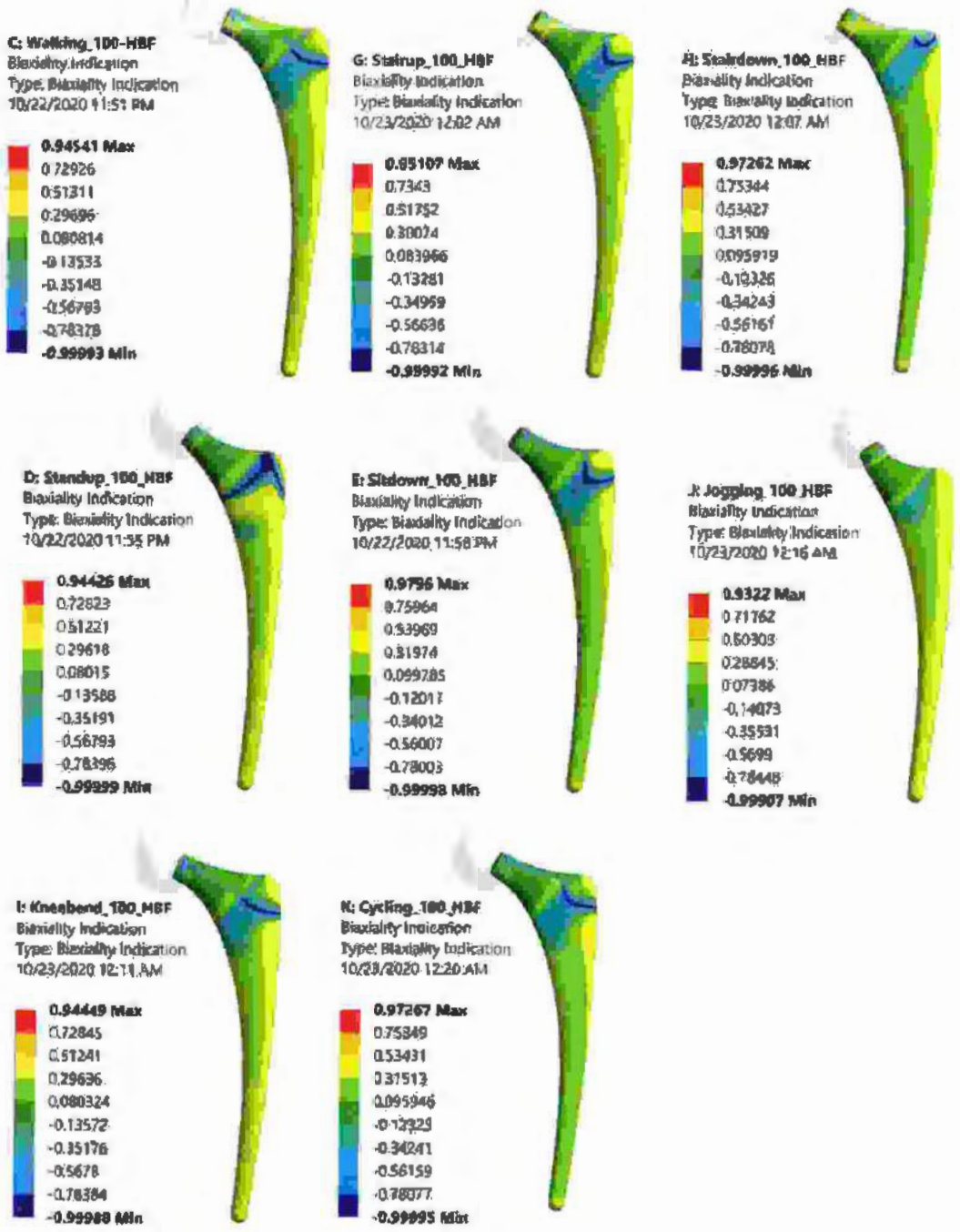

Figure_Apx A- 6: Bi axiality Indication contour of different activities for body weight of 100 Kg SBF Treated Ti-27Nb.

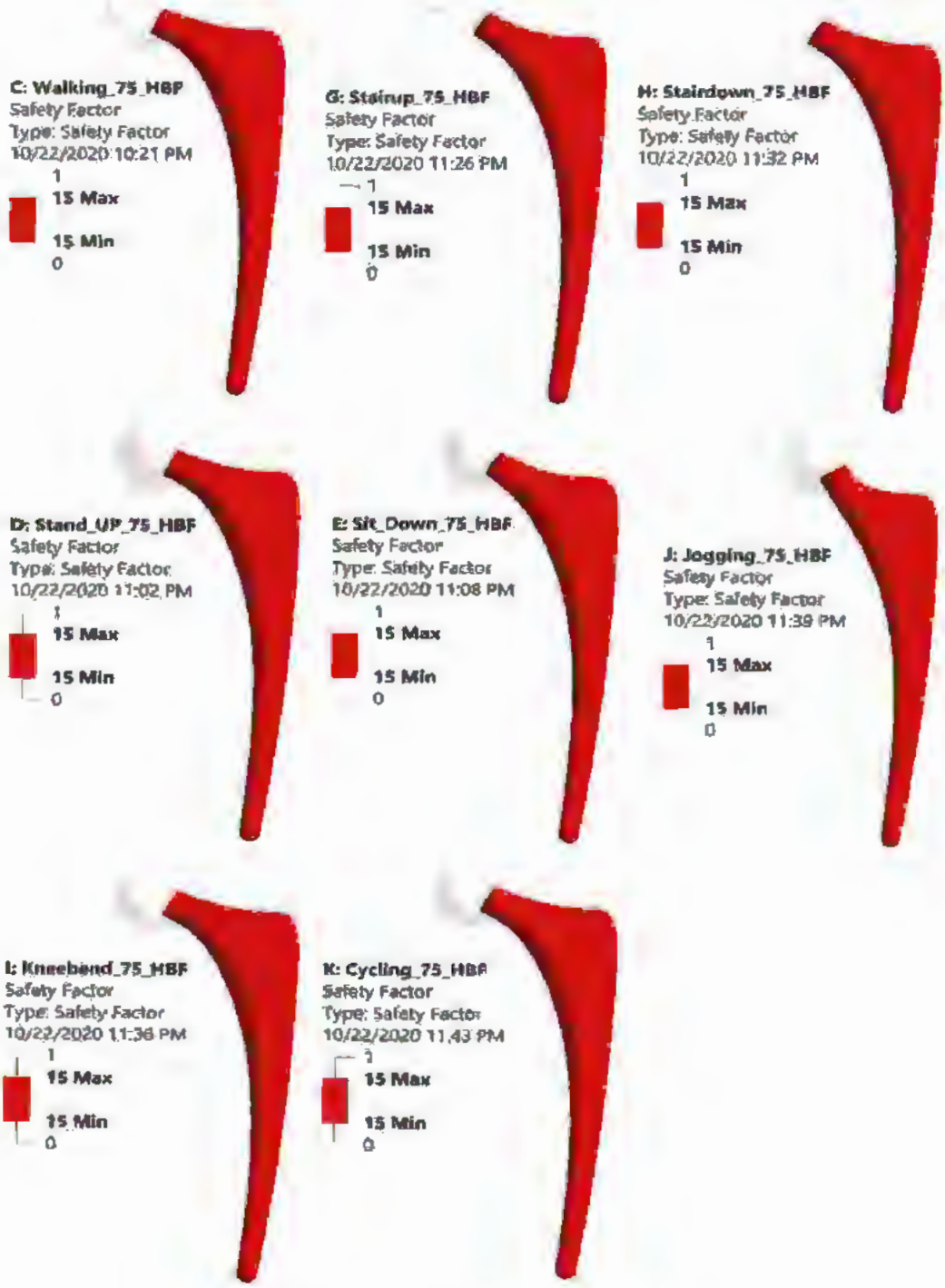

Figure_Apx A- 7: Fatigue FOS contour of different activities for body weight of 75 Kg SBF Treated Ti-27Nb.

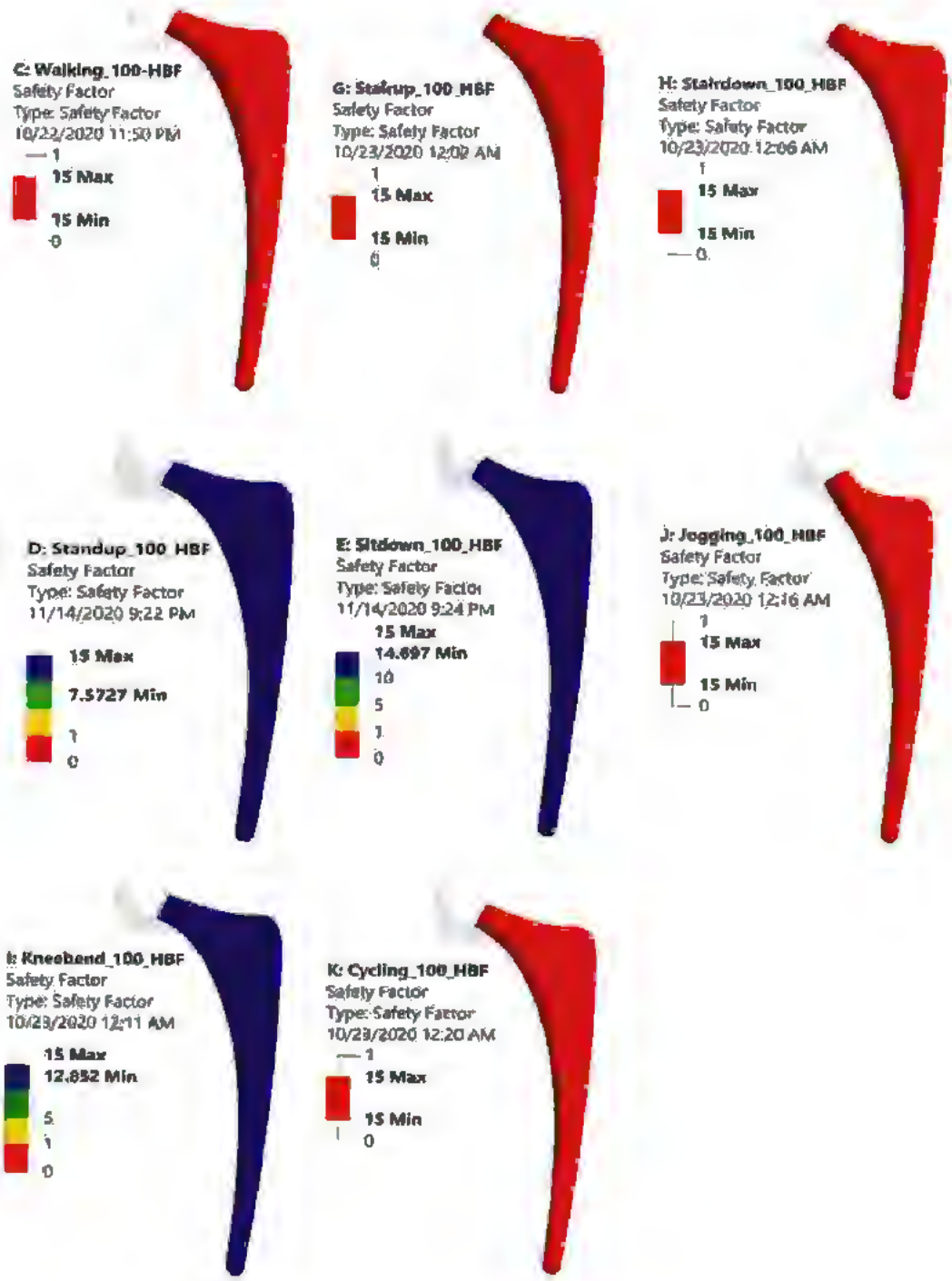

Figure_Apx A-8: Fatigue FOS contour of different activities for body weight of 100 Kg SBF Treated Ti-27Nb.

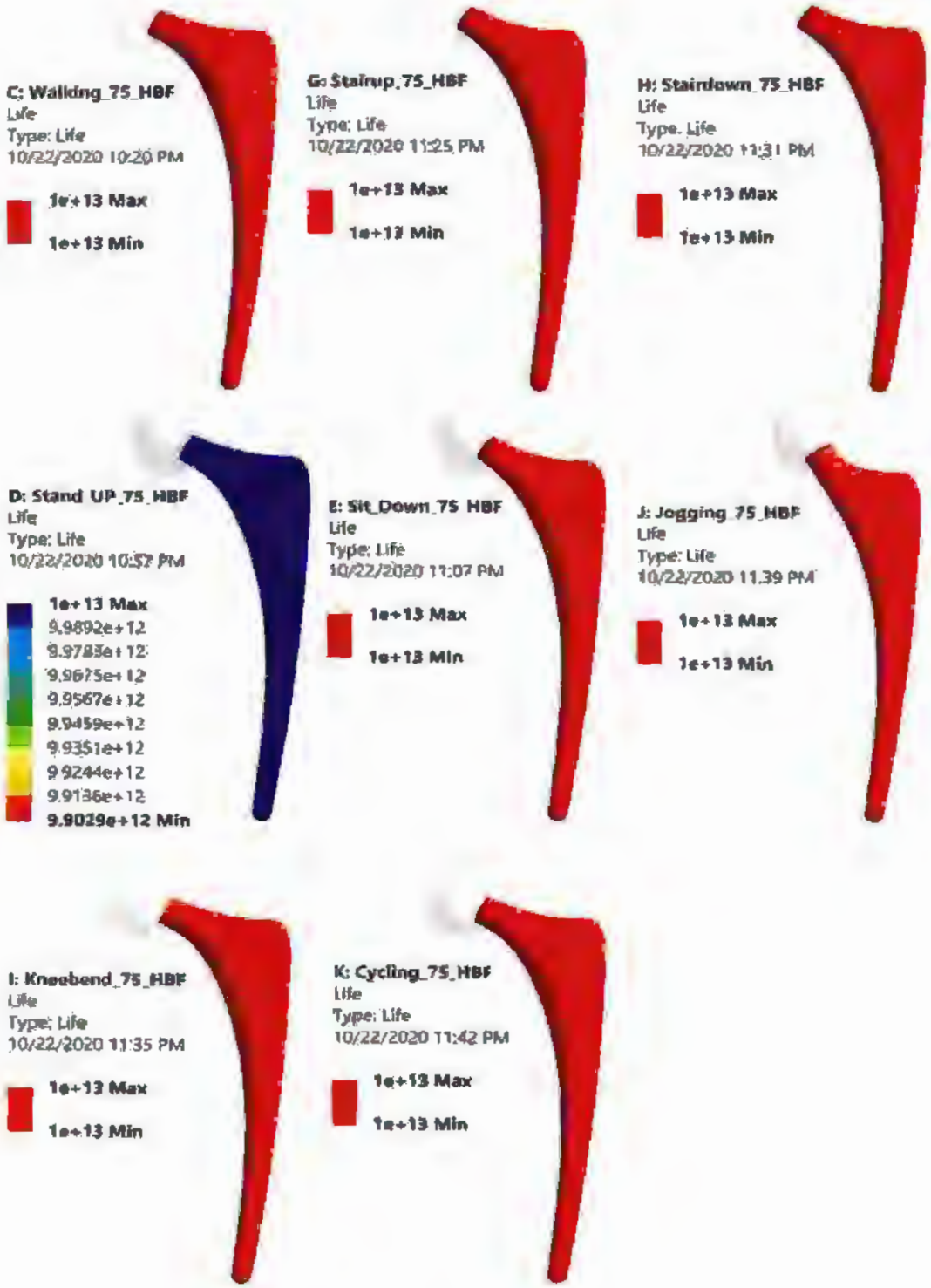

Figure_Apx A- 9: Fatigue life contour of different activities for body weight of 75 Kg SBF Treated Ti-27Nb.

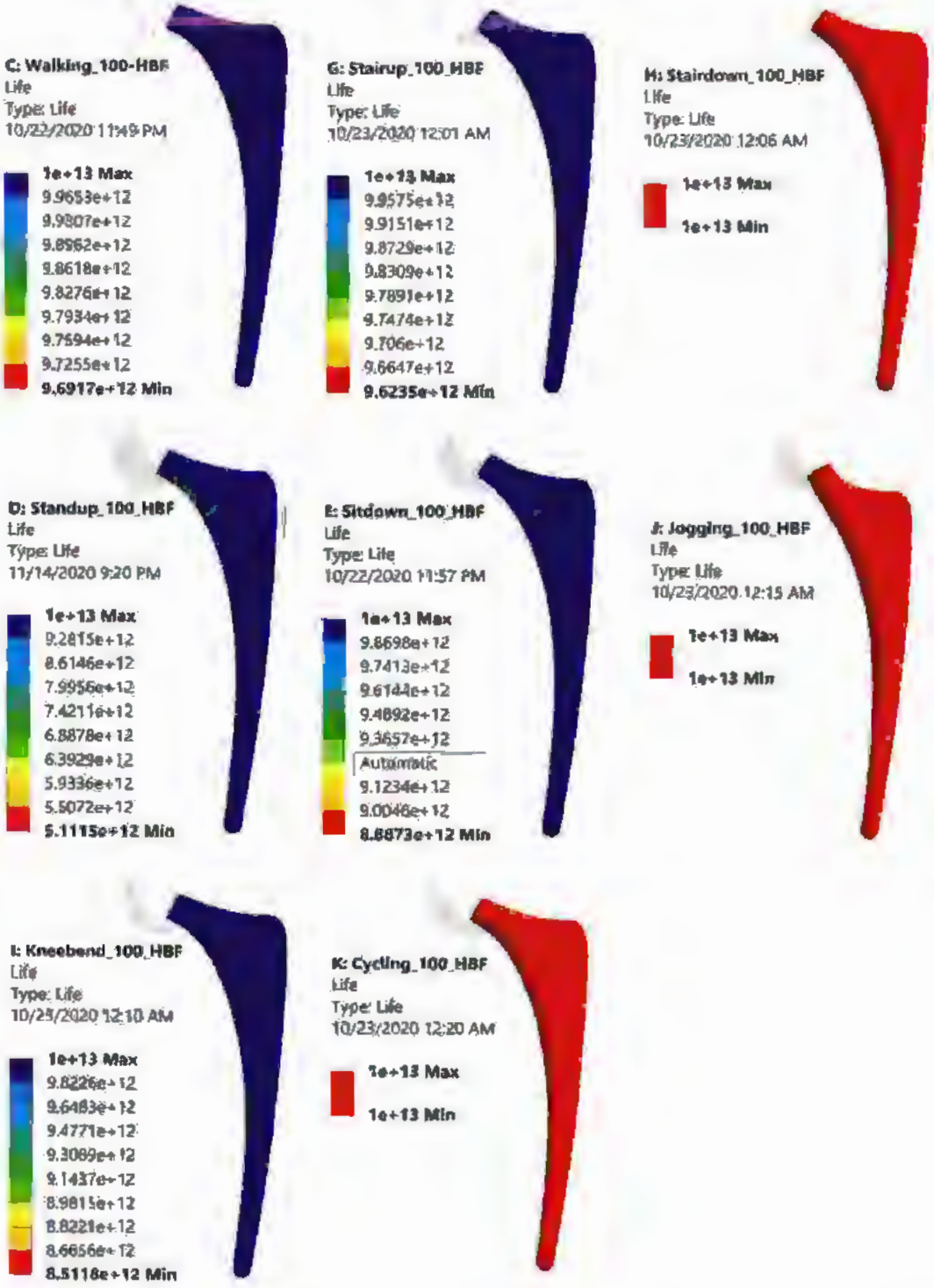

Figure_Apx A- 10: Fatigue life contour of different activities for body weight of 100 Kg SBF Treated Ti-27Nb.

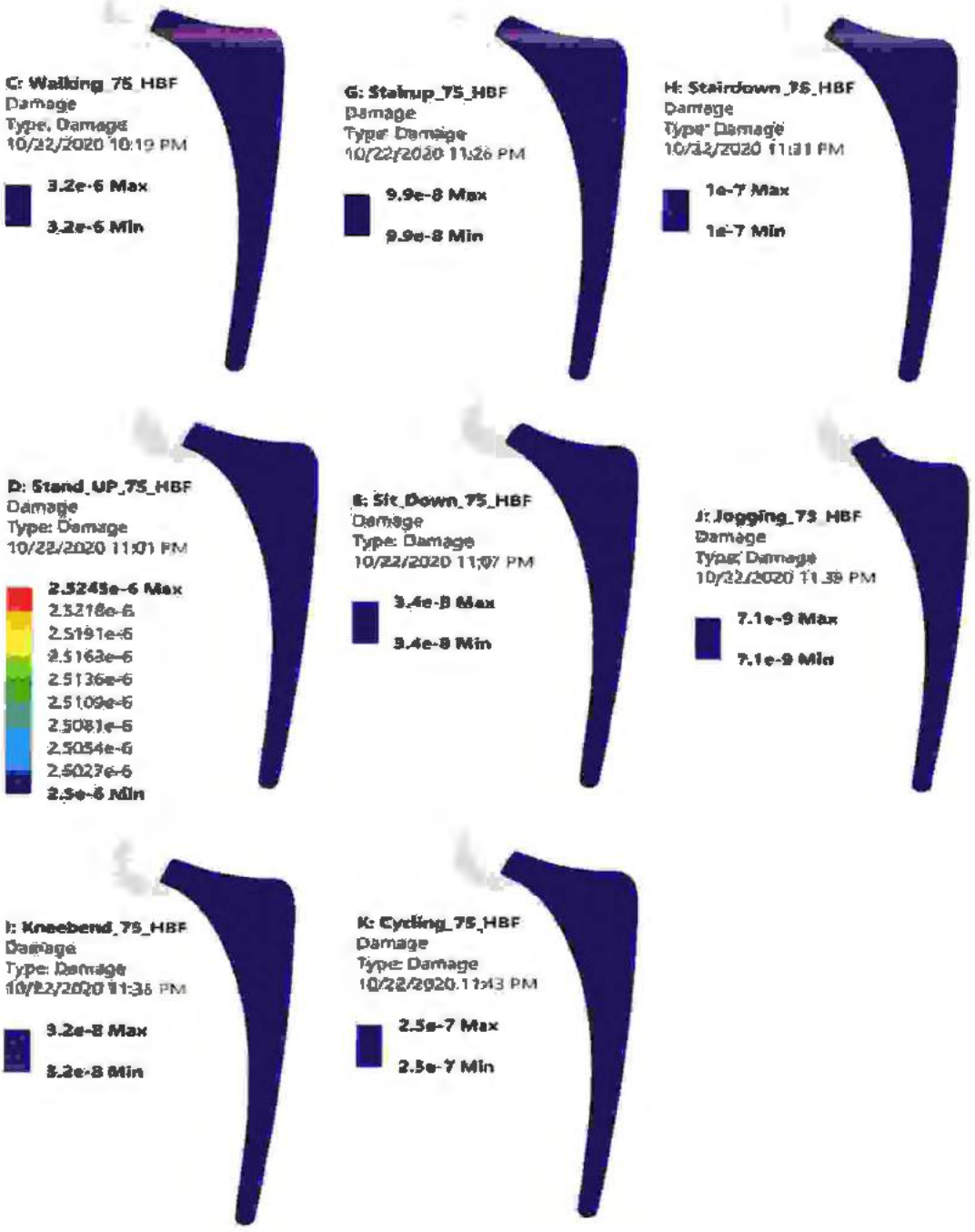

Figure_Apx A- 11:Fatigue Damage contour of different activities for body weight of 75 Kg SBF Treated Ti-27Nb.

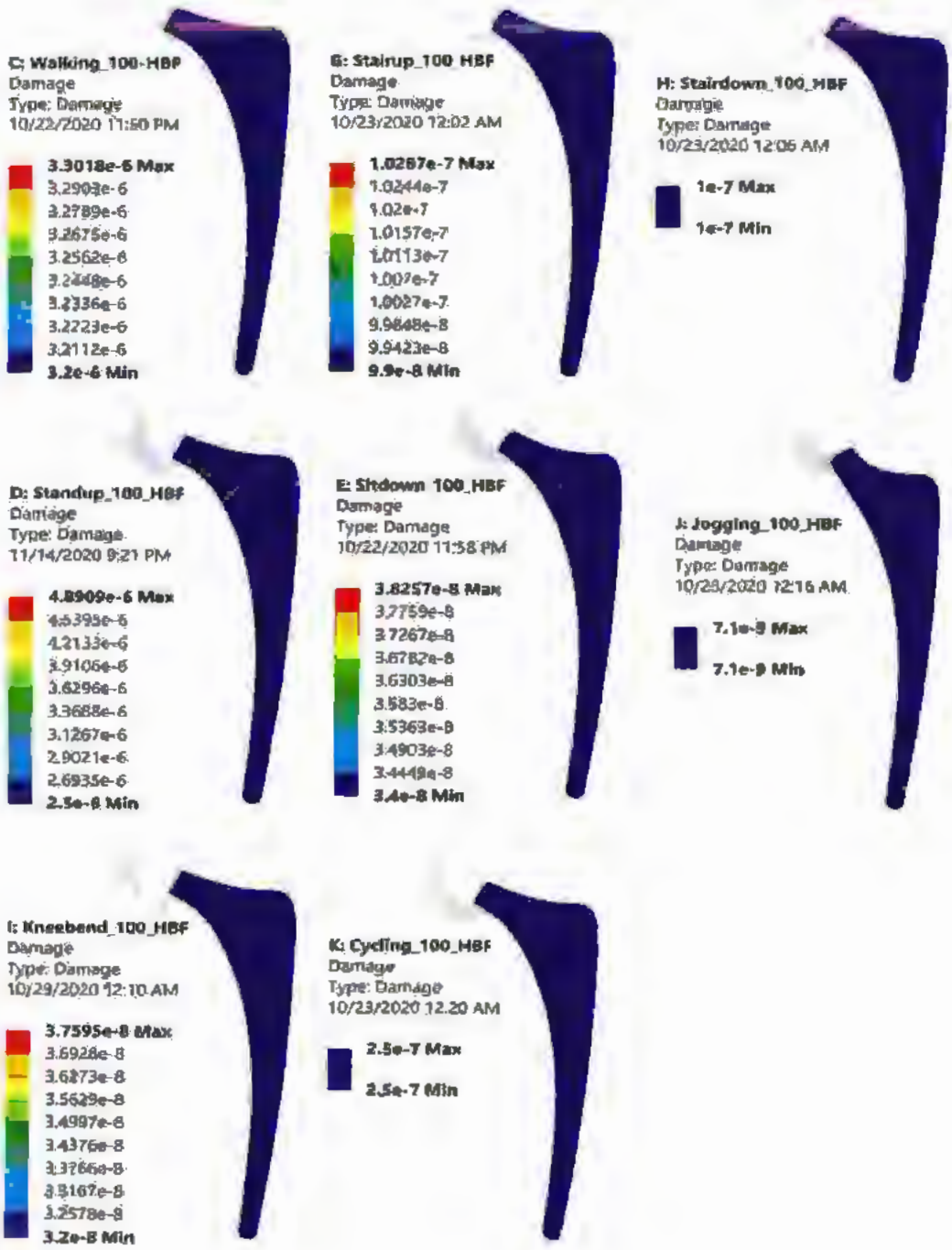

Figure_Apx A- 12: Fatigue Damage contour of different activities for body weight of 100 Kg SBF Treated Ti-27Nb.

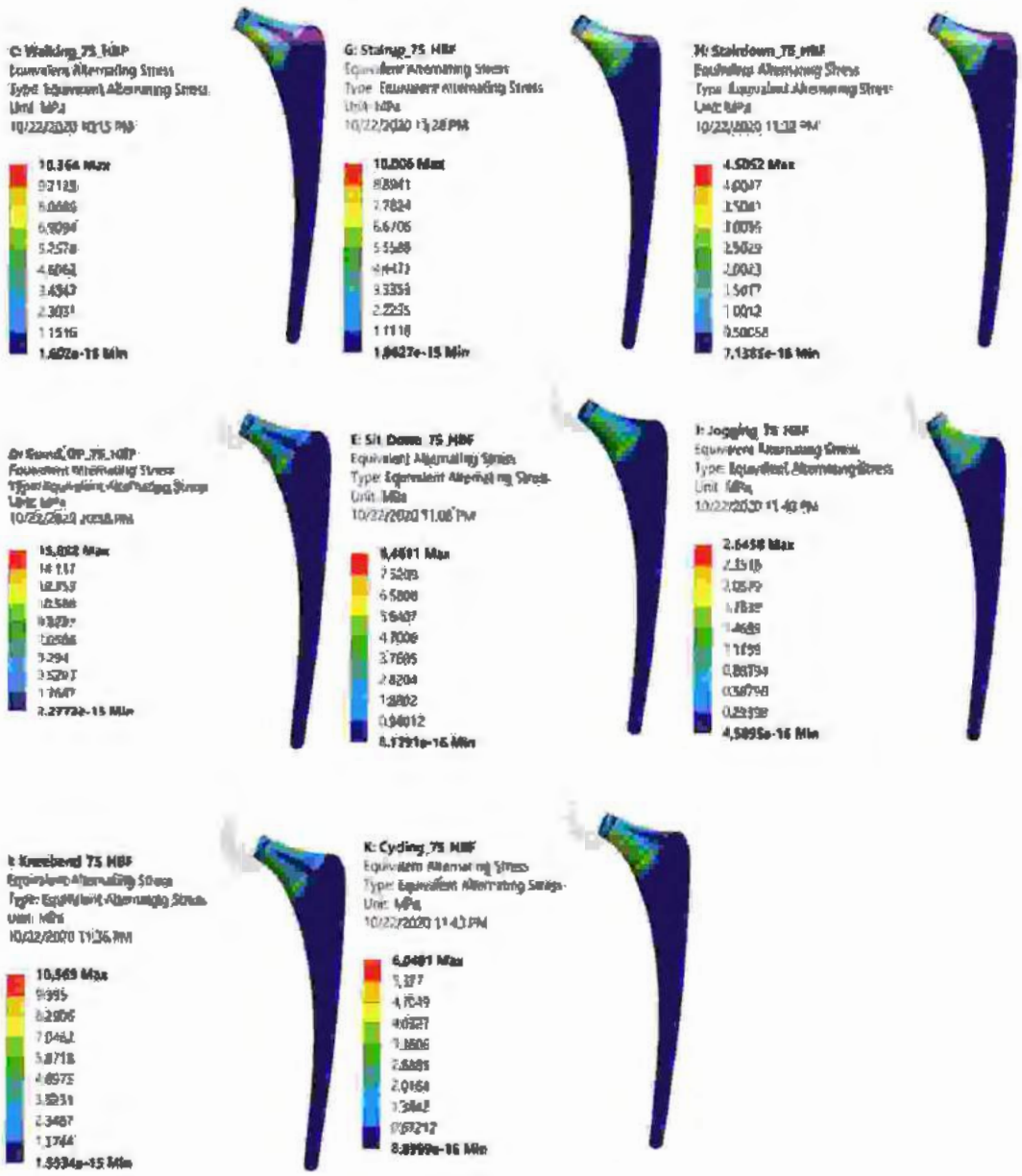

Figure_Apx A- 13:Equivalent Alternating Stress contour of different activities for body weight of 75 Kg SBF Treated Ti-27Nb.

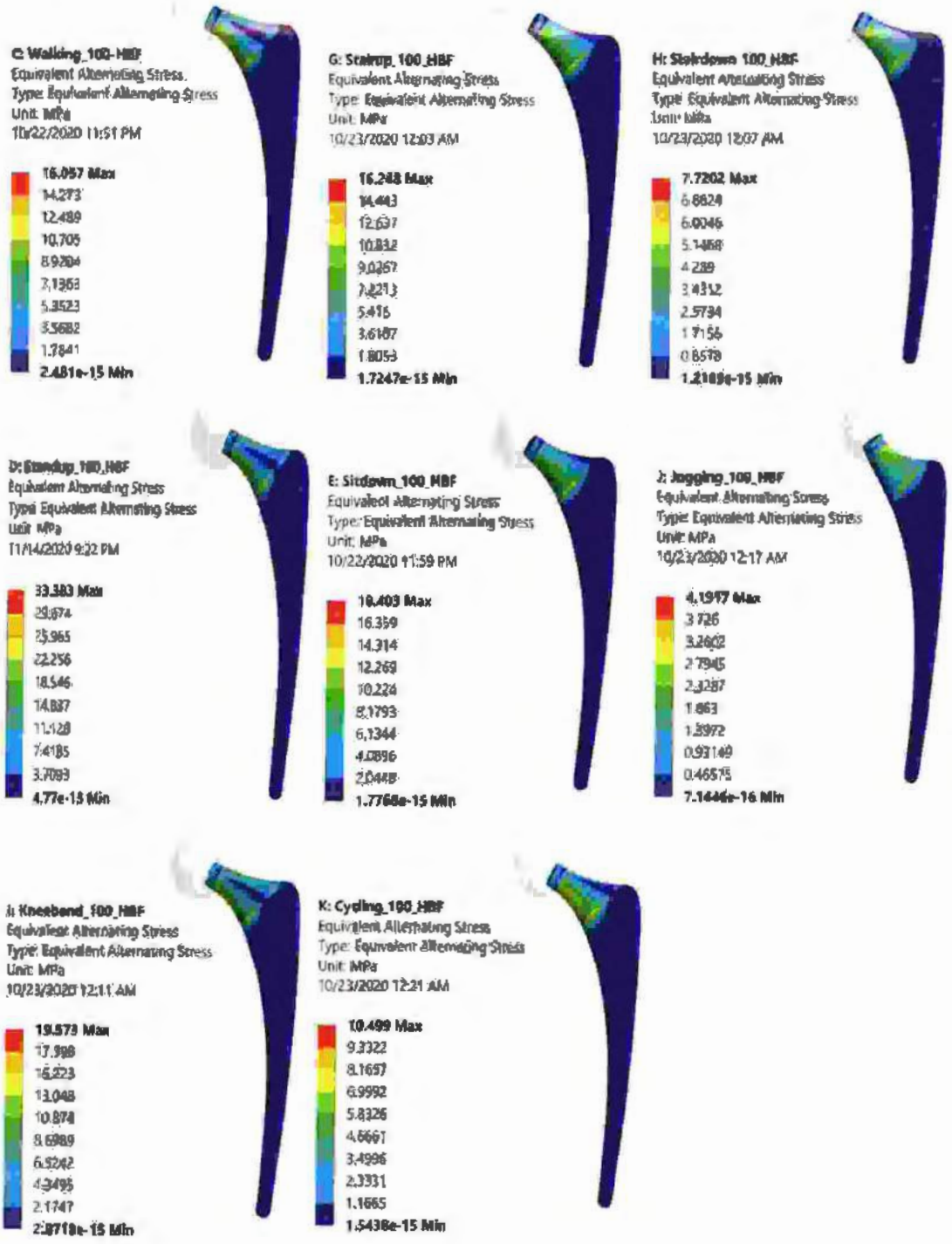

Figure_Apx A- 14: Equivalent Alternating Stress contour of different activities for body weight of 100 Kg SBF Treated Ti-27Nb

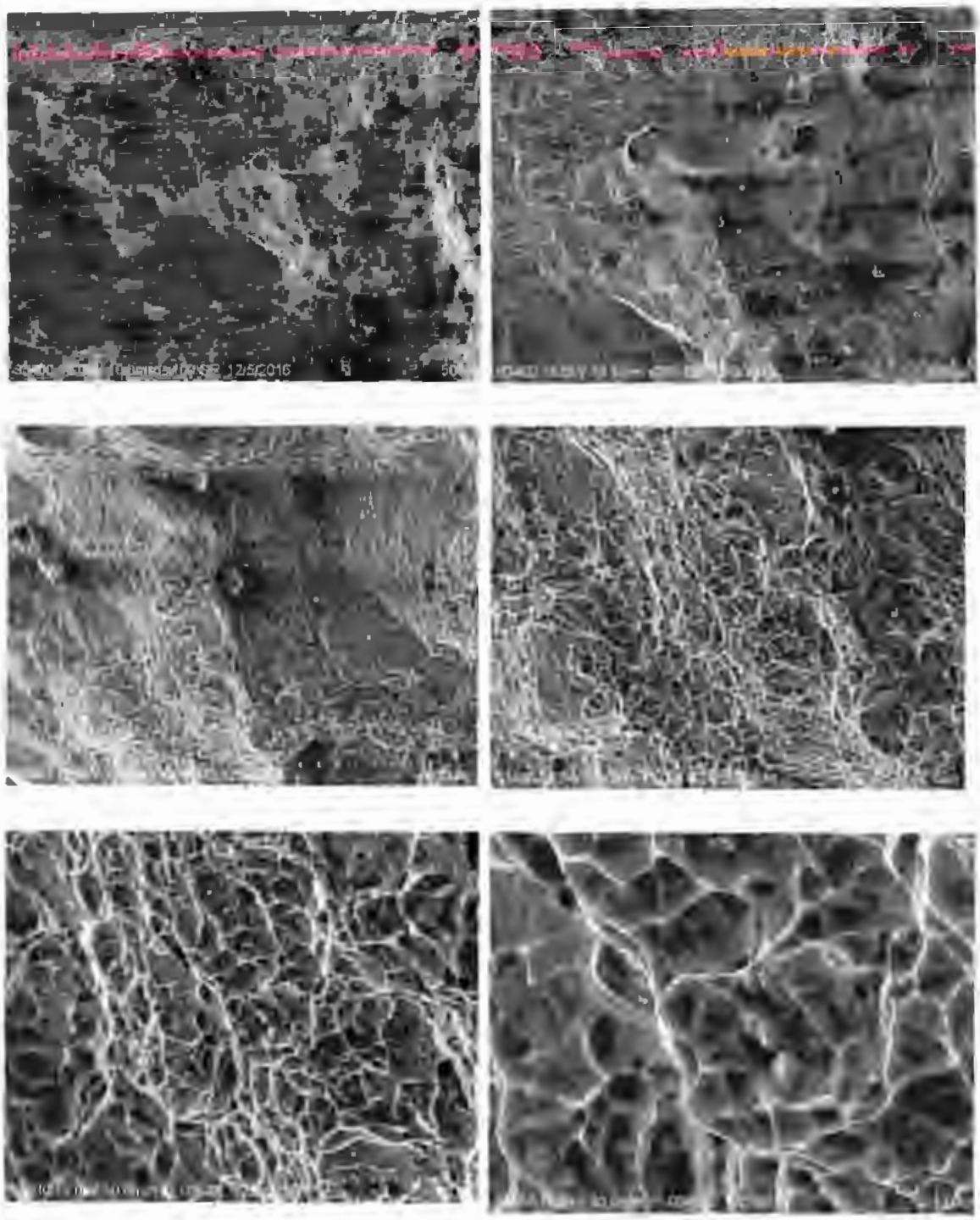

Figure_Apx A- 15: SEM micrograph showing the fractured surface of tensile specimen

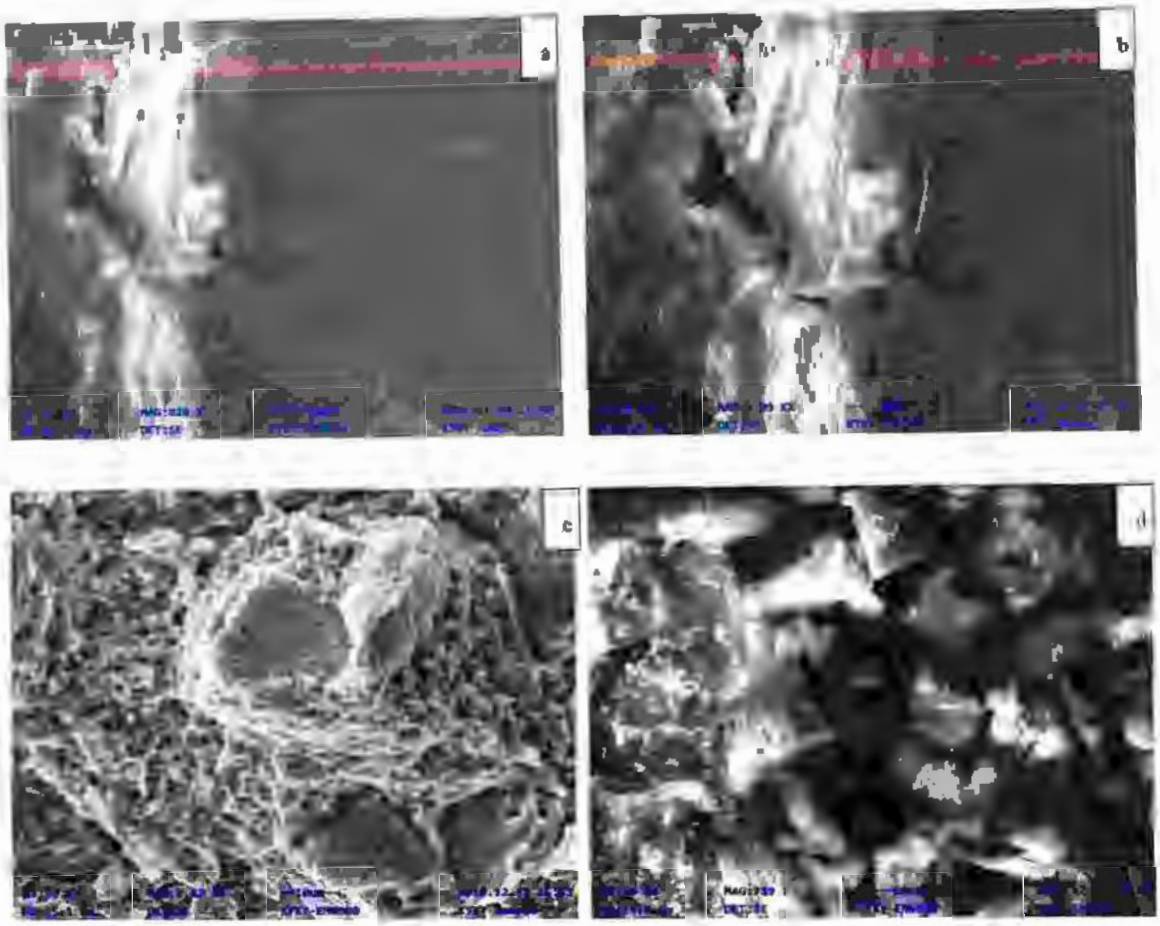

Figure_Apx A- 16: Ti-27Nb untreated specimen SEM analysis after fatigue crack growth at different µm. (a & b) stable crack growth region. (c) unstable crack growth region (d) pre crack region

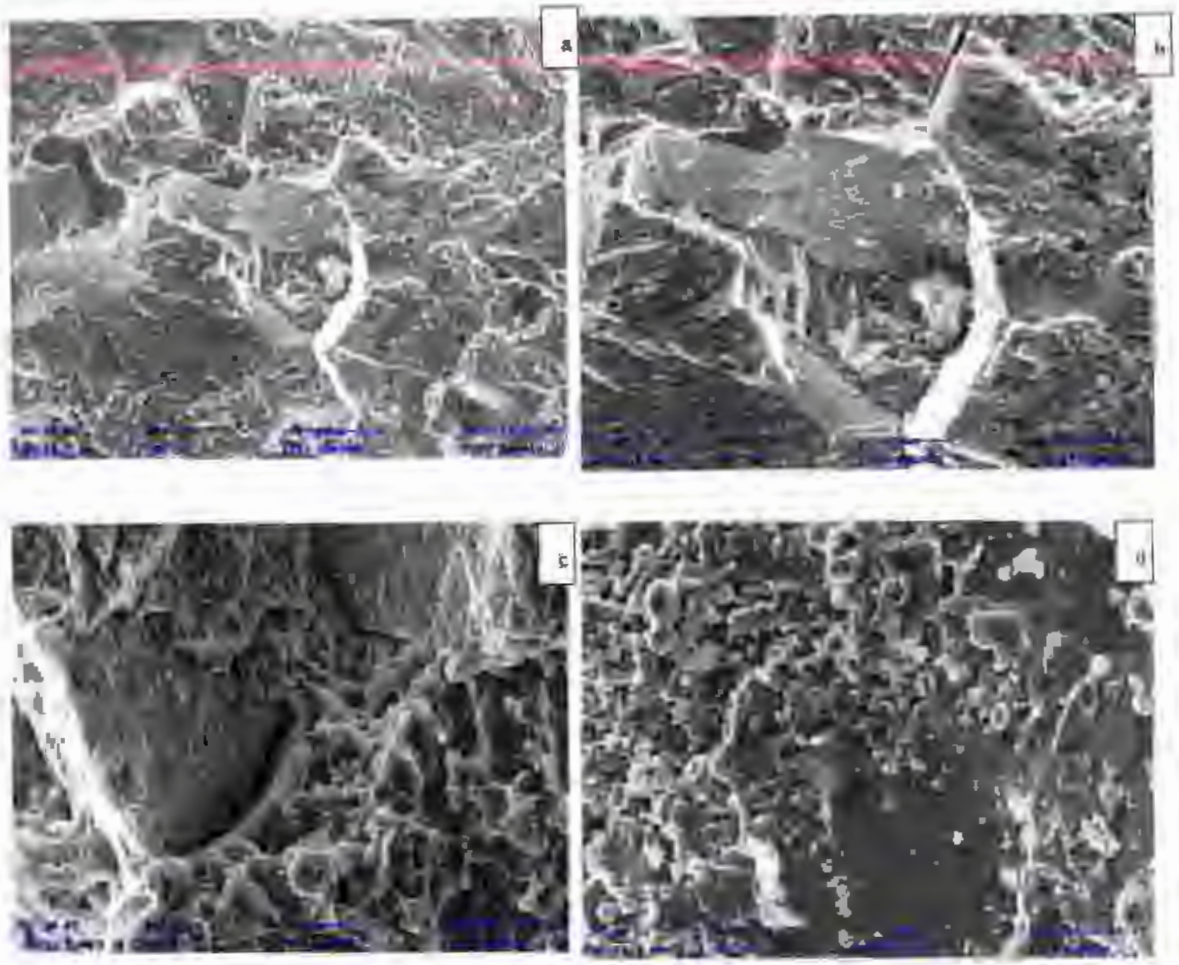

Figure_Apx A- 17: Ti-27Nb 504 Hrs treated specimen SEM analysis after fatigue crack growth at different µm. (a & b) stable crack growth region. (c) unstable crack growth region (d) pre crack region

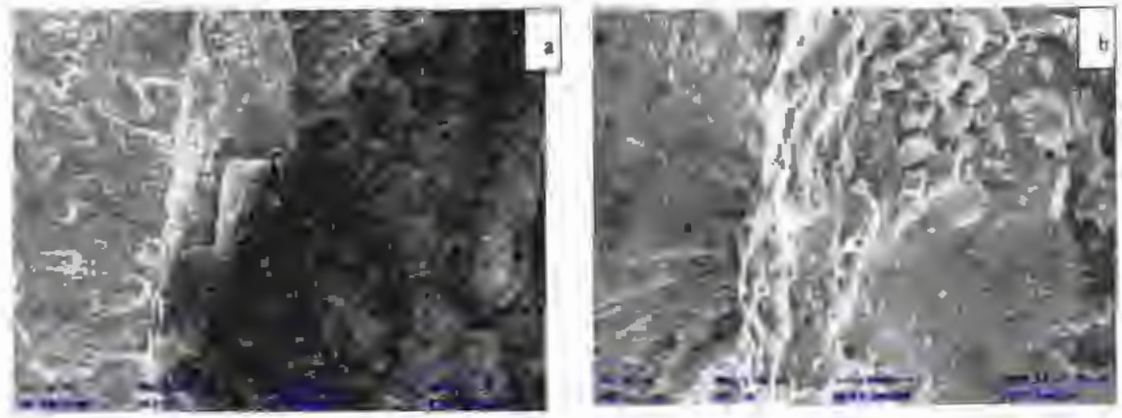

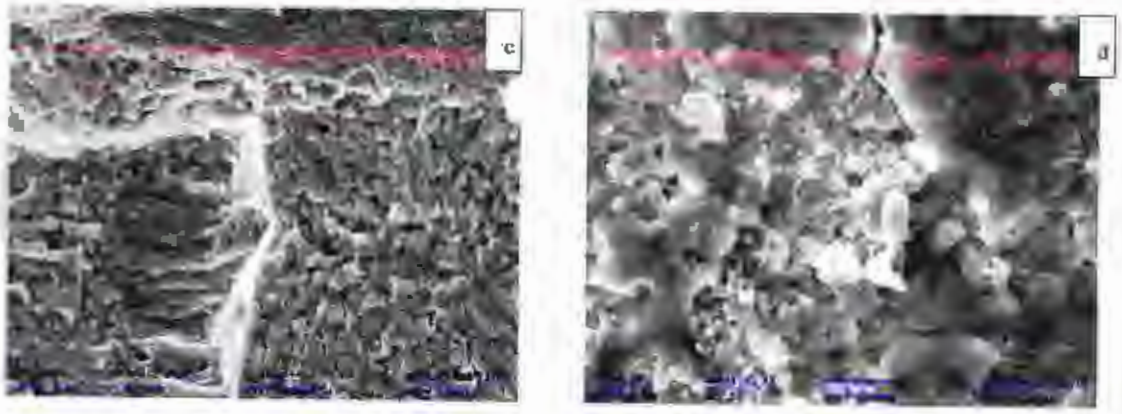

Figure_Apx A- 18: Ti-27Nb 816 Hrs treated specimen SEM analysis after fatigue crack growth at different µm. (a & b) stable crack growth region. (c) unstable crack growth region (d) pre crack region

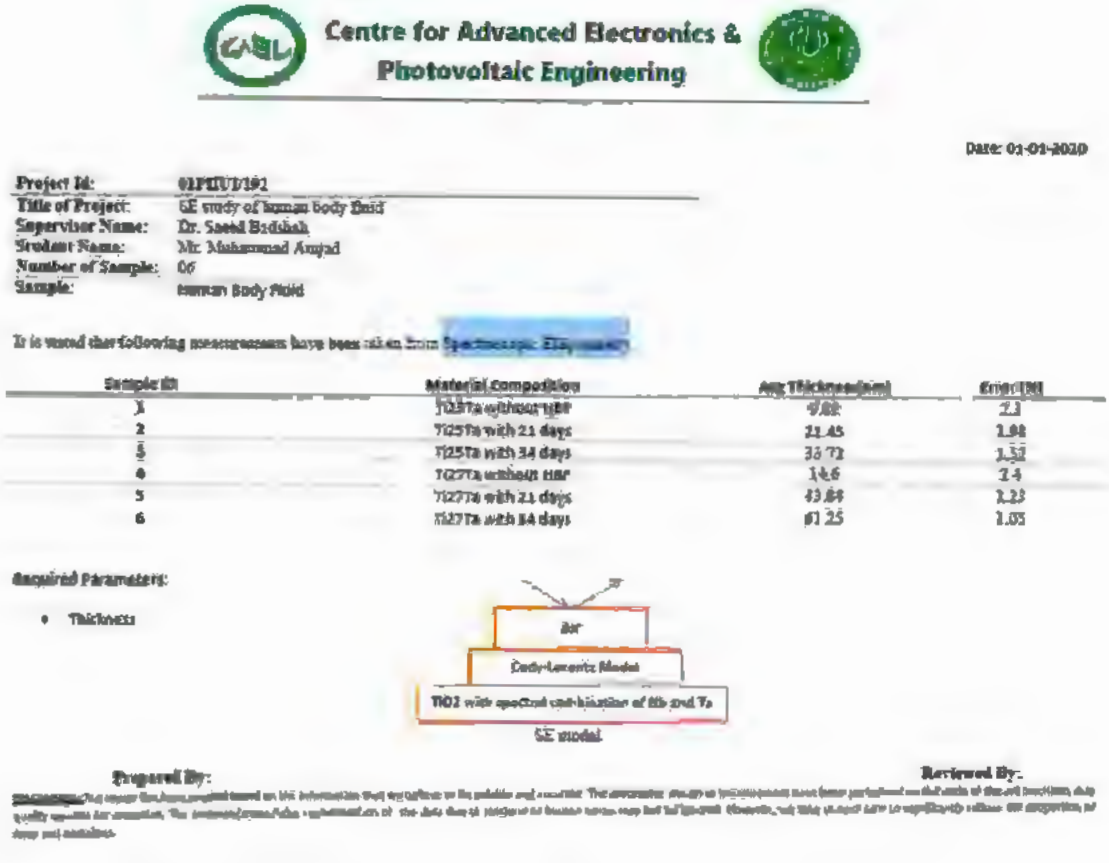

Centre for Advanced Electronics & Photovoltaic Engineering

Date: 01-01-2020

Project Id:	01PIUD192
Title of Project:	SE study of human body fluid
Supervisor Name:	Dr. Saeed Ur-Rehman
Student Name:	Mr. Muhammad Amjad
Number of Sample:	06
Sample:	Human Body Fluid

It is stated that following measurements have been taken from Spectroscopic Ellipsometry

Sample ID	Material composition	Avg Thickness(nm)	Error (%)
1	Ti25Ta without HBF	9.82	2.3
2	Ti25Ta with 21 days	21.45	1.84
3	Ti25Ta with 34 days	33.72	1.32
4	Ti27Ta without HBF	14.6	2.4
5	Ti27Ta with 21 days	43.84	1.23
6	Ti27Ta with 34 days	61.25	1.05

Required Parameters:

- Thickness

Prepared By: Reviewed By:

Figure_Apx A- 19: Spectroscopic Ellipsometry Ti-27Nb and Ti-25Ta